SEISMIC RESERVOIR CHARACTERIZATION: A FEASIBILITY STUDY USING SEISMIC SITE SURVEY DATA FOR SHALLOW GAS PILOT PROJECT IN PENINSULAR MALAYSIA

HASLINA BINTI MOHAMED

FACULTY OF SCIENCE
UNIVERSITY OF MALAYA
KUALA LUMPUR

2018

SEISMIC RESERVOIR CHARACTERIZATION: A FEASIBILITY STUDY USING SEISMIC SITE SURVEY DATA FOR SHALLOW GAS PILOT PROJECT IN PENINSULAR MALAYSIA

HASLINA BINTI MOHAMED

DISSERTATION SUBMITTED IN PARTIAL FULFILMENT OF THE REQUIREMENTS FOR THE DEGREE OF MASTER OF SCIENCE (PETROLEUM GEOLOGY)

DEPARTMENT OF GEOLOGY
FACULTY OF SCIENCE
UNIVERSITY OF MALAYA
KUALA LUMPUR

2018

UNIVERSITY OF MALAYA
ORIGINAL LITERARY WORK DECLARATION

Name of Candidate: HASLINA BINTI MOHAMED

Matric No: SGI 120005

Name of Degree: MASTER OF SCIENCE (PETROLEUM GEOLOGY)

SEISMIC RESERVOIR CHARACTERIZATION: A FEASIBILITY STUDY USING SEISMIC SITE SURVEY DATA FOR SHALLOW GAS PILOT PROJECT IN PENINSULAR MALAYSIA ("this Work"):

Field of Study: Site survey, seismic petro-physics, rock physics, AVO, seismic inversion and reservoir characterization.

I do solemnly and sincerely declare that:

(1) I am the sole author/writer of this Work;
(2) This Work is original;
(3) Any use of any work in which copyright exists was done by way of fair dealing and for permitted purposes and any excerpt or extract from, or reference to or reproduction of any copyright work has been disclosed expressly and sufficiently and the title of the Work and its authorship have been acknowledged in this Work;
(4) I do not have any actual knowledge nor do I ought reasonably to know that the making of this work constitutes an infringement of any copyright work;
(5) I hereby assign all and every rights in the copyright to this Work to the University of Malaya ("UM"), who henceforth shall be owner of the copyright in this Work and that any reproduction or use in any form or by any means whatsoever is prohibited without the written consent of UM having been first had and obtained;
(6) I am fully aware that if in the course of making this Work I have infringed any copyright whether intentionally or otherwise, I may be subject to legal action or any other action as may be determined by UM.

Candidate"s Signature Date:

Subscribed and solemnly declared before,

Witness"s Signature Date:

Name:

Designation:

SEISMIC RESERVOIR CHARACTERIZATION: A FEASIBILITY STUDY USING SEISMIC SITE SURVEY DATA FOR SHALLOW GAS PROJECT IN PENINSULAR MALAYSIA

ABSTRACT

Exploration Malaysia of PETRONAS Carigali Sdn Bhd (PCSB) recently embarked on a Shallow Gas (SG) project where most of the leads and prospects were identified based on strong seismic amplitude anomalies that satisfied at least one of the conventional Direct Hydrocarbon Indicator (DHI) criteria. However, the strong amplitude anomalies can be due to low saturation gas, silty gas sand, high porosity brine sand and overpressure sand. This non-uniqueness in the interpretation of the seismic amplitude anomaly has made the SG project a challenging task and hence the needs for this research study. Well log and seismic data are acquired by PCSB specifically for unconsolidated clastic sediments at shallow-depth were made available for the study. The sonic logs were acquired using a new Acoustic Sonic Tool (AST) and the input seismic was from a high resolution 2D site survey which was reprocessed into a pseudo 3D data. Since there is limited literature and suitability of pseudo 3D seismic site survey data for seismic reservoir characterization analysis are still unknown, this research aimed at studying the feasibility of using these input data to: 1) understand the relationship of rock type, porosity, water saturation and pressure to the elastic properties; 2) ascertain the suitability of site survey data for AVO and Inversion study at shallow clastics depth interval; and 3) predict lithology, porosity, and if possible water saturation and reservoir pressure through forward modelling and inversion. To achieve the aim, the following activities were executed in four phases: 1) input data QC and conditioning; 2) elastic logs and seismic forward modeling; 3) seismic inversion processing; and 4) seismic reservoir characterization analysis and interpretation. The results are encouraging. The elastic *in situ* and modeled elastics logs showed good trend match with the global AI-Vp/Vs crossplot. The established AI-Vp/Vs from the GD-1 well produced clear understanding of elastic properties changes to rock type, hydrocarbon phase, porosity, water saturation and pore pressure. Seismic forward model analysis result clearly demonstrated that seismic amplitude from unconsolidated shallow sand is highly sensitive to gas fill, followed by hydrocarbon saturation, porosity, volume of clay and pore pressure. An excellent well to seismic tie with stable wavelet produced consistent AVO response between the synthetic seismic and observed seismic response thus indicating that both datasets are suitable for seismic inversion processing. High correlation value of 80 - 90% match between inverted AI - Vp/Vs trace and measured AI - Vp/Vs logs confirmed the input site survey seismic data are feasible for seismic reservoir characterization analysis. The predicted sand results match the well result, and the interpreted sand fairway is consistent with shallow marine sand deposition. It is therefore concluded that the pseudo3D seismic site survey data are feasible for seismic reservoir characterization interpretation and analysis. Value of site survey seismic data for seismic reservoir characterization in shallow-depth clastics has been demonstrated here. It is recommended to apply this scheme to other areas so as to improve confidence in drilling shallow gas prospect and especially placing wells at optimal drilling locations.

Keywords: Site survey, rock physics, AVO, inversion and reservoir characterization.

PENCIRIAN TAKUNGAN MELALUI SEISMIK: KAJIAN KELAYAKKAN MENGGUNAKAN DATA SEISMIK DARI TINJAUAN TAPAK UNTUK EXPLORASI GAS PADA KEDALAMAAN CETEK DI SEMENANJUNG MALAYSIA

ABSTRAK

Exploration Malaysia PETRONAS Carigali Sdn Bhd (PCSB) menjalankan explorasi gas di kedalaman yang cetek (kedalaman tidak lebih dari 1200m), di mana kebanyakan petunjuk dan prospek yang telah dikenal pasti adalah berdasarkan anomali amplitud seismik yang kuat dan memenuhi sekurang-kurangnya satu kriteria indikator hidrokarbon. Walau bagaimanapun, anomali amplitud yang kuat boleh juga disebabkan oleh ketepuan gas yang rendah, pasir lumpur berkandungan gas, pasir yang poros berkandungan air atau takungan yang bertekanan tinggi, Oleh kerana tiada keunikan didalam pentafsiran anomali amplitud seismic, cabaran untuk penafsiran anomali yang tepat telah mendorong kajian ini dilakukan. Tujuan utama kajian adalah: 1) Memahami hubungan jenis batu, keliangan, ketepuan, dan tekanan keliangan terhadap sifat elastic; 2) menentukan kesesuaian "pseudo3D" seismik data yang direkodkan semasa tinjauan-tapak untuk kajian "AVO" dan "Penyongsangan Seismik" pada kedalaman cetek; dan 3) meramalkan jenis batuan, keliangan, ketepuan hidrokarbon dan tekanan takungan jika boleh. Untuk mencapai matlamat, aktiviti berikut telah dilaksanakan dalam empat fasa: 1) penyemakan kualiti dan pembetulan; 2) permodelan log elastik dan seismik; 3) penyongsangan seismic "Pseudo3D"; dan 4) analisis dan pencirian takungan seismik. Hasilnya menggalakkan kerana trend AI-Vp/Vs yang dicadangkan adalah sama dengan bacaan yang dibuat dari telaga GD-1. Pemahaman yang jelas terhadap perubahan sifat elastik dengan jenis batuan, fasa hidrokarbon, keliangan, ketepuan air dan tekanan keliangan diperolehi dari permodelan. Hasil analisa model seismik menunjukkan dengan jelas bahawa amplitud seismik dari batuan yang belum terkondisasi sangat sensitif terhadap cecair gas, diikuti oleh ketepuan hidrokarbon, keliangan kandungan tanah liat dan tekanan liang. Sintetik seismik dan seismik sebenar mempunyai persamaan yang tinggi dan trend “AVO” yg sama membuktikan bahawa seismik data tersebut sesuai digunakan untuk kajian “AVO” and penyonsangan seismik. Penafsiran jenis batuan daripada seismik juga sama seperti dicerap dari telaga (pada resolusi seismic). Berdasarkan dari keputusan analisa di atas, kajian ini menyimpulkan bahawa input data log AST dan “Pseudo3D” tersebut adalah sesuai digunakan untuk analisa dan penafsiran gas di kawasan yang cetek. Kajian ini mensyorkan penggunaan kajian ini di digunakan untuk penafsiran dan analisa pencirian takungan seismic di kawasan yang lain bagi meningkatkan keyakinan dalam potensi kejayaan menjumpai gas di kedalaman yang cetek.

Kata kunci: Tinjauan tapak, fizik batuan, AVO, penyongsangan seismic dan pencirian takungan.

ACKNOWLEDGEMENTS

Thank you to PCSB management (Ahmad Bukhari, Amiruddin Mansor, Ismail Saad, Ahmad Aznan, Roszendy Danial, Salihin Samsuri, Abdul Aziz, Zabidi, Suhaileen Shahar) and technical personnel (Syazwani Suhairi, Mustaza Musa, Martin Brewer, Jahan Zeb, Farhan Khan, Siti Fahimah and Faiqah Mohamed) for input data permission and technical support. My lecturer and supervisors Dr. Ralph Kugler, Dr. Meor Hakif , Dr. Noer El Hidayah and Prof. Wan Hasiah for academic support. QI team in PETRONAS CariGali and my family for their continous encouragement. CGG-Jason (formely Fugro-Jason) for sponsoring Jason sofware license in 2013 - 2014 and Halliburton for allowing Mr. Azizul Yahya to support PETRONAS Processing Team. Special thanks to Dr. Maxwell Meju for his consistent motivation, guidance and volunteer in reviewing this dissertation.

TABLE OF CONTENTS

Abstract iii

Abstrak v

Acknowledgements vii

Table of Contents viii

List of Figures xi

List of Tables xvii

List of Symbols and Abbreviations xviii

List of Appendices xix

CHAPTER 1: INTRODUCTION 1

1.1 Background and problem definition 1

1.2 Data issues and research motivation 4

1.2.1 Seismic data challenges 4

1.2.2 Well data challenges 7

1.3 Aims and objective of the study 11

1.4 Data sources 12

1.5 Outline of the research approach 15

1.6 Key deliverables 15

CHAPTER 2: LITERITURE REVIEW 16

2.1 Geologic setting and stratigraphy of study area 16

2.2 Rock and elastic properties of unconsolidated rocks 19

2.2.1 Empirical rock physics relationships......21
2.2.2 Rock physics template (RPT)......23
2.3 High resolution site survey seismic......24
2.4 Seismic reservoir characterization......26

CHAPTER 3: METHODOLOGY......28
3.1 Well log QC & conditioning......28
3.1.1 Well log QC......28
3.1.2 Well log data conditioning......33
3.2 Seismic data QC and conditioning......37
3.3 Petrophysical Interpretation......43
3.3.1 Volume of clay (V_{clay}) estimation......43
3.3.2 Porosity estimation......44
3.3.3 Water saturation estimation......45
3.4 Rock physics modeling......46
3.4.1 Fluid Phase and Saturation Perturbation......46
3.4.2 Porosity perturbation......46
3.4.3 Pore pressure perturbation......46
3.4.4 Volume of clay perturbation......47
3.5 Seismic Forward Model & AVO crossplot......51
3.6 Simultaneous AVO inversion......54
3.6.1 Well to seismic calibration......55
3.6.2 Wavelet extraction......57
3.6.3 Low frequency model......58
3.6.4 Seismic Inversion and Quality Check......60
3.6.5 Interpretation and analysis......65
3.6.6 Analysis of cross plots and inversion results......65

3.6.7 Bayesian probabilistic method for lithology probability prediction......... 67

3.6.8 Porosity prediction... 69

CHAPTER 4: RESULTS AND DISCUSSION.. 71

4.1 Rock and elastic properties of B-group unconsolidated sediments in the pilot study area…….. 71

4.2 Suitability of site survey seismic data for AVO and Inversion study.................... 79

4.3 Seismic reservoir prediction of lithology, porosity, fluid and pressure through forward model and inverted seismic... 81

CHAPTER 5: CONCLUSION AND RECOMMENDATION................................. 85

References 87

Appendix A: Regional study of ai – vp/vs, group-I malay basin of offshore peninsular malaysia; Unpublished poster. 94

Appendix B: Seismic gather conditoning qc plots 95

Appendix C: A look into gassmann"s equation... 103

Appendix D: Rock physics modeling results 109

I. Fluid phase and hydrocarbon sensitivity analysis 109

II. Porosity sensitivity analysis 113

III. Pore pressure sensitivity analysis 117

IV. Clay volume sensitivity analysis 121

LIST OF FIGURES

Figure 1.1: Peninsular Malaysia Gas Field and Production Facilities. The pilot study area is surrounded by gas fields and within production facility. 2

Figure 1.2: Schematic diagram and seismic section of shallow gas prospect and plays identified during Shallow Gas Project. 2

Figure 1.3: Seismic section across well GD-1 and RMS amplitude map extracted from Intra B1.5 horizon. The seismic section and intra B1.5 RMS amplitude map shows at least three criteria that give high confidence of hydrocarbon presence (After Suhairi & Jalil , 2014). 3

Figure 1.4: Surface seismic CDP offset showing lack of seismic signal at near angle stack from conventional seismic acquisition and processing. 5

Figure 1.5: Angle stack seismic section from site survey data shows strong amplitude events at 270ms and 370ms (NFMJ, 2014). 6

Figure 1.6: GD-1 composite well log. The composite log is showing the availability of GR, Density, Compressional and Shear sonics, within the B-group of shallow clastics interval. The red box higlighted the missing interval..8

Figure 1.7: Well correlation between GD-1 and DS-1. Both wells acquired complete elastic logs at B group interval using the same AST tool, enabling reliable elastic logs comparison. The low water saturation log within the B group at DS-1 give a good calibration reservoir-fluid and elastic logs. 9

Figure 1.8: a) AI-Vp/Vs crossplot and histogram color coded by wells. The green points are from GD-1 well has lower AI and higher Vp/Vs as compared to DS-2. b) top right cross plot of AI-Vp/Vs color coded by depth (TVDss). The cold color shows elastic properties of AI and Vp/Vs log data from GD-1 well while the hot color are from DS-1. This cross plot shows normal depth compaction trend. 10

Figure 1.9: Study area basemap and seismic section showing vertical zone of interest. 14

Figure 1.10: Research process flow and contents. 15

Figure 2.1: GD-1 site survey area is surrounded by oil and gas field (modified after Hutchinson & Tan, 2009). 17

Figure 2.2: Distribution of source, reservoir and seal rock in the Malay Basin (Hutchison & Tan, 2009). 18

Figure 2.3: Rock physics properties change with depositional environment and burial depth. These geologic trends must be taken into account during hydrocarbon reconnaissance of seismic data (Avseth, Mukerij, & Mavko, 2010). 19

Figure 2.4: Schematic illustration of porosity-depth trends for sands and shales. (Avseth, Fleshe & Wijngaaeden, 2003). 20

Figure 2.5: Conceptual trends for siliciclastic lithologies at constant confining pressures (Odegaard et al., 2004). 24

Figure 2.6: Seismic gather comparison from 2D processing and pseudo3D processing (Panea et al., 2013) 25

Figure 2.7: Seismic inversion to porosity prediction from site survey data (Vardy et al., 2015). Panel (a) shows the subset of a single channel boomer profile, (b) the synthetic seismic profile generated by the inversion, and (c) through (e) the P-wave velocity, density, and porosity profiles estimated from the impedance using empirically derived relationships. 27

Figure 3.1: Well log QC plot. In GD-1, caliper logs show two different logging run. Gamma ray log showed full coverage but the several logs are missing and highlighted in red. 29

Figure 3.2: Histogram and Crossplot of input density and p-velocity logs color coded by volume of clay within the B-Group. 32

Figure 3.3: Histogram and Crossplot of input p-velocity and s-velocity logs color coded by volume of clay within the B-Group. Hydrocarbon-bearing points lie off trend. 32

Figure 3.4: GD-1 and DS-2 well logs plot of conditioned data. The data gap from the input Vp, Vs and Density (blue curve) filled with synthetic logs (black) that shows good match of depth trend. 34

Figure 3.5: Histogram and Crossplot comparison of before and after conditioning of p-velocity and density logs color coded by Vclay in the B-Group. 35

Figure 3.6: Histogram and Crossplot comparison of before and after conditioning of p-velocity and s-velocity logs color coded by Vclay in the B-Group. 36

Figure 3.7: Histogram and Crossplot comparison of before and after conditioning of AI and Vp/Vs logs in B-Group. 36

Figure 3.8: Seismic frequency bandwidth QC of input data. (a) Amplitude spectra QC plot from depth 400 – 1400ms. (b) Band limited seismic sections 0 Hz to 170 Hz. (c) Comparison of band limited seismic sections. 38

Figure 3.9: GD-1 well synthetic and seismic gather tie at three different acquisition spacings. Observed seimic reflector from all the input seismic gathers are not aligend and contaminated with multiples..39

Figure 3.10: Radon demultiple QI-4 QC plot. The red arrow highlighted multiple crossing the reflector. 100ms cut-off window removed most of the multiples and improved the data signal. 200ms cut-off window still have multiples. Cut-off window of 100ms used as final product. 41

Figure 3.11: Seismic amplitude and frequency sections of near, mid and far angle stacks. 41

Figure 3.12: RMS amplitude extracted at window 250 – 7500ms to observe non-geological effect. Two low amplitude lines at direction NE-SW observed at all stacks are non-geological effect. 42

Figure 3.13: Porosity - P-Velocity - Volume of Clay relationship. 48

Figure 3.14: Porosity - S-Velocity - Volume of Clay relationship. 49

Figure 3.15: Density – P-Velocity – Volume of Clay relationship. 50

Figure 3.16: Schematic format of a seismogram forward and inverse model (after Schroeder, 2011). 51

Figure 3.17: An incident p-wave produces four resulting waves, consisting of two reflected waves and two transmitted waves. Incidence angle of P-wave, $\boldsymbol{\theta 1} = \boldsymbol{\theta}$ for P-wave angle reflectivity. 52

Figure 3.18: The AVO classes (Castagna & Backus. 1992; Simm & Bacon., 2014). 53

Figure 3.19: Simultaneous AVO Inversion Workflow (Adapted from Jason CGG training manual). 54

Figure 3.20: GD-1 well synthetic and seismic calibration of near stack. This well tie QC plot of each panel describes as followings. Panel 1) wavelet used to generate synthetic seismic; 2) vertical scale in two way time (ms); 3) seismic traces at the well location; 4) synthetic seismic generated from convolution of well log reflectivities and wavelet; 5) cross correlation of seismic and synthetic at each displayed traces; 6) relative drift of final time-depth curve from the well checkshot; 7) Facies sand and shale from well log; 8) AI and Vp/Vs well log; 9) vertical scale in depth and 10) legend for cross-correlation value. Observe the AI property of B1, B2 and B3 sands are higher than shale. Seismic amplitude at the top of these sands are correspond to peak of seismic amplitude (black). Over the whole interval, the seismic and the synthetic have good match with cross-correlation more than 70%. However, at the Top of B1 sand, small mismatch of amplitude observed indicating stronger well reflectivities than seismic. Thus the same mismatch of inverted seismic and well log is expected at B1 sand. 55

Figure 3.21: GD-1 well synthetic and seismic calibration of mid stack. AI property of B1, B2 and B3 sands are higher than shale. Seismic amplitude at the tops of these sands correspond to peak amplitude (black). 56

Figure 3.22: GD-1 well synthetic and seismic calibration of far stack. AI property of B1, B2 and B3 sands are higher than shale. Seismic amplitude at the tops of these sands correspond to peak amplitude (black). 56

Figure 3.23: Composite of wavelets extracted from near, mid and far stacks from GD-1. 57

Figure 3.24: Seismic sections and interpreted horizon of top B-1 time map. A) Seismic at inline-84 across the GD-1 well with Vclay log, well formation tops and Top B-1 horizon. B) Seismic crossline 725. C) Relative Geological Time (RGT) model at inline-84. D) Top B-1 time structure map and GD-1 well location. Observe the Top B-1 reservoir map at the seismic peak, the well is located within structure crest..................58

Figure 3.25: Seismic sections and interpreted horizon of top B-2 time map. 59

Figure 3.26: Seismic sections and interpreted horizon of top B-3 time map. 59

Figure 3.27: Cross section of low frequency model of AI, Vp/Vs and density. 60

Figure 3.28: Well calibration and comparison of measured and inverted elastic logs at GD-1 well location at bandlimited bandwidth (relative domain). 62

Figure 3.29: Well calibration and comparison of measured and inverted elastic logs at GD-1 well location at full bandwidth (absolute domain). The result showed high correlation of inverted and measured logs that give high confidence of inverted properties for interpretation and analysis away from the well location. 63

Figure 3.30: Cross section of seismic and inverted AI and Vp/Vs of bandpass (relative domain) and full bandwidth (absolute domain). Observe continuity of seismic reflectors and layers of inverted bandpass (relative) are similar. The inverted full bandwidth show two dominant contrast of AI and Vp/Vs are consistent with the low frequency trends in the figure 3.27. 64

Figure 3.31: Localized AI – Vp/Vs rock physics template with modeled elastic-rock properties log. The inverted traces points are display in the purple color falls within the high porosity brine sand, clean shale and 20% oil sand. 66

Figure 3.32: Histogram and Crossplot of AI – Vp/Vs color coded by lithology with probability density function (PDF) from GD-1 well data. 67

Figure 3.33: QC plot of actual and predicted lithology based on the established probability density function (PDF) at the GD-1 well location. 68

Figure 3.34: Predicted lithology probability sections and most likely lithology based on the established probability density function. 68

Figure 3.35: Cross plot of AI and porosity total, color-coded by lithology. 69

Figure 3.36: Acoustic Impedance section across GD-1 well (Top). Porosity total section across GD-1 (Bottom). 70

Figure 4.1: Comparison of conceptual (a) and localized (b-f) AI-Vp/Vs rock physics templates. The template for b – f are derived through rock physics modeling from various property perturbation at GD-1 well. 72

Figure 4.2: Synthetic seismic forward model responses for 20% gas and 80% gas. Observed significant amplitude brightening with gas. 73

Figure 4.3: Synthetic seismic response at near, mid and far of *in situ* porosity, +5% and +10%. 74

Figure 4.4: Histogram of relative seismic amplitude differences from synthetic seismic angles stack of all forward model analysis 76

Figure 4.5: Histogram of average amplitude changes from all the synthetic seismic stacks for amplitude sensitivity ranking. 77

Figure 4.6: AVO crossplot summary shown is a composite of modeled synthetic seismic response from various perturbations. 78

Figure 4.7: GD-1 synthetic and seismic gathers calibrations. Shown is the AVO crossplot for top sand for B1, B2 and B3 reservoirs. 80

Figure 4.8: A composite section of input seismic, inverted traces and predicted lithology and porosity. 81

Figure 4.9: B1 sand reservoir characterization analysis. Top left: Seismic section with volume of clay log at GD-1 well, top sand horizons. Top middle: seismic amplitude on the horizon. Top right: Porosity map (PHIT). Bottom left: Sand probability section. Bottom middle: RGB color blend of decomposed frequency map extracted on the horizon. Bottom right: sand probability map extracted on the horizon. 82

Figure 4.10: B2 sand reservoir characterization analysis. Top left: Seismic section with volume of clay log at GD-1 well, top sand horizons. Top middle: seismic amplitude on the horizon. Top right: Porosity map (PHIT). Bottom left: Sand probability section. Bottom middle: RGB color blend of decomposed frequency map extracted on the horizon. Bottom right: sand probability map extracted on the horizon. 83

Figure 4.11: B3 sand reservoir characterization analysis. Top left: Seismic section with volume of clay log at GD-1 well, top sand horizons. Top middle: seismic amplitude on

the horizon. Top right: Porosity map (PHIT). Bottom left: Sand probability section. Bottom middle: RGB color blend of decomposed frequency map extracted on the horizon. Bottom right: sand probability map extracted on the horizon. 84

Figure 5.1: Pore pressure trend line in AI-Vp/Vs RPT 118

Figure 5.2: Synthetic seismic at near, mid and far of *in situ*, clay volume 10% and 20%. 123

Figure 5.3: Synthetic seismic at near, mid and far of *in situ*, clay volume 30% and 40%. 123

Figure 5.4: AVO crossplot at clay volume of 10%, 20%, 30% and 40%. 124

Figure 5.5: Histogram of synthetic seismic amplitude differences (%) at clay volume of 10%, 20%, 30% and 40%. 124

LIST OF TABLES

Table 1.1: Summary of fluid type and contacts extracted from GD-1 Petrophysical Report (Chiew & Zakaria, 2014)....................4

Table 1.2: Well data checklist of all raw data provided in this study. 12

Table 1.3: Site survey seismic data checklist data provided in this study 13

Table 2.1: Elastic Properties Nomenclature. 22

Table 3.1: Elastic parameters of mineral, rock and fluid (Bianco, 2011). 30

Table 3.2: Rock Properties Nomenclature 43

Table 3.3: Velocity-density-porosity-clay relationship established from unconsolidated sand of GD-1 well 47

LIST OF SYMBOLS AND ABBREVIATIONS

For examples:

AI	:	Acoustic Impedance
AST	:	Array Sonic Tool
AVO	:	Amplitude Versus Offset
DHI	:	Direct Hydrocarbon Indicator
MPM	:	Malaysia Petroleum Management
PCSB	:	PETRONAS Carigali Sdn Bhd
QC	:	Quality Check
RPT	:	Rock Physics Template
SG	:	Shallow Gas
SMRE	:	Surface Related Multiple Elimination
WSTT	:	Wave Sonic Cross dipole
XPM	:	Exploration Peninsular Malaysia

LIST OF APPENDICES

Appendix A: Regional study of AI – Vp/Vs, group-I Malay Basin of offshore Peninsular Malaysia; Unpublished poster ………………………………….. 93

Appendix B: Seismic gather conditioning qc plots …………………………. 94

Appendix C: A look into Gasmann‟s equation ……………………………… 102

Appendix D: Rock physics modeling results………………………………… 108

CHAPTER 1: INTRODUCTION

This chapter contains the background of the Shallow Gas (SG) project and seismic reservoir characterization issues at depth less than 1000 mss that motivate this research as a pilot study. The aims and objectives of the pilot study, and the outline of the research approach are also described in this chapter.

1.1 Background and problem definition

Exploration Peninsular Malaysia (XPM) of PETRONAS Carigali Sdn. Bhd and Malaysia Petroleum Management (MPM) have a great interest in finding gas reserves from clastics within shallow intervals in Malay and Penyu Basins. Several fields such as Lawit B2 sand (760 – 1100 mss), Tabu D & E sands (750 mss) and Teluk D & E sands (750 mss) are currently producing gas from shallow reservoirs which has motivated both XPM and MPM to conduct a Shallow Gas (SG) project (Figure 1.1). The SG project is defined by four criteria: 1) area of the study is confined to Malay and Penyu Basin, 2) maximum depth is approximately of 1200m, 3) Formation pressure ranging from 400-1200 psi and 4) Unconsolidated sand.

Through SG project initiative by XPM and MPM, several shallow gas leads and prospects have been identified from hydrocarbon trap style and seismic amplitude anomaly (Figure 1.2). These amplitude anomalies were recognized from bright amplitude of full stack seismic, where a higher chance of success was given to structural trap with supporting amplitude anomaly (Roden et al., 2005 & 2012).

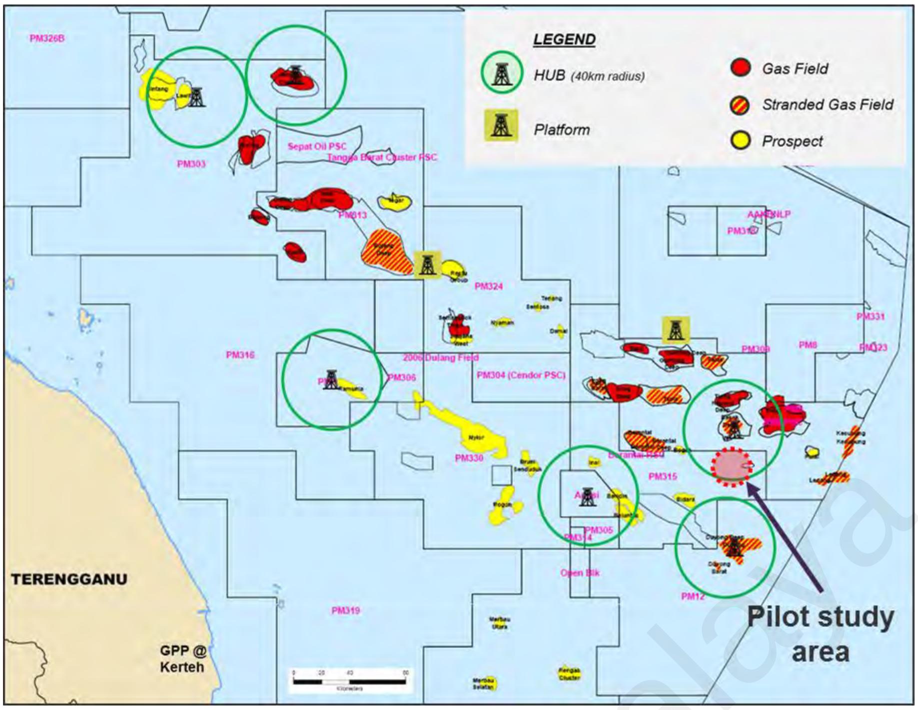

Figure 1.1: Peninsular Malaysia Gas Field and Production Facilities. The pilot study area is surrounded by gas fields and within production facility.

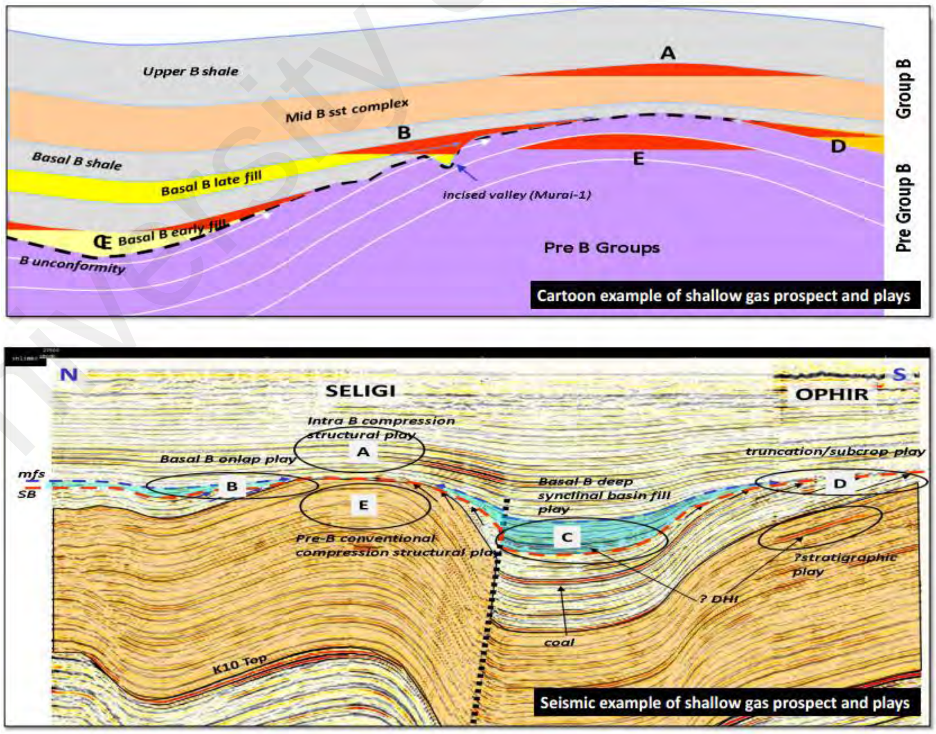

Figure 1.2: Schematic diagram and seismic section of shallow gas prospect and plays identified during Shallow Gas Project.

Qualitatively, high confidence of hydrocarbon prediction is obtained when the seismic amplitude anomalies satisfies one or all the following criteria: 1) down-dip fit to structure (at least locally); 2) flat spot with correct polarity (hard kick); 3) amplitude shutoff; (4) phase change at contact; (5) frequency drop below gas reservoirs; and (6) pock marks and gas wipe-out (Ghosh et al., 2010; Brown, 2003). However, these anomalies were also found at low saturation gas (biogenic gas), silty gas sand, high porosity brine sand and overpressure sand. Figure 1.3 shows an example of excellent amplitude anomalies that satisfied more than one criteria for hydrocarbon prediction (Suhairi & Jalil, 2014). Although the amplitude anomalies indicate the presence of hydrocarbon, the well result at the predicted reservoir turned out as water bearing Table 1.1. This non-uniqueness in the interpretation of the seismic amplitude anomaly is the major challenge for this SG project.

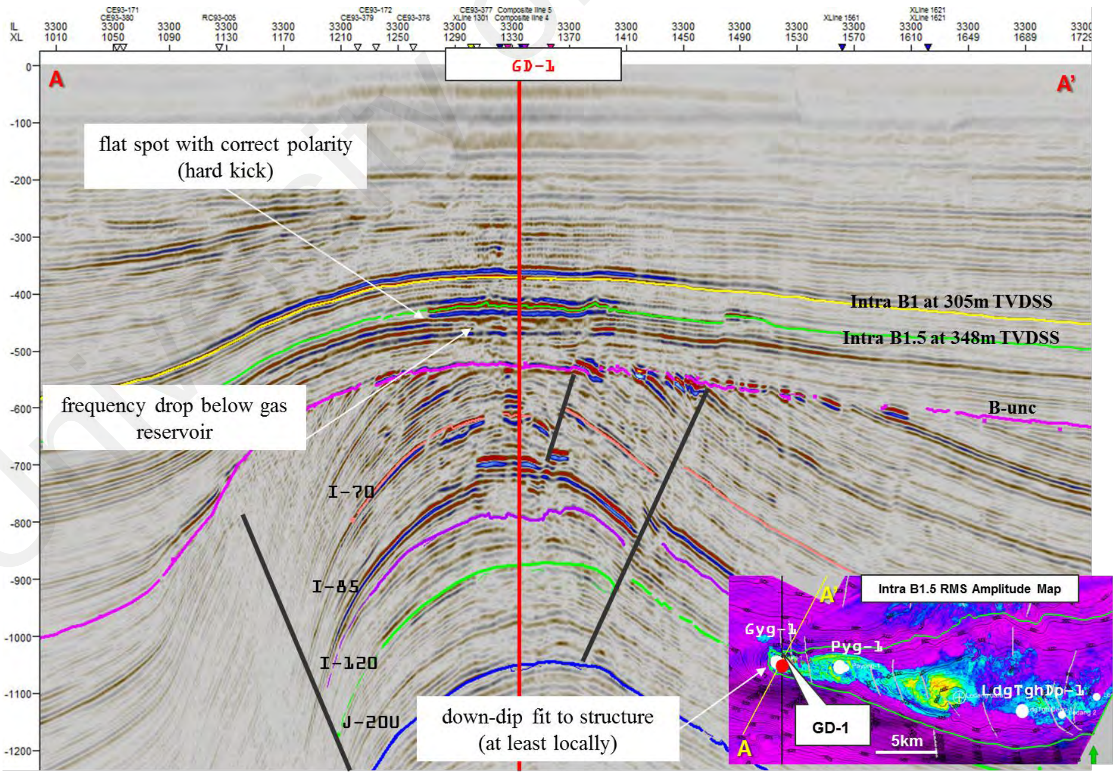

Figure 1.3: Seismic section across well GD-1 and RMS amplitude map extracted from Intra B1.5 horizon. The seismic section and intra B1.5 RMS amplitude map shows at least three criteria that give high confidence of hydrocarbon presence (After Suhairi & Jalil , 2014).

Table 1.1: Summary of fluid type and contacts extracted from GD-1 Petrophysical Report (Chiew & Zakaria, 2014).

Zone	Depth (m MDDF)	Interpretation Sources	H2S/C02 presence	Fluid Type
Intra B-1	329 - 348	• No Density Neuron crossover • Low resistivity • Pressure data not available due to tight & lost seal	None	Water
Intra B-1.5	390 - 400	• No Density Neutron crossover • Low resistivity	None	Water

Typically, quantitative analysis of seismic reservoir characteristic through Amplitude Versus Offset (AVO) and Seismic Inversion study will be carried out to determine the reservoir properties and fluid type (Avseth et al., 2010; Simm & Bacon, 2014). However at shallow depth, we often face challenges such as: 1) lack of near offset trace in seismic data, and 2) lack of complete elastic log suite (density, P & S sonic) or poor data quality which make the AVO and Seismic Inversion studies not feasible (Onajite, 2017).

1.2 Data issues and research motivation

This subchapter describes the two main data issues of seismic reservoir characterization in shallow clastics that motivated this feasibility research study.

1.2.1 Seismic data challenges

Conventional marine seismic tool is typically designed to acquire signal from deep reflector (estimated more than 1000 mss) with long offset distance between the seismic source and first seismic receiver. As a result, the recorded seismic at the shallow depth is lacking in useful near offset trace which is dominated by higher noise in near angle stack as seen in Figure 1.4.

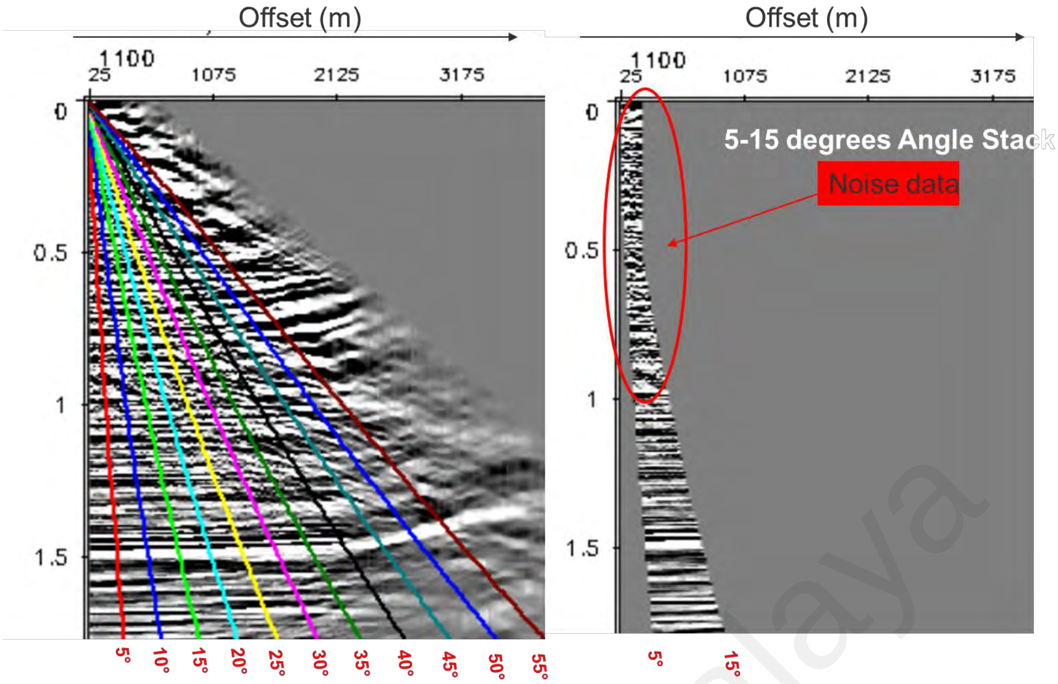

Figure 1.4: Surface seismic CDP offset showing lack of seismic signal at near angle stack from conventional seismic acquisition and processing.

A possible solution to this seismic data issue comes from site survey data. Site survey acquisition design has often shorter length of short-receiver separation thus enabling to record the near offset traces (Roger, 2001).

In March 2014, the high density site survey data at 12.5m of shot and 12.5 m of group interval was acquired at GD area for the use of 1) shallow hazard analysis, and 2) to support this pilot study. AVO analysis was then carried out by Teknik Lengkap contractor on two (2) 2D test lines (Nur, 2014). Seismic angle stack section QC plot (Figure 1.5) showed the high density site survey acquisition data have successfully recorded signal from near offset traces. AVO anomaly was observed at shallow clastics within the B group. However, during that study, there was no well within the site survey area, hence the AVO calibration to well reservoir properties was not possible.

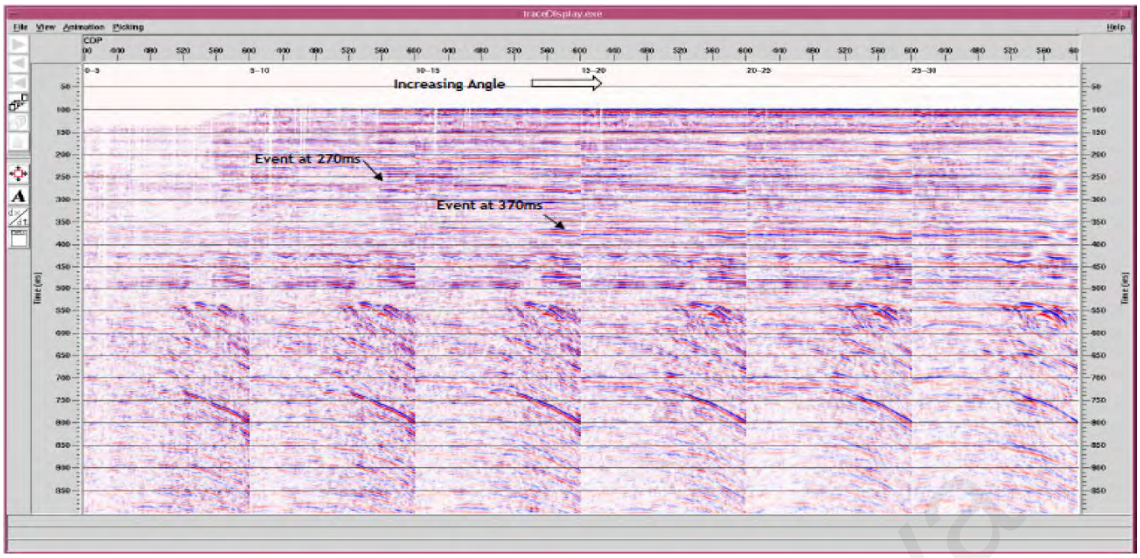

Figure 1.5: Angle stack seismic section from site survey data shows strong amplitude events at 270ms and 370ms (Nur, 2014).

Following a discussion with PCSB‟s Quantitative Geophysics technical expert, Mr. Martin Brewer on the two test lines, it was found out that the processed site survey data is not optimum for AVO analysis since Surface Related Multiple Elimination (SRME) processing (Naidu et al., 2013) were not done. Without this processing, the seismic data is contaminated by multiple reflections which can produce false AVO response. Thus, seismic reprocessing was recommended with complete processing sequence and amplitude preservation for AVO and Inversion studies.

The GD site survey data was initially reprocessed by Mr. Mohd Azizul for his Master degree research project with objectives 1) to find the optimum processing sequence for AVO/Inversion study and 2) to convert the 2D high density site survey data into 3D volume (Yahya, 2015). However, to further improve the seismic imaging, the site survey data was then reprocessed by PETRONAS Processing Group with support from Azizul. The reprocessing was completed and delivered to PCSB in October 2016 (Khan & Zohdi, 2016). The reprocessed site survey seismic data enable one to the test usability of the data for AVO and Seismic Inversion studies.

1.2.2 Well data challenges

Another challenge for shallow clastics study is the typically incomplete elastic log suite (density, compressional & shear sonic) or poor data quality. Low exploration interest at shallow depth caused lack of interest to acquire sonic data in this interval. In the past, sonic velocity logging tool mostly recorded velocity of mud, instead of velocity of the unconsolidated rock.

In the last few years, Halliburton Company designed sonic tools to record a reliable compressional and shear sonic logs from an unconsolidated and consolidated sediment named Array Sonic Tool (AST) and Wave Sonic Cross dipole (WSTT) (Morris et al., 1984; Sun et al., 2016).

In September 2014, XPM drilled a well named GD-1 within the high resolution site survey area. Two sonic logging tools were used to cater specific requirement. 1) AST logging tool was run at depth interval of 380 - 680 m for unconsolidated sediment and 2) Conventional dipole sonic WSTT logging tool was run at depth interval of 680 m to well TD for consolidated sediment. Figure 1.6 below showing the coverage of elastic logs (density, p-sonic and s-sonic) within the shallow clastics interval. A gap of elastic logs and interpreted logs between 380 m to 680m of logs are due to poor data.

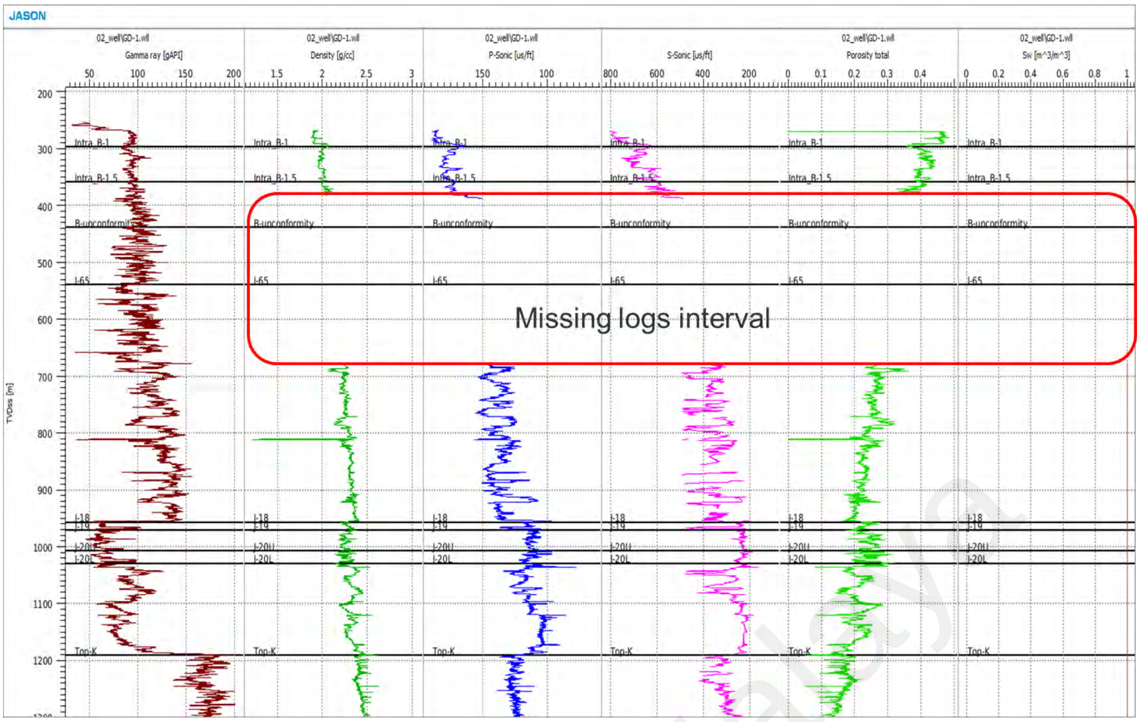

Figure 1.6: GD-1 composite well log. The composite log is showing the availability of GR, Density, Compressional and Shear sonics, within the B-group of shallow clastics interval. The red box higlighted the missing interval.

GD-1 well encountered water-bearing reservoir, hence calibration of hydrocarbon elastic properties for unconsolidated reservoir was not available. Due to this reason, rock and elastic logs from DS-1 well located 54 km to the south west of GD-1 were used as another reference for interpretation and analysis of inversion result. Figure 1.7 showed a well correlation and elastic log coverage between the two wells. DS-1 is structurally deeper than GD-1. Since both wells acquired elastic logs using the same AST tool, a reliable cross plot analysis can be made.

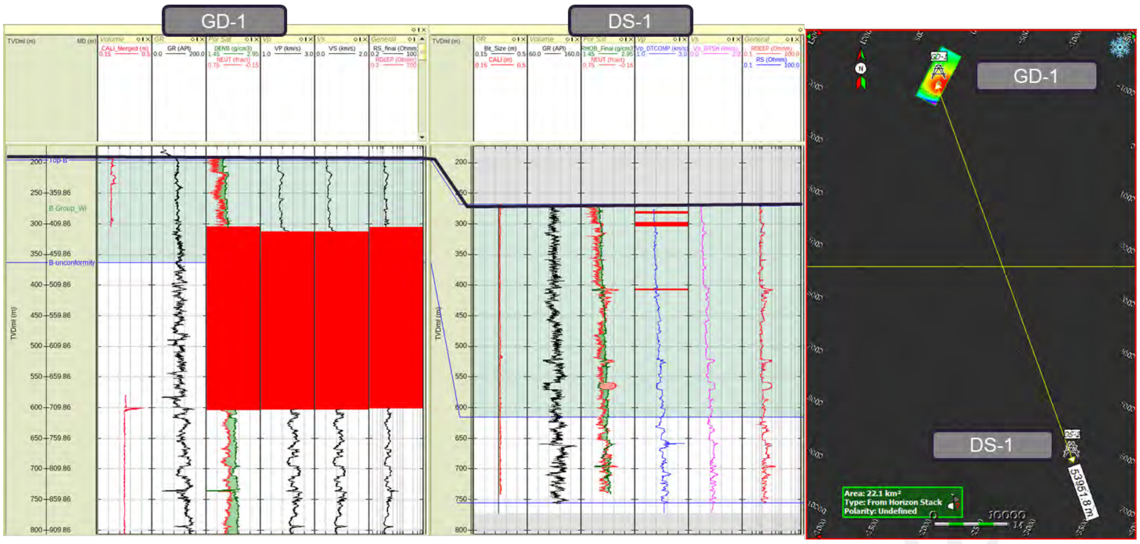

Figure 1.7: Well correlation between GD-1 and DS-1. Both wells acquired complete elastic logs at B group interval using the same AST tool, enabling reliable elastic logs comparison. The low water saturation log within the B group at DS-1 give a good calibration reservoir-fluid and elastic logs.

The elastic properties of Acoustic Impedance (AI) and Vp/Vs calculated from the input density, p-sonic and s-sonic logs were then compared between GD-1 and DS-1 well. Well feasibility study was carried out in 2014 using the two wells. Histogram in Figure 1.8 (a) shows GD-1 has lower AI and higher Vp/Vs as compared to DS-1. The crossplot of AI-Vp/Vs color coded depth on Figure 1.8 (b) showed both wells are having in the same depth trend. The crossplot confirmed the reliability for elastic-rock/fluid properties calibration between these two wells. The well feasibility study result support the quest to deepen the understanding of the elastic property response to the changes of reservoir, fluid and pressure in the unconsolidated sediment.

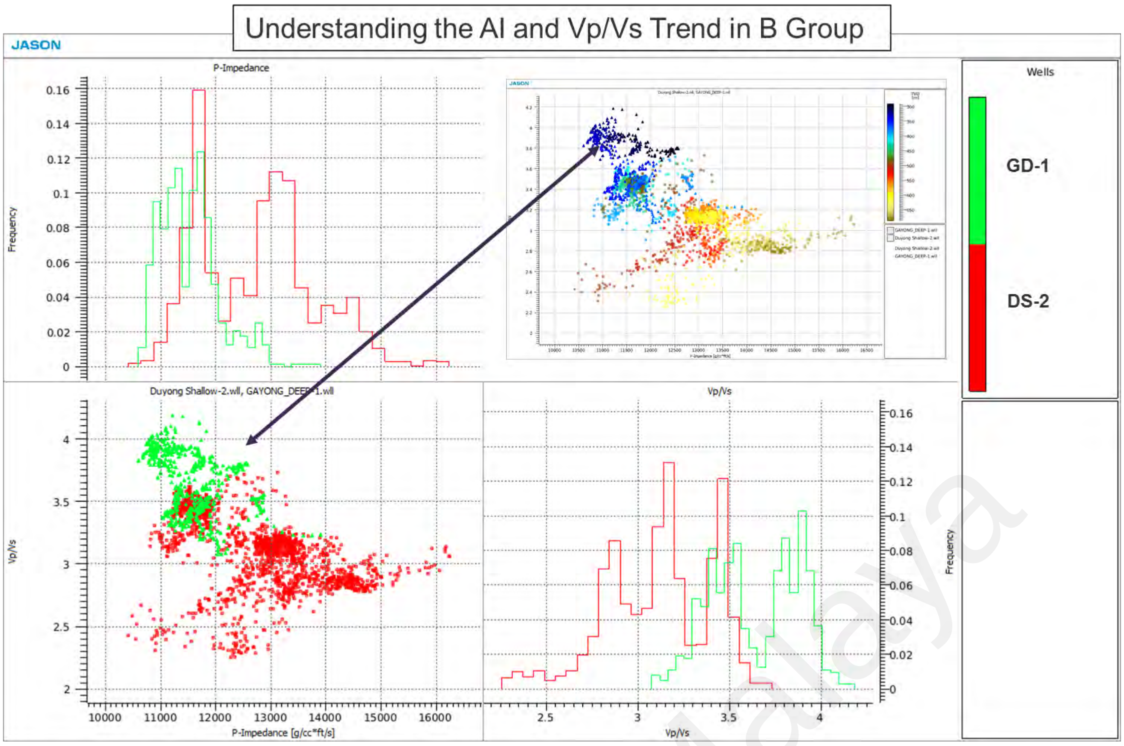

Figure 1.8: a) AI-Vp/Vs crossplot and histogram color coded by wells. The green points are from GD-1 well has lower AI and higher Vp/Vs as compared to DS-2. b) top right cross plot of AI-Vp/Vs color coded by depth (TVDss). The cold color shows elastic properties of AI and Vp/Vs log data from GD-1 well while the hot color are from DS-1. This cross plot shows normal depth compaction trend.

1.3 Aims and objective of the study

The aim of this dissertation research is to conduct a feasibility study for shallow gas detection using unconventional data input of: 1) new acoustic logging tool (AST) for unconsolidated sediment and 2) pseudo3D seismic data from 2D high resolution site survey acquisition. This feasibility study served as pilot project of seismic reservoir characterization using site survey data for shallow clastics in Malay Basin, offshore Peninsular Malaysia. This study interest is from late Upper Miocene to Upper Pliocene of the B stratigraphic group.

The main objectives of this study are to:

I. Ascertain whether the use of unconventional sonic logs and the pseudo3D site survey data are feasible for AVO and Inversion study in shallow clastics interval.
II. Understand the relationship of different rock type, porosity, water saturation and pressure to elastic properties through rock physics modeling and seismic forward model.
III. Predict the lithology and porosity, and if possible water saturation and reservoir pressure through forward modelling and inverted site survey seismic data.

Technically, the success of this pilot study will increase confidence for future drilling of shallow gas prospects and enable provision of an optimum well location from site survey data.

From business perspective, this pilot study will enable exploration of more potential shallow gas for hydrocarbon resource addition and maximizing the value of the investment in site survey data.

1.4 Data sources

Data for this study is provided by PETRONAS CariGali Sdn. Bhd. (PCSB). Due to confidentiality of the data, different names were used for well and site survey. Two well data were made available, GD-1 and DS-1. Both wells have all the elastic logs within the unconsolidated sediment section. The available input well data are listed in Table 1.2. The input seismic data are from 9 sq. km of GD-1 site survey seismic data. 2D and Pseudo3D seismic data were made available as listed in the Table 1.3. In this study, only the reprocessed Pseudo3D data were used. Figure 1.9 shows a basemap of study area and seismic section across GD-1. The basemap shows the high resolution 2D data coverage, the Pseudo3D seismic data coverage and GD-1 well location. The seismic section shows the vertical zone of study interest.

Table 1.2: Well data checklist of all raw data provided in this study.

Well Data	GD-1	DS-1
Caliper (Cali)	Y	Y
Gamma Ray (GR)	Y	Y
Spectral Gamma Ray (CGR)	X	X
Micro-Resistivity (MSFL)	Y	Y
Shallow-Resistivity (Rs)	Y	Y
Medium-Resistivity (Rm)	Y	Y
Deep Resistivity (Rd)	Y	Y
Compressional-wave Travel Time (DTC)	Y	Y
Shear-Wave Travel Time (DTS)	Y	Y
Density (RHOB)	Y	Y
Neutron Porosity (NPHI)	Y	Y
Spontaneous Potential (SP)	X	X
Photoelectric Factor (PEF)	Y	Y
Well Location	Y	Y
Well Deviation	N	N
Well Top	Y	Y
Checkshot	Y	Y
Pressure Data	Y	Y
Cutting Description	Y	Y
Core Data	X	X
Core Description	X	X

Table 1.3: Site survey seismic data checklist data provided in this study

Processed Seismic Data	2D	Pseudo3D
Seismic Gather		
25 m line spacing	N	Y
50 m line spacing	N	Y
100 m line spacing	N	Y
25m line spacing - gather flattening	N	Y
Full stack		
Raw	Y	Y
Scaled	Y	Y
Angle stacks (25 m line spacing)		
05 - 10 deg	N	Y
10 - 15 deg	N	Y
15 - 20 deg	N	Y
20 - 25deg	N	Y
25 - 30 deg	N	Y
30 - 35 deg	N	Y
35 - 40 deg	N	Y
Seismic velocity (stacking)	N	Y

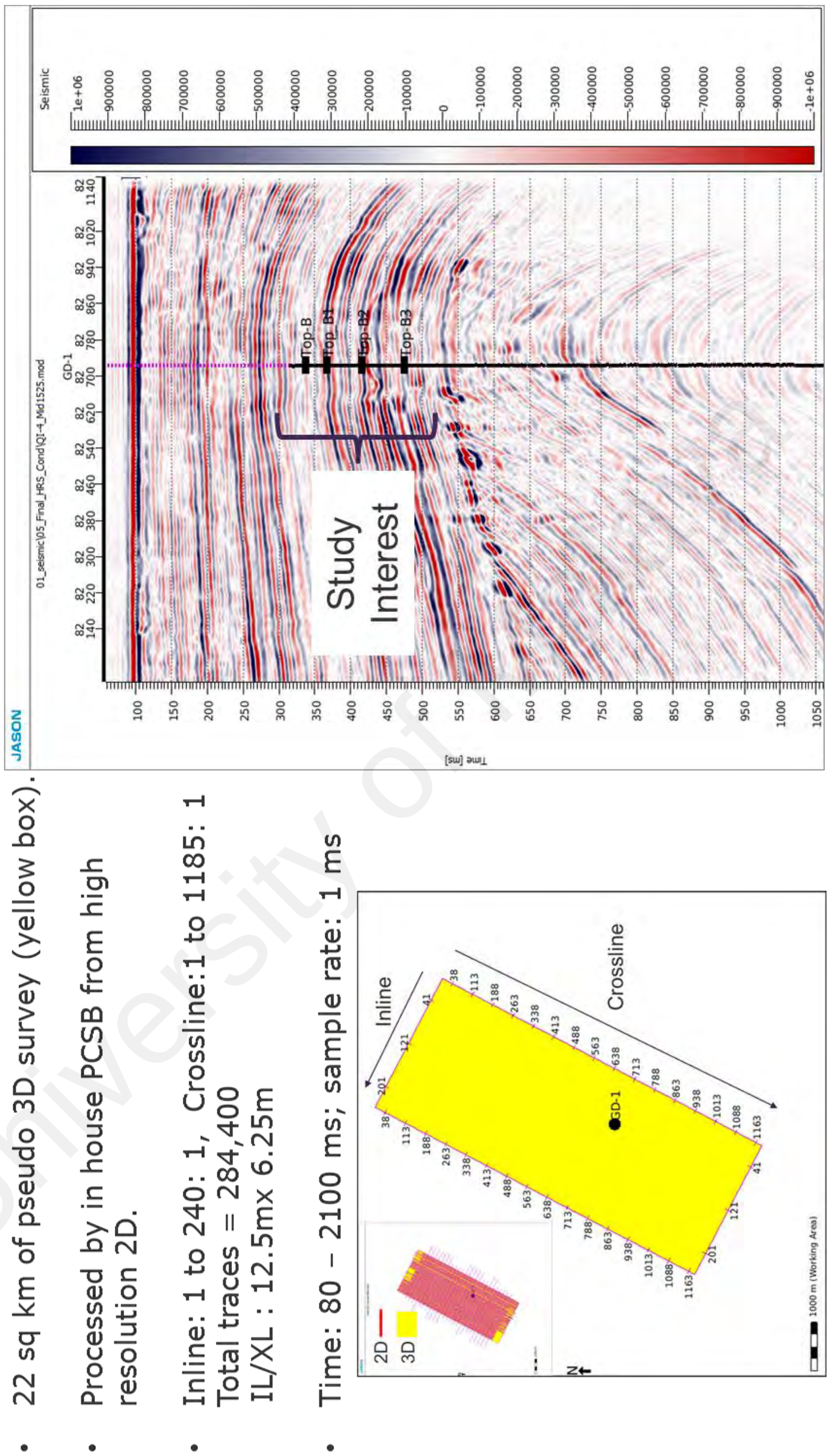

Figure 1.9: Study area basemap and seismic section showing vertical zone of interest.

1.5 Outline of the research approach

This research was designed based on the process flow to meet the research objectives as shown in the Figure 1.10. There are five (5) chapters with each chapter containing several sub-chapters that relate to the subsequent chapter.

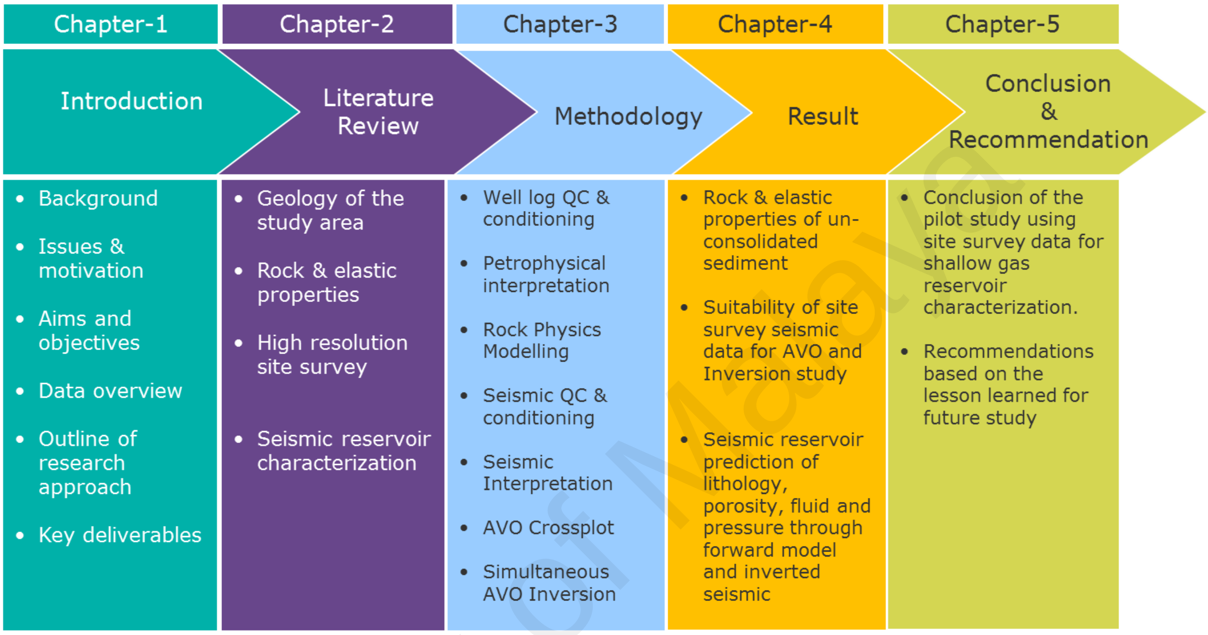

Figure 1.10: Research process flow and contents.

1.6 Key deliverables

At the end of the study, candidate is expected to deliver final product to PETRONAS and University Malaya as listed below.

a. PETRONAS

Final log data in las format Inversion product volumes in SEGY format and final power point presentation. Thesis in softcopy and hard copy.

b. University Malaya

Thesis in softcopy and hard copy.

CHAPTER 2: LITERITURE REVIEW

This chapter summaries previous literature and studies relevant to this research.

2.1 Geologic setting and stratigraphy of study area

The pilot study area is located in the south of Malay Basin, offshore Peninsular Malaysia. The area is surrounded by Ophir oil field and Ledang gas field as shown in Figure 2.1. Several major tectonic event control the structure of the study area. During Lower Oligocene, extensional tectonic activity resulted in formation of grabens, half grabens and depressions creating depo-centers in which Group Pre-M, M, L and K sediments were deposited. Extensional faulting ceased in the Upper Oligocene, generally synchronous with the upper part of the Group K. Thereafter from early Lower Miocene to late Middle Miocene, thermal/tectonic subsidence was the dominant activity, which Groups J to D were deposited. During late Lower Miocene to mid Middle Miocene (Late Group H to F time), compressional deformation set in. This period saw local inversion of pre-existing half grabens and major uplift of the SE part of the Malay Basin. This uplift led to the basin wide B-unconformity of middle Upper Miocene age. From late Upper Miocene to Quaternary gentle subsidence without significant tectonic activity along with marine flooding has been the dominant tectono-stratigraphic event (Tjia, 1994 &1999; Tan, 2009; Mansor et al., 2014).

Figure 2.1: GD-1 site survey area is surrounded by oil and gas field (Tan, 2009).

Stratigraphic interest for shallow gas pilot study is from late Upper Miocene to Upper Pliocene in the B group as shown in Figure 2.2. The chart shows that during this age, the B group sediment is dominated by coastal plain and offshore shale with some thin beds of marine & delta front sand deposited during slow subsidence (Madon, 1999). This group is characterized by seismic facies with parallel configuration, high amplitude and high frequency (Sulaiman, Hamzah & Samsudin, 2016). GD-1 well result shows the presence of shallow marine sediment dominated by marine mud and silts (Dzhafri et al., 2014).

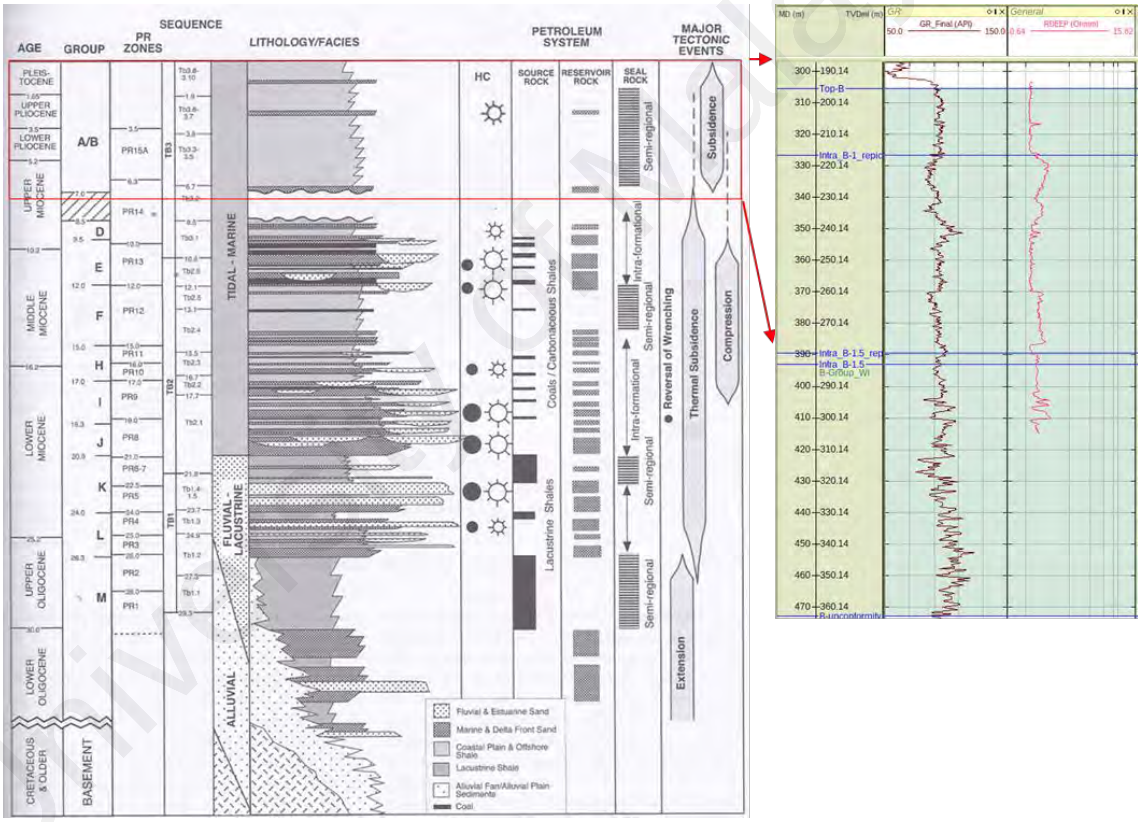

Figure 2.2: Distribution of source, reservoir and seal rock in the Malay Basin (Tan, 2009).

2.2 Rock and elastic properties of unconsolidated rocks

The B group sediment of the study area is dominated by marine mud and silts at depth less than 700m; where the sediment is expected to be unconsolidated (Sulaiman et al., 2016; Dzhafri et al., 2014). The rock and elastics properties of unconsolidated and consolidated sediments are different as the rock physics properties change with the 1) depositional environment and 2) burial depth (Avseth, 2010). Changes of rock and elastics properties with depth is the commonly understood as shown in the schematic section in Figure 2.3.

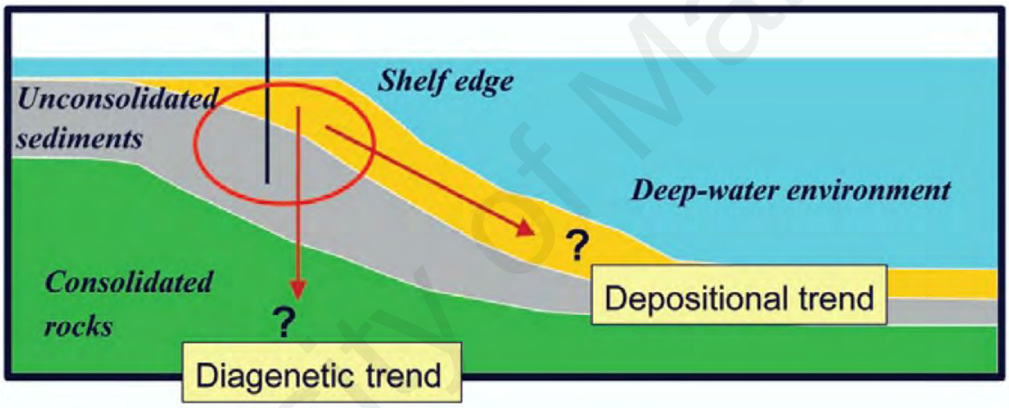

Figure 2.3: Rock physics properties change with depositional environment and burial depth. These geologic trends must be taken into account during hydrocarbon reconnaissance of seismic data (Avseth, Mukerji, & Mavko, 2010).

The elastic properties of velocities and densities of siliciclastic sedimentary rocks increase with depth due to compaction and porosity reduction as shown in schematic porosity-depth section in Figure 2.4 by Avseth, Fleshe, and Wijngaaeden (2003). During deposition, the pure shale has higher porosity as compare to sand. Sediment is still unconsolidated and loose; the sand-to-sand grain contact is very minimal. After a certain depth of burial, the sediment is more compacted due to overburden stress where the mineral grains start to align. Shale platy mineral is more compacted and lost the porosity at much higher rate, while the sand grain start to pack or crushing but still have inter-grain porosity making the porosity of sand is relatively higher than shale. At deeper depth, the high overburden stress induced diagenesis process in the shale and the sand. Greater changes are seen in sand as the diagenesis cause the pore space to be filled with cement. This makes the sand to have lower porosity than shale.

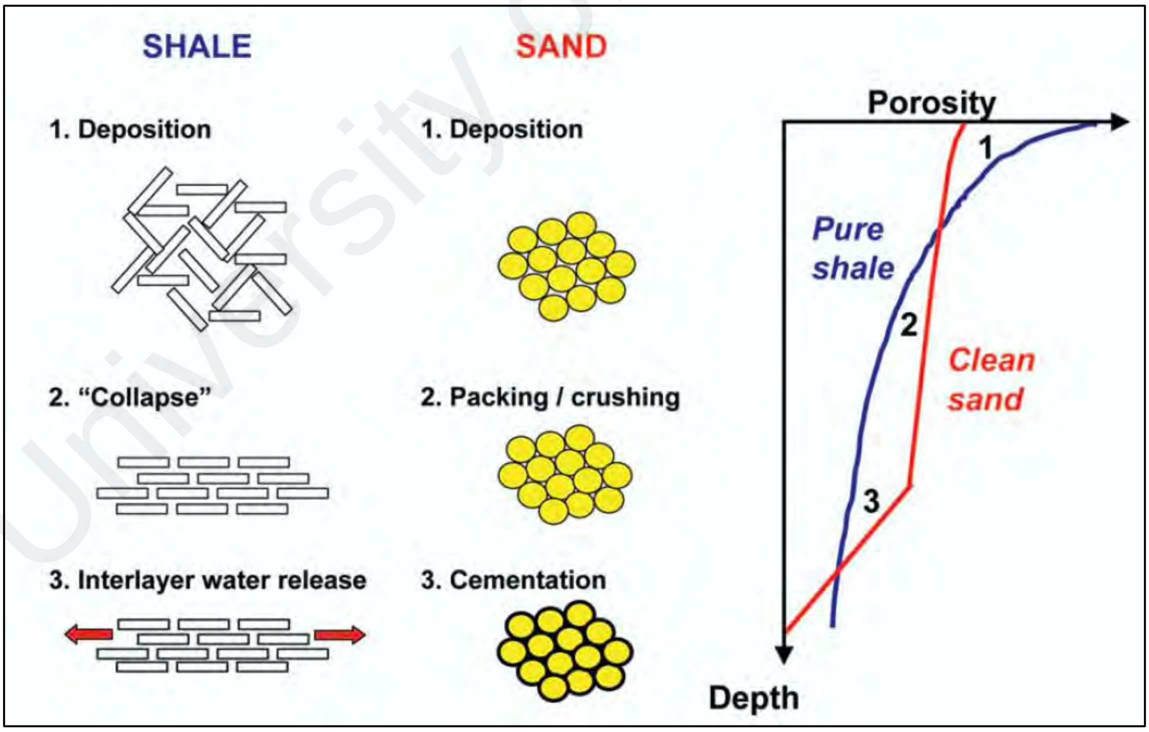

Figure 2.4: Schematic illustration of porosity-depth trends for sands and shales. (Avseth, Fleshe & Wijngaaeden, 2003).

Changes of elastic properties due to depositional trend require further insight in understanding, as the rock properties varies with environment of deposition (Paul & Bruno, 2013). Changes in depositional trend has significant changes of elastic properties that are controlled by lithology, mineral composition, texture, pore fluids, temperature and pressure gradient (Gardner et al., 1974; Eastwood & Castagna, 1983; Castagna, Batzle, & Eastwood., 1985; Miller & Steward, 1990; Avseth et al., 2003 & 2010; Bjorlykke, 2014).

To date, there is no rock and elastic properties relationship that has been done for group-B of the Malay Basin which is motivation for this research.

2.2.1 Empirical rock physics relationships

In the study of rock and elastic properties of the unconsolidated rock, a rock physics diagnostic is a must in order to understand the local variation (Avseth, 2000 & 2010; Hossain & MacGregor, 2014; Wollner, Yang, & Dvorkin, 2017). The rock physics diagnostic uses cross-plots between the rock and its elastics properties relationships. In this study, empirical model approach is more practical to validate input log data quality and for generating synthetics elastic logs by calibrating the input data to the known rock-elastic relationship. Below is a list of various rock-elastic properties relationships available in the literature.

- Velocity - density (Gardner et al., 1974; Castagna et al., 1985)
- Velocity - porosity (Wyllie et al., 1956; Geertsma & Smith, 1961; Gardner et al., 1974; Raymer et al., 1980; Tosaya, 1982; Han, 1986; Nur, 1992, Nur et al.,1998).
- Velocity – porosity - clay (Tosaya, 1982; Castagna, 1985; Han, 1986; Nur 1992, Nur et al., 1998).

2.2.2 Rock physics template (RPT)

There are many types of rock physics template (RPT). Vp/Vs vs. P-Impedance cross plot are now widely used to understand the changes of lithology, mineralogy, burial depth, diagenesis, pressure and temperature since this was introduced by Avseth & Wijngaaeden in 2003. Conceptual trend for siliciclastics lithologies at constant pressure in Figure 2.5 give an overview of AI and Vp/Vs trend with increase of shaliness (Vclay), cement volume, porosity, pore pressure and gas saturation for siliciclastic rock (Odegaard & Avseth, 2004). The trend has to be calibrated to the local geology prior to interpretation and analysis (Odegaard & Avseth, 2004; Avseth, 2010; Simm & Bacon, 2014). Within Malay Basin, this RPT is commonly used to predict lithology and fluid at prospect and field scales (Mohamed & Danial, 2013; Lubis et al., 2016). To some extent, the template has been used for regional study. For example, the RPT was used to understand the lateral variation of elastic and rock properties within the stratigraphic Group-I in the Malay Basin (Ralim & Mohamed, 2015), The result has helped seismic interpreters to better understand amplitude variation with contrast from sub-basin to another as shown in Appendix-A.

Although there are many calibration of RPT for Malay Basin, to date, none of the existing studies include shallow clastic interval of depth less than 700 m.

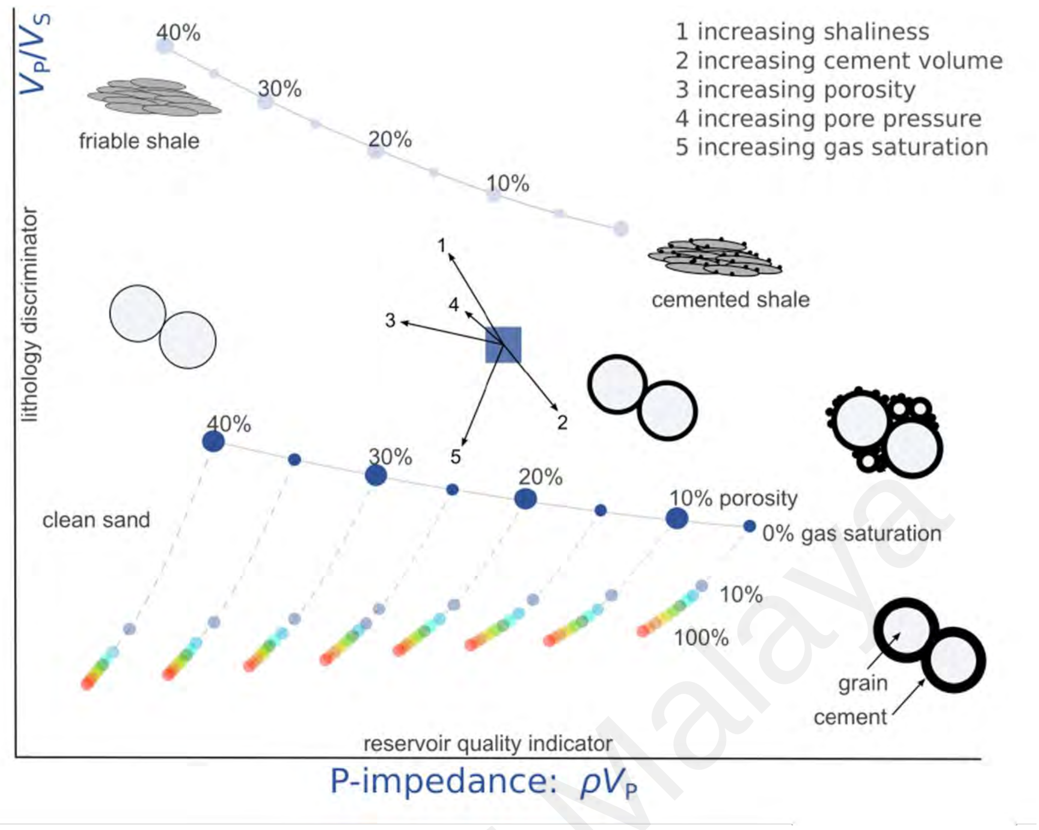

Figure 2.5: Conceptual trends for siliciclastic lithologies at constant confining pressures (Odegaard et al., 2004).

2.3 High resolution site survey seismic

Digital seismic acquisition for high resolution site survey data is defined as 2D site survey acquisition with trace interval of 12.5m (Roger, 2001). This data is not only used for shallow gas (bright spot) analysis, but also for shallow strata delineation up to 2 to 3 seconds beneath the seabed. However, the effectiveness of the site survey data depends on number of factors such as the seismic pulse penetration, vertical and horizontal accuracy. Study example by Versteeg, Verschuren, Henriet and Batist (1992) concludes that the selection of pseudo3D 3D bin size is dependent on the complexity of the subsurface structural features to give a good 3D subsurface image.

2D versus Pseudo3D seismic data processing in the AVO Analysis was carried out by Panea, Rayner, Schultz and Manea (2013). The study result concludes: 1) reflected waves are clearer on Common Depth Point (CDP), Common Reference Survey (CRS) and PSTM gathers processed using pseudo-3D geometry and, 2) reflections in target intervals can be seen on larger offset intervals on the gathers processed using pseudo-3D geometry (Figure 2.6). The result has served to motivate the geoscience community to produce 3D pseudo seismic from the site survey data and testing the AVO response at different shot point spacing (Khan & Zohdi, 2016).

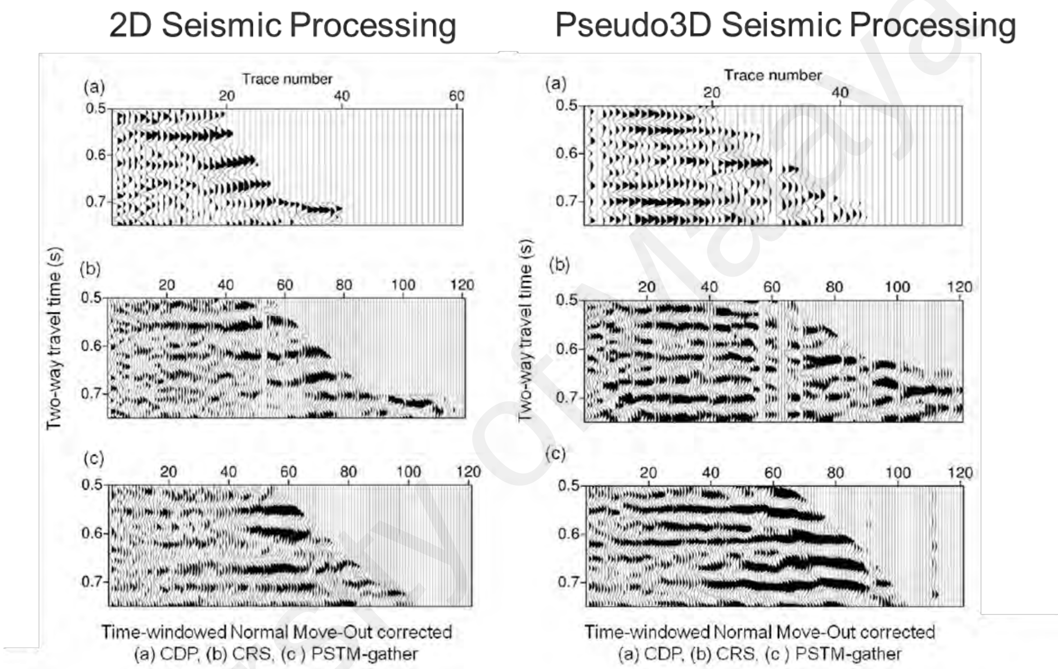

Figure 2.6: Seismic gather comparison from 2D processing and pseudo3D processing (Panea et al., 2013)

There is great interest in using site survey seismic data for rock properties prediction in the shallow clastic (Vardy, 2015) where the research effort also focus on the development of seismic inversion algorithm (Vardy et al., 2015 & 2016).

2.4 Seismic reservoir characterization

The seismic reservoir characterization objective is to predict subsurface reservoir properties such as lithology, fluid, porosity, saturation, net-to-gross and reservoir fairway from seismic data (Ostrander, 1984; Castagna & Backus., 1993; Hilterman, 2001; Abhinav, 2012). The prediction from seismic sometimes cover the prediction of permeability from a relationship with porosity (Adekanle & Enikanselu, 2013) or facies (Simm & Bacon., 2014) and pore pressure (Hawkins et al., 2004; Banik et al., 2013). AVO and Inversion are well known technologies that have widely been applied for quantitative interpretation of reservoir (Avseth, 2000; Ross, 2000). The derived elastic properties were then linked to rock properties through rock physics relationship as stated in Section 2.2. However, most of the inversion study carried on conventional seismic and logs are focused on consolidated rocks (Cheng et al., 2008; Mohamed & Danial, 2013; Mohamed et al., 2015; Yoong et al., 2016;Lubis et al., 2016).

Seismic inversion using site survey data for reservoir characterization has less coverage and limited case study examples presented. Although the interest of using site survey data for seismic reservoir characterization started more than 20 years (Roger, 2001), the interest turned into practical applications in the recent years (Vardy, 2015 & 2016). The latest seismic inversion project using high density site survey data are able to predict soil properties at higher resolution (Vardy, Vanneste, Henstock, Morgan, & Pinson, 2015) as shown in Figure 2.7 below. To date, this project research is the first case study in Malay Basin of using site survey seismic data for reservoir characterization.

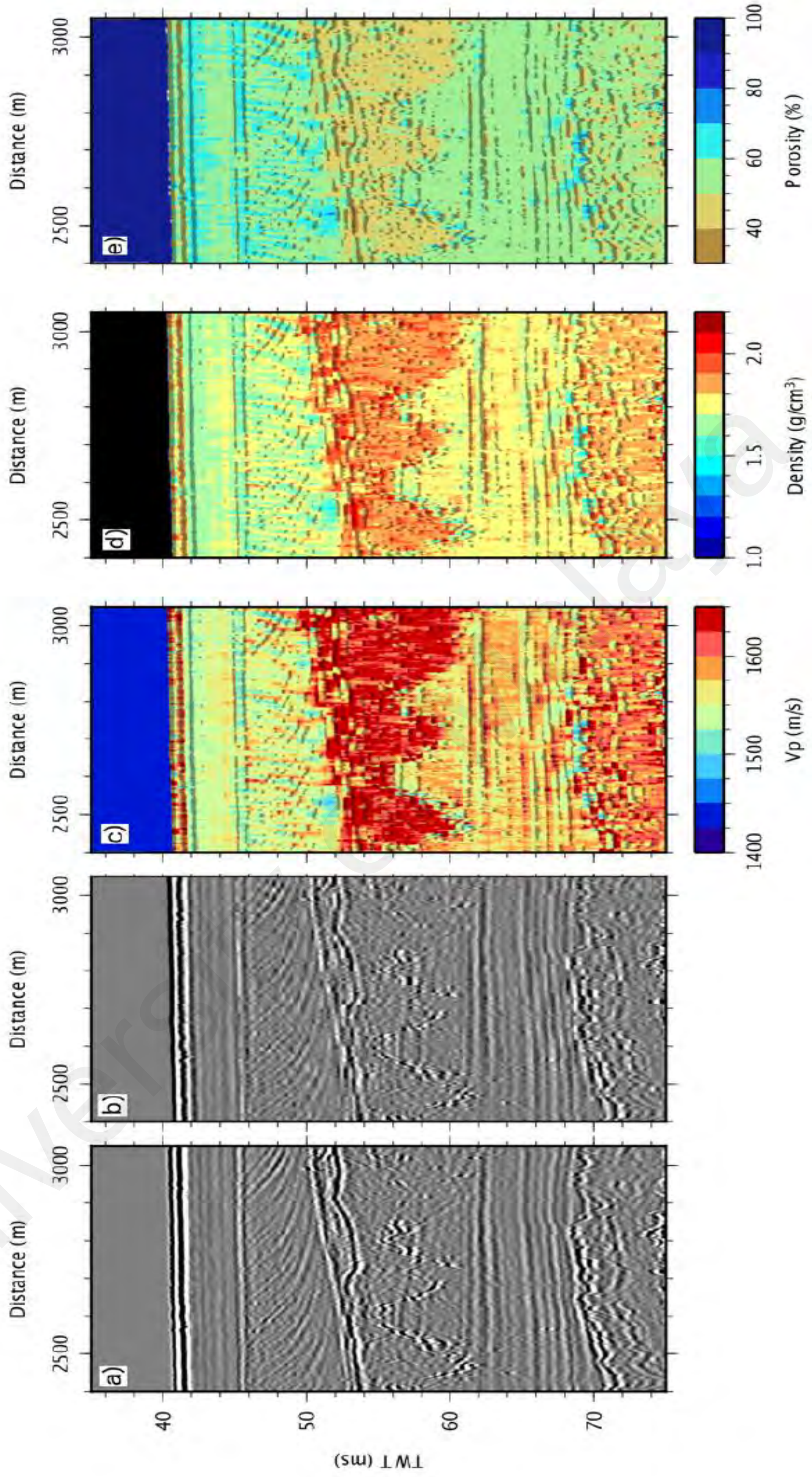

Figure 2.7: Seismic inversion to porosity prediction from site survey data (Vardy et al., 2015). Panel (a) shows the subset of a single channel boomer profile, (b) the synthetic seismic profile generated by the inversion, and (c) through (e) the P-wave velocity, density, and porosity profiles estimated from the impedance using empirically derived relationships.

CHAPTER 3: METHODOLOGY

This chapter describes and explains the research methodology used in the study. The sub-topics for this chapter include the key research questions, the research design, and the research procedures adopted.

3.1 Well log QC & conditioning

Well data is one of the critical input in seismic reservoir characterization analysis. An iterative workflow of log conditioning, petrophysical interpretation, rock physics modelling and synthetics-to-seismic matching is applied to ensure the sonic and density logs represent the true *in situ* properties of the rock (Sidi et al., 2007). Thus, well log QC prior to a detailed study is important.

3.1.1 Well log QC

The main objective of the well log data QC is to determine the different logging tools, environmental effects, missing sections, borehole rugosity and misaligned data in depth. The integrating of input logs data were assessed through the following QC plots.

a. Well log QC plot (Figure 3.1). The caliper logs showed borehole size in the B-group. GD-1 well was drilled using 8 ½" (22 cm) bit size and DS-2 well was drilled using 12 ¼" (32 cm) bit size. All the important logs for this study are available and the logs value are within the plausible data ranges, where the specified units are consistent with the values in Table 3.1. The caliper log provides information on the borehole rugosity and environmental effects where both wells showed good borehole conditioned. Note the gap in the log highlighted in red as missing section. Misaligned data was not observed as all the logged responses are depth consistent.

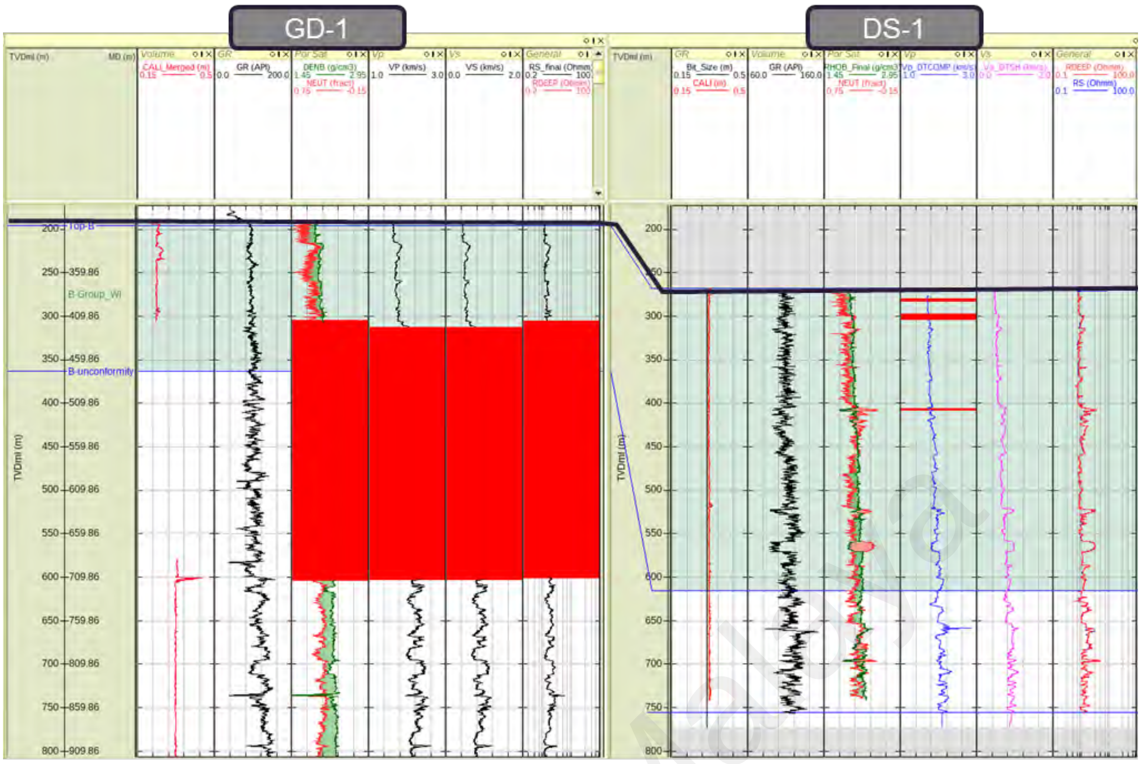

Figure 3.1: Well log QC plot. In GD-1, caliper logs show two different logging run. Gamma ray log showed full coverage but the several logs are missing and highlighted in red.

Table 3.1: Elastic parameters of mineral, rock and fluid (Bianco, 2011).

Elastic parameters		E Young's modulus [$kg \cdot m^{-1}s^{-2}$]	ν Poisson's ratio [dimensionless] aka σ	K bulk modulus [$kg \cdot m^{-1}s^{-2}$] aka volumetric modulus	μ shear modulus [$kg \cdot m^{-1}s^{-2}$] aka rigidity, G	λ 1st Lamé parameter [$kg \cdot m^{-1}s^{-2}$] aka incompressibility	V_P P-wave velocity [m/s] aka compressional vel	V_s S-wave velocity [m/s] aka shear velocity	Γ $V_P:V_S$ ratio [dimensionless]
	Density [kg/m^3]	[GPa]	[dimensionless]	[GPa]	[GPa]	[GPa]	[m/s]	[m/s]	[dimensionless]
Quartz	2650	95	0.07	37	44	8	6008	4075	1.47
Feldspar (mean)	2620	40	0.32	37.5	15	28	4685	2393	1.96
Plagioclase	2630	70	0.35	76	26	59	6487	3144	2.06
Calcite	2710	84	0.32	77	32	56	6645	3436	1.93
Dolomite	2870	117	0.30	95	45	65	7349	3960	1.86
Anhydrite	2980	72	0.23	45	29	26	5299	3120	1.70
Siderite	3960	135	0.32	124	51	90	6963	3589	1.94
Pyrite	4930	305	0.15	147	132	59	8094	5174	1.56
Sandstone, 10 p.u.	2500	32-105	~0.05-0.10	15-18	7-24	1-3	2500-4500	1725-3103	~1.45-1.5
Limestone, 10 p.u.	2540	97-280	~0.33	37-71	9-26	18-53	3800-6500	1900-3250	~2.0
Shale, 5 p.u.	2500	20-160	~0.27	16-36	2-19	3-24	1800-5000	1000-2777	~1.8
Water (brine)	1030	0	0.5	2.3	0	2.3	1507	0	undefined
Oil (40 API)	830	0	0.5	1.6	0	1.6	1226	0	undefined

b. Histogram and crossplot QC plot enables to check data consistency between wells and comparison against typical relationship of density - p-velocity (Gardner et al., 1974) and p-velocity and s-velocity (Greenberg et al., 1992). Figure 3.2 shows that the DS-2 reservoir is faster and denser as compared to reservoir from the GD-1. The crossplot of Vp and Density color-coded by volume of shale showed the elastics properties are consistent with depth trend and lithological trend. Figure 3.3 shows that the DS-1 has higher Vs then well GD-1. The Vp-Vs crossplot color-coded by volume of clay showed consistent Vp-Vs trend. Points further away from the outlier are hydrocarbon bearing reservoirs.

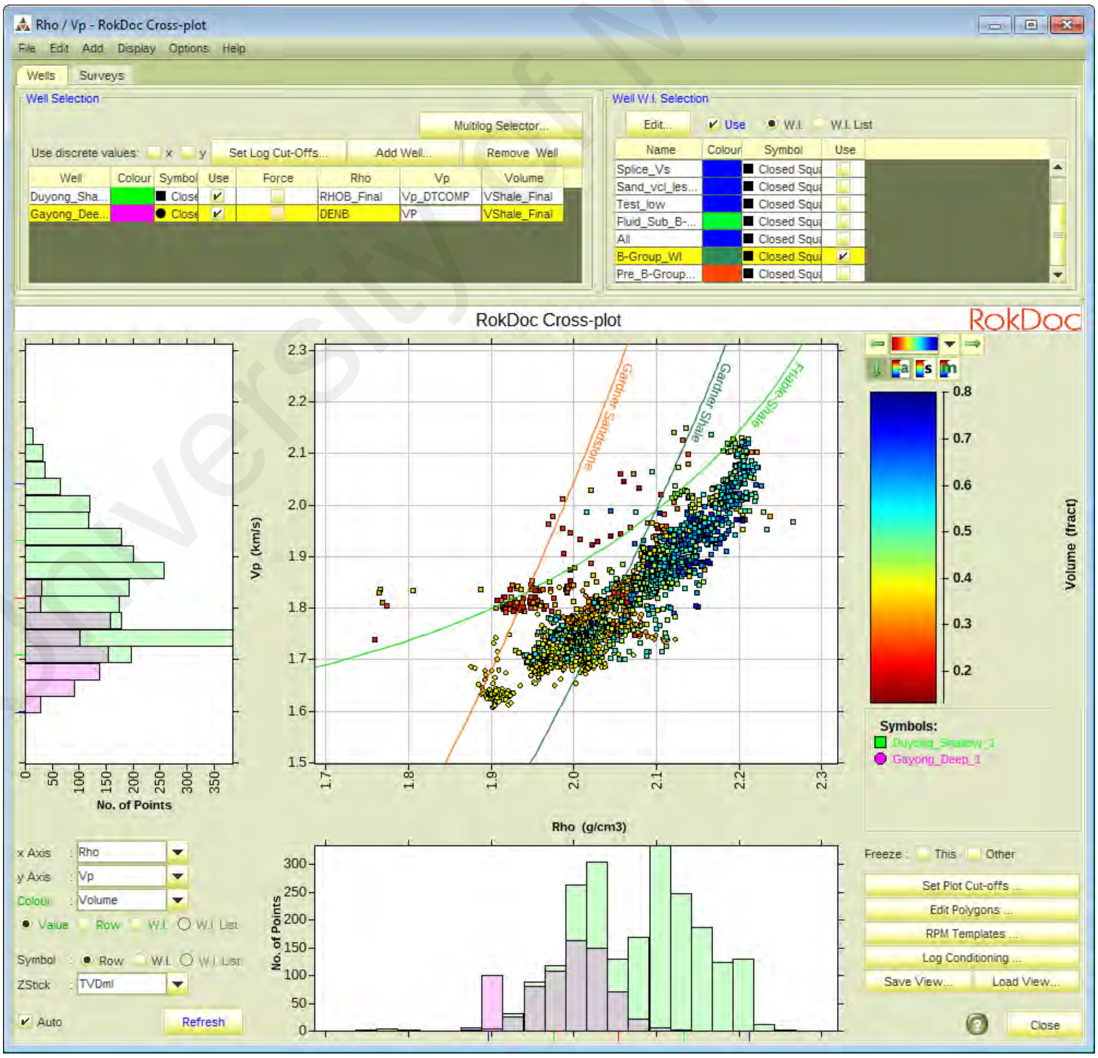

Figure 3.2: Histogram and Crossplot of input density and p-velocity logs color coded by volume of clay within the B-Group.

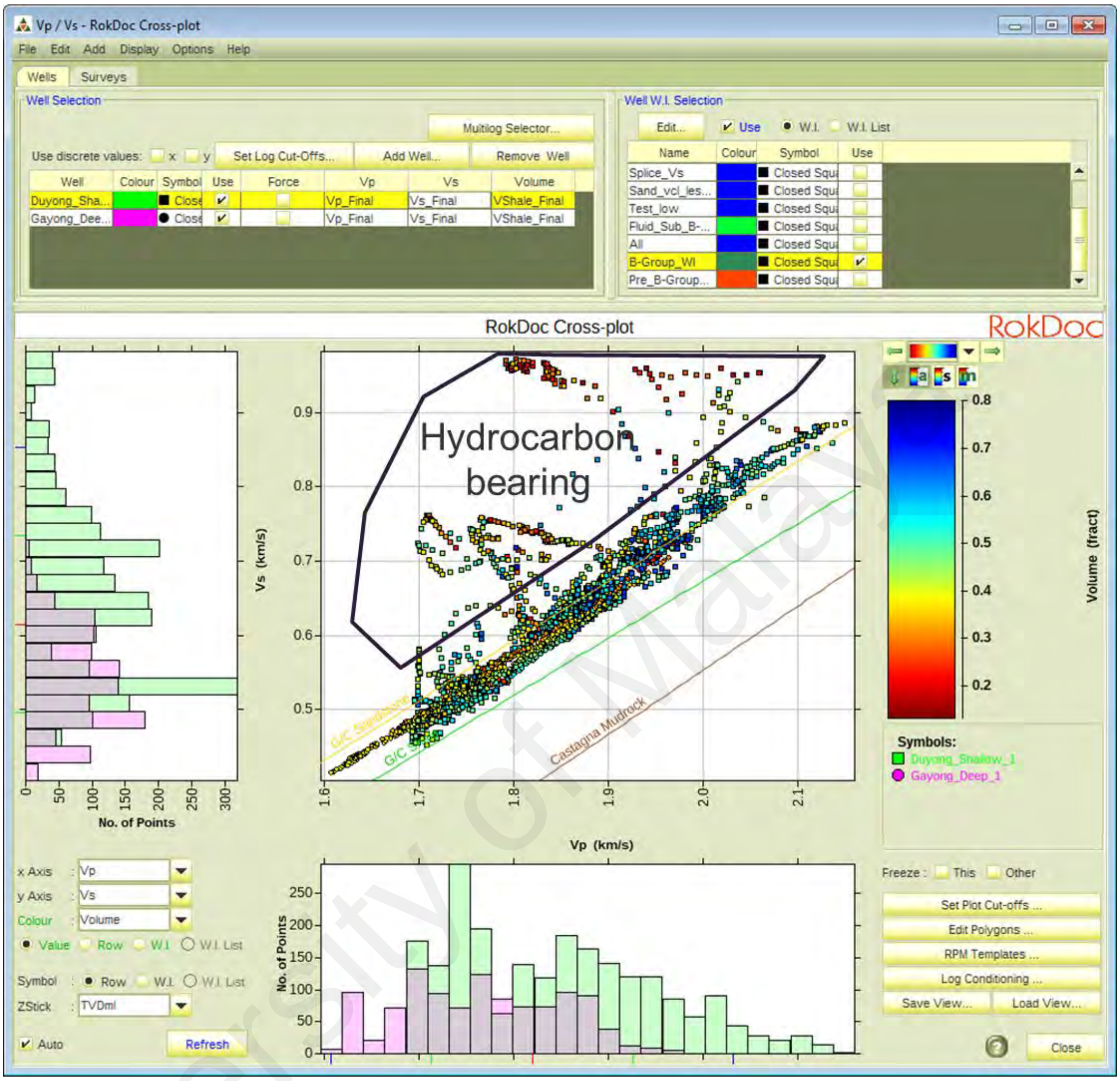

Figure 3.3: Histogram and Crossplot of input p-velocity and s-velocity logs color coded by volume of clay within the B-Group. Hydrocarbon-bearing points lie off trend.

3.1.2 Well log data conditioning

Data conditioning was carried out to fill-in the gap in resistivity, p-velocity, s-velocity and density. For DS-1, the well logs gap are small and were filled by log interpolation. For well GD-1, the big gap in well logs were filled the through four steps:

i. Resistivity log through multi-linear relationship of GR-Resistivity,

ii. P-velocity log using Faust (1953) relationship,

$$Vp = 2.2888\left(Z\frac{Ro}{Rw}\right)^{1/6}$$

Where;

Vp = Compressional velocity in km/s

Rw = Water resistivity of formation water

Ro = Water saturated formation

Z = Depth in km

iii. Density logs using Gardner (1974) relationship,

$$\rho_0 = 1.741\,Vp^{0.25}$$

Where;

ρ_0 = Bulk density in g/cm^3

Vp = Compressional velocity in km/s

iv. S-velocity logs using Greenberg & Castagna (1992).

$$Vs = -0.055\,Vp^{0.2} + 1.1017Vp - 1.031$$

Where;

Vp = Compressional velocity in km/s

Vs = Shear velocity in km/s

The conditioned logs were then compared with the log plot and cross plot to observe the consistency of the conditioned data in terms of depth trend and obeying the rock – physics trend. Figure 3.4 below shows log plot that contain logs before and after conditioning. The synthetic logs that filled the gap of density, compressional velocity and shear velocity are consistent with the depth trend.

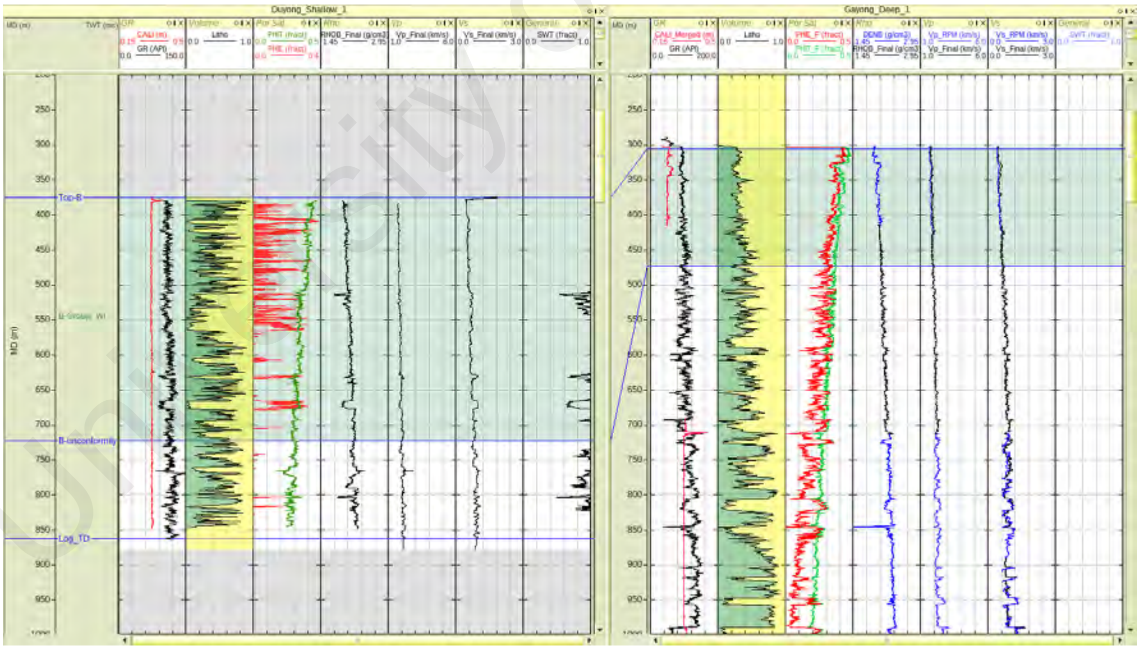

Figure 3.4: GD-1 and DS-2 well logs plot of conditioned data. The data gap from the input Vp, Vs and Density (blue curve) filled with synthetic logs (black) that shows good match of depth trend.

Once the gaps are filled, the data was cross-checked against the input data through cross-plots. The conditioned data is expected to follow the rock-elastic trends. In Figure 3.4 to Figure 3.6 below, the additional points are highlighted with circle symbol. Overall, the conditioned data follow the rock physics trends confirming that the log data is ready for the subsequent standard analysis.

Crossplot of the AI and Vp/Vs in Figure 3.7 shows the raw and conditioned data. Notice the clear lithology separation between sand and shale. This observation indicates the lithology discrimination is feasible using this unconventional logs.

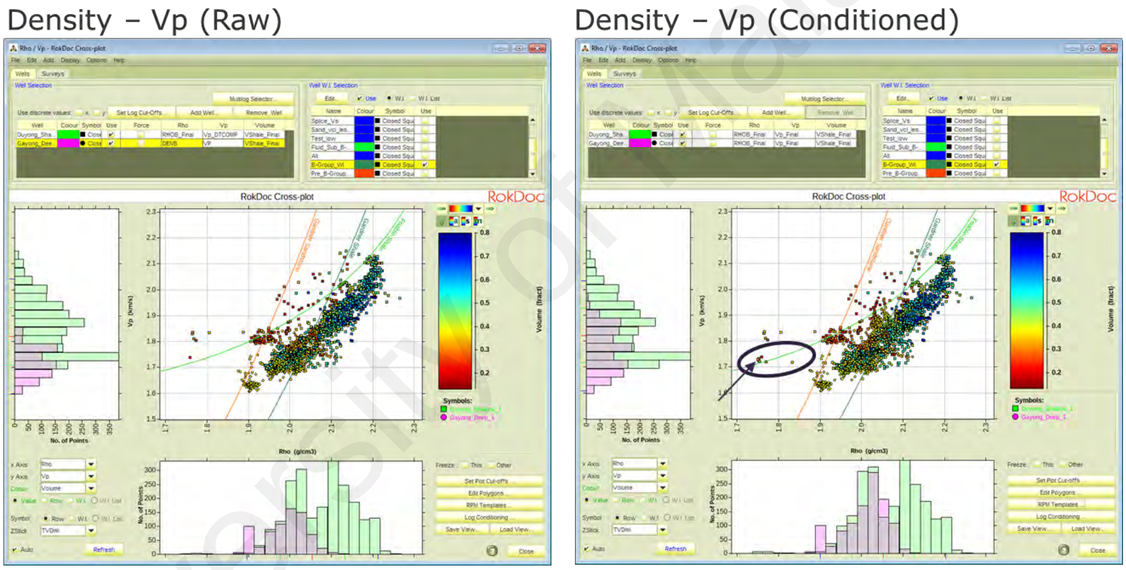

Figure 3.5: Histogram and Crossplot comparison of before and after conditioning of p-velocity and density logs color coded by Vclay in the B-Group.

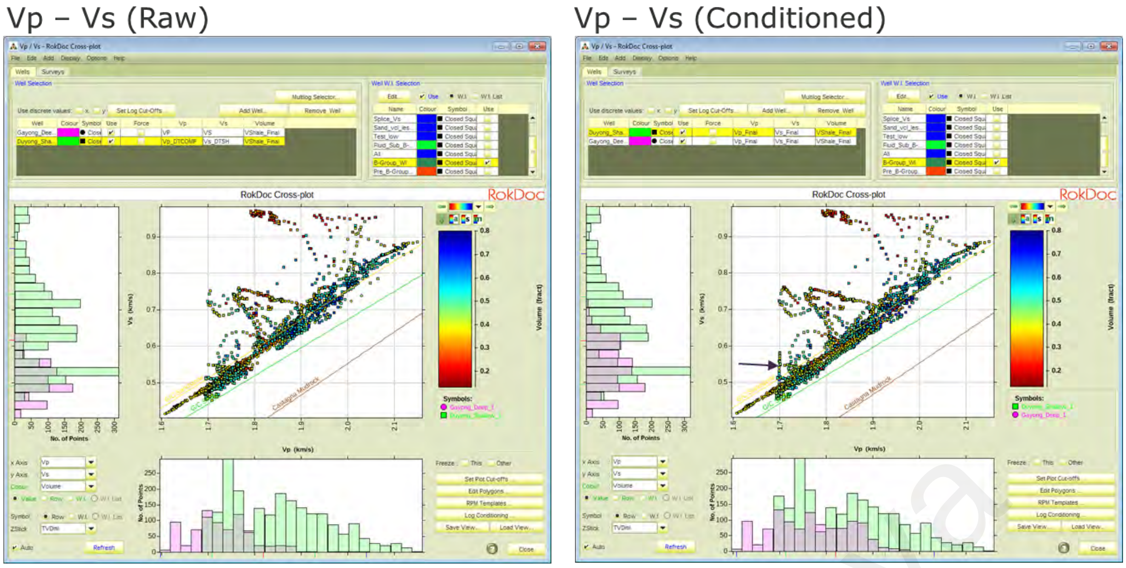

Figure 3.6: Histogram and Crossplot comparison of before and after conditioning of p-velocity and s-velocity logs color coded by Vclay in the B-Group.

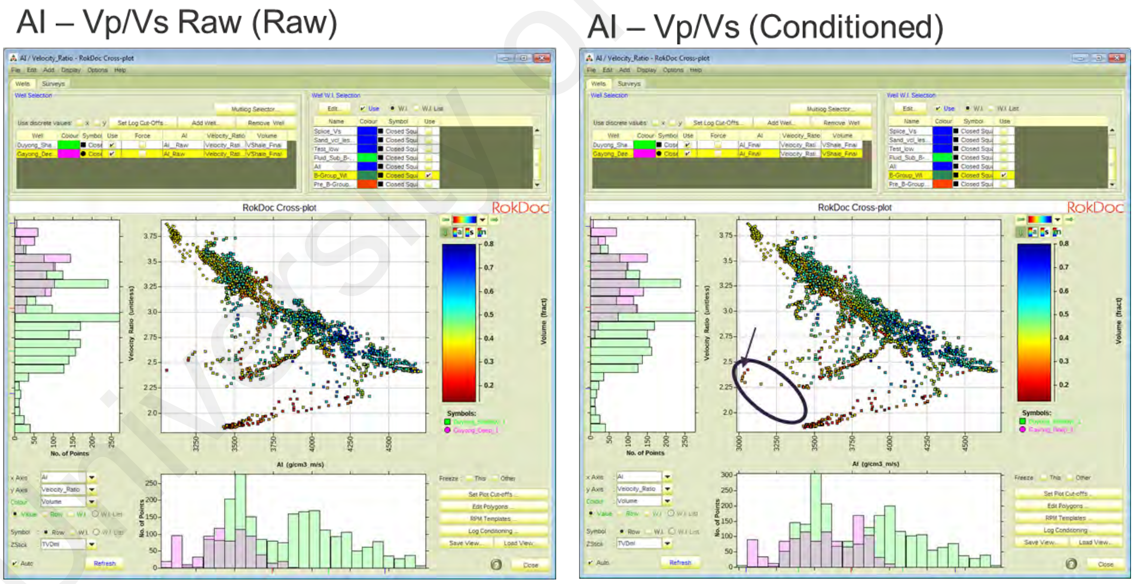

Figure 3.7: Histogram and Crossplot comparison of before and after conditioning of AI and Vp/Vs logs in B-Group.

3.2 Seismic data QC and conditioning

Well data is one of the critical input in the reservoir characterization. The input seismic data would ideally be noise free, multiple free, true amplitude, correctly imaged and wide bandwidth. Processed seismic data will never fully satisfy these criteria, however the closer to these objectives the better.

In this study, full stack, angles stacks and seismic gather were supplied by PCSB for QC and conditioning. Seismic frequency bandwidth QC plot in Figure 3.8 was used to differentiate signal and noise through bandpass filtering of the seismic. High signal appear as coherent amplitude that follow the structure/geology, while coherent noise do not. Although seismic amplitude spectrum of the full stack at less than 20dB down show frequency ranges between 8 – 160 Hz, seismic noise can be observed at 120-130 Hz. Hence, the bandwidth for full stack is selected between 8 – 120 Hz.

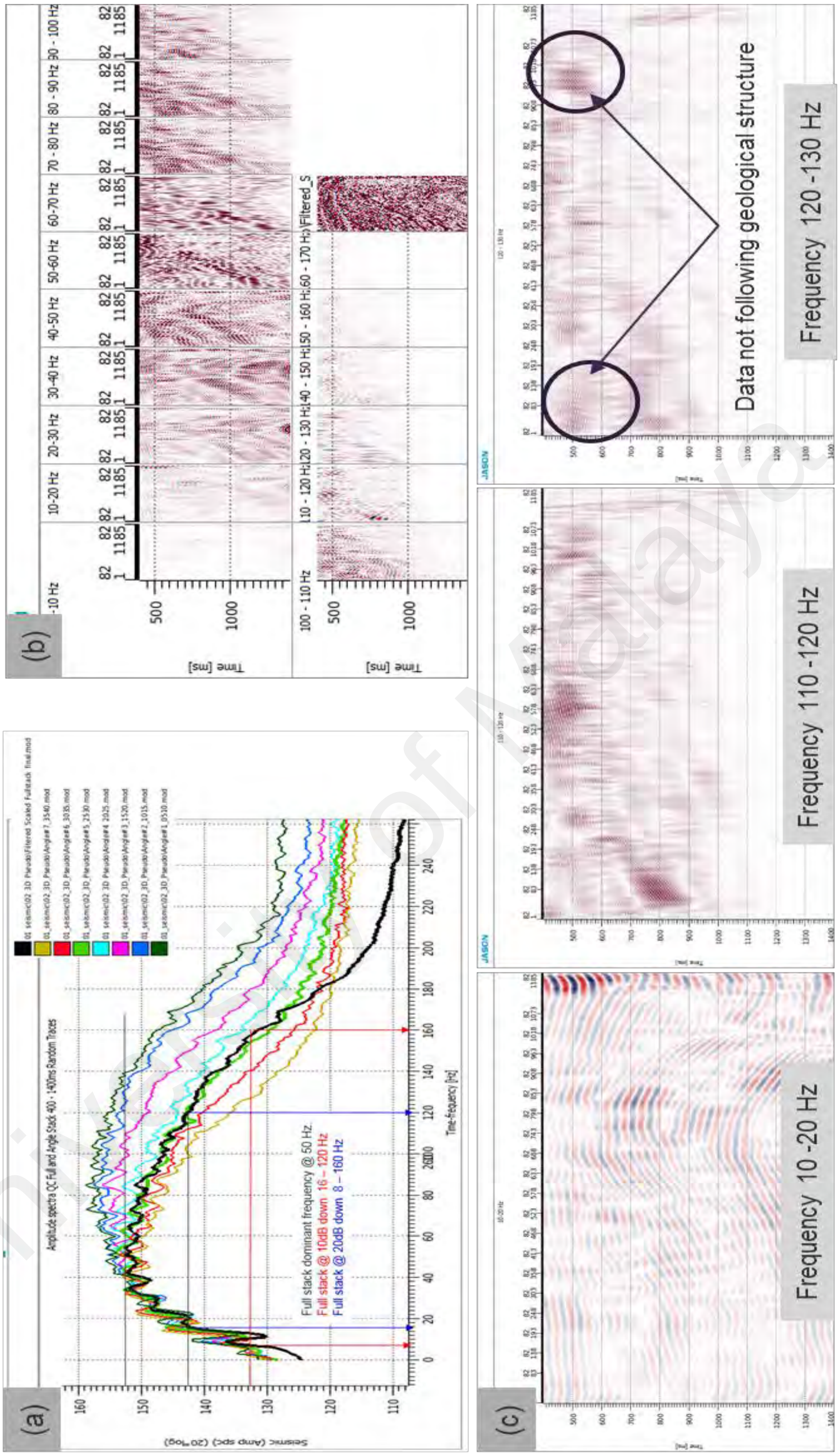

Figure 3.8: Seismic frequency bandwidth QC of input data. (a) Amplitude spectra QC plot from depth 400 – 1400ms. (b) Band limited seismic sections 0 Hz to 170 Hz. (c) Comparison of band limited seismic sections.

Comparison of input seismic gather with synthetic seismic from well logs provide QC plot of the seismic gather alignment that is crucial for AVO and Inversion processing. Figure 3.9 QC plots show input seismic gathers at three different acquisition source-receiver spacing and the synthetic gathers. This QC plots highlighted that all the input gathers are contaminated with multiples. Thus seismic gathers conditioning were necessary.

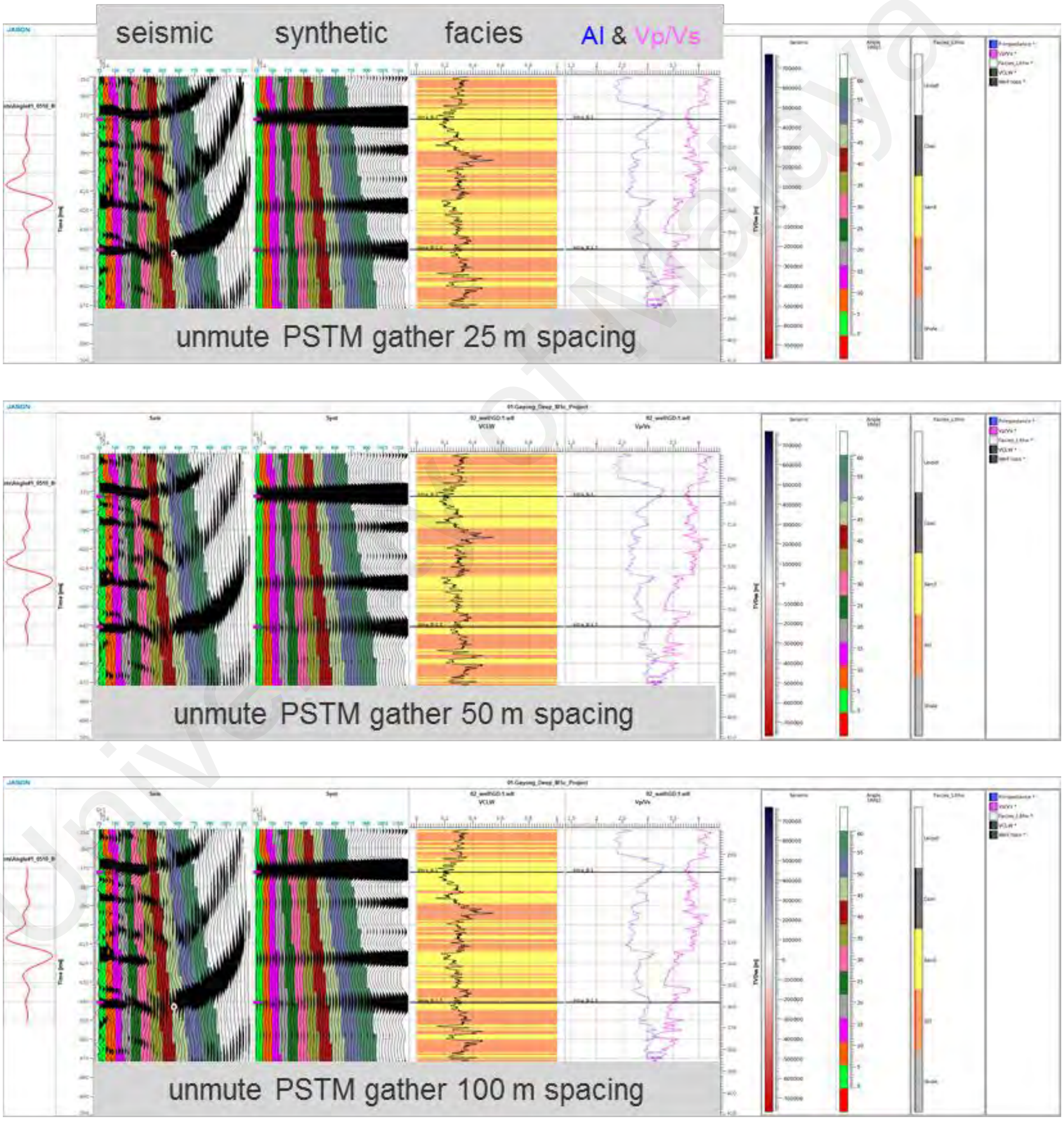

Figure 3.9: GD-1 well synthetic and seismic gather tie at three different acquisition spacings. Observed seimic reflector from all the input seismic gathers are not aligend and contaminated with multiples.

Seismic gather conditioning was performed with objective to increase signal to noise ratio, trace alignment of seismic reflector and zero phasing. The input gather were tested through seven reprocessing sequence (QI-1 to QI-7) as listed below. Complete QC plots from each processing sequence are available in the Appendix-B.

- QI-1: Frequency Bandpass – to suppress noise
- QI-2: Angle Mute - remove faulty data within angle range
- QI-3: Super Gathers – to enhance signal to noise ratio
- QI-4: Parabolic Radon Transform – to correct for noise and multiples.
- QI-5: Trim statics – to correct time alignment.
- QI-6: Zero phasing - to transform seismic data from non-zero phase to zero phase
- QI-7: Offset dependent scaling - Correct the systematic offset-dependent amplitude distortion in the gathers.

Conditioned seismic gather from sequence QI-4 (Figure 3.10) show better quality in terms of seismic reflector continuity and was selected for the subsequence analysis. Three (3) angle stacks were generated from QI-4 conditioned gather; 5-10 degrees, 15-25 degrees and 25-35 degrees.

Seismic amplitude and frequency sections at time 300 – 600 ms (within zone of interest) showed consistent image and reflector continuity at all angle stacks. The far stacks have lower background amplitude as compared to the near and the mid stacks. The frequency bandwidth is between 20 – 120 Hz. See Figure 3.11.

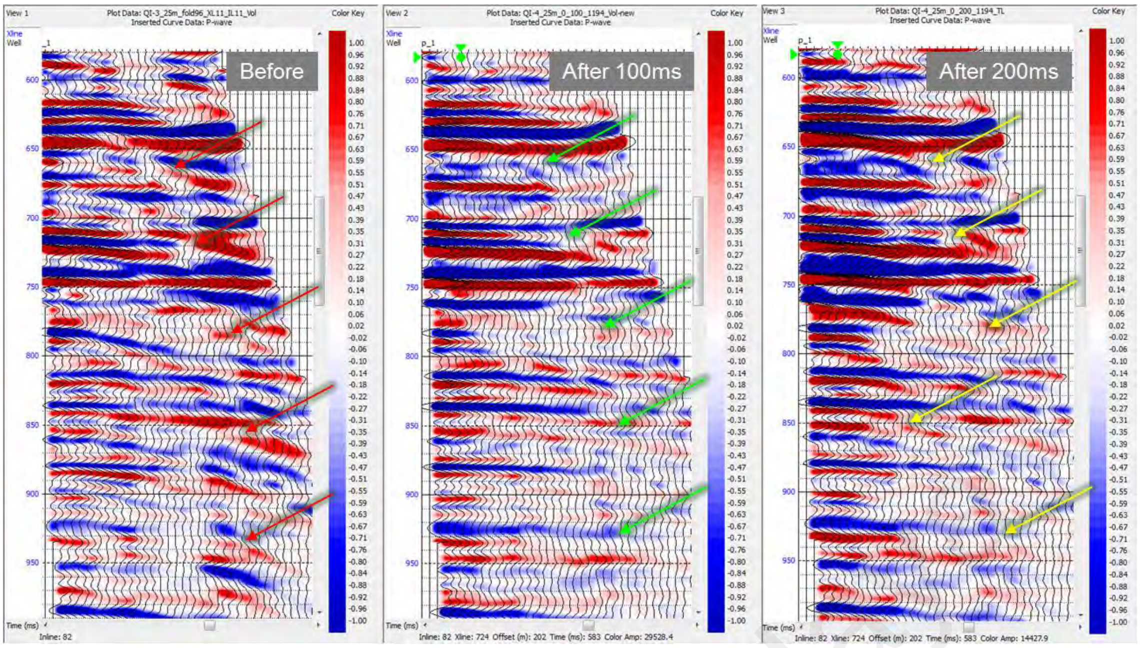

Figure 3.10: Radon demultiple QI-4 QC plot. The red arrow highlighted multiple crossing the reflector. 100ms cut-off window removed most of the multiples and improved the data signal. 200ms cut-off window still have multiples. Cut-off window of 100ms used as final product.

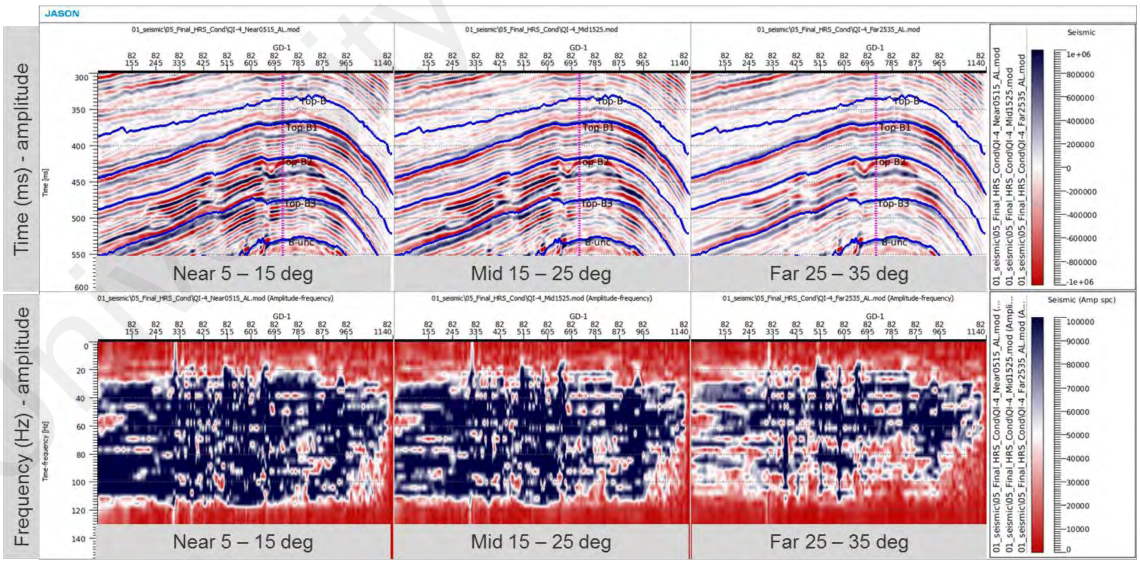

Figure 3.11: Seismic amplitude and frequency sections of near, mid and far angle stacks.

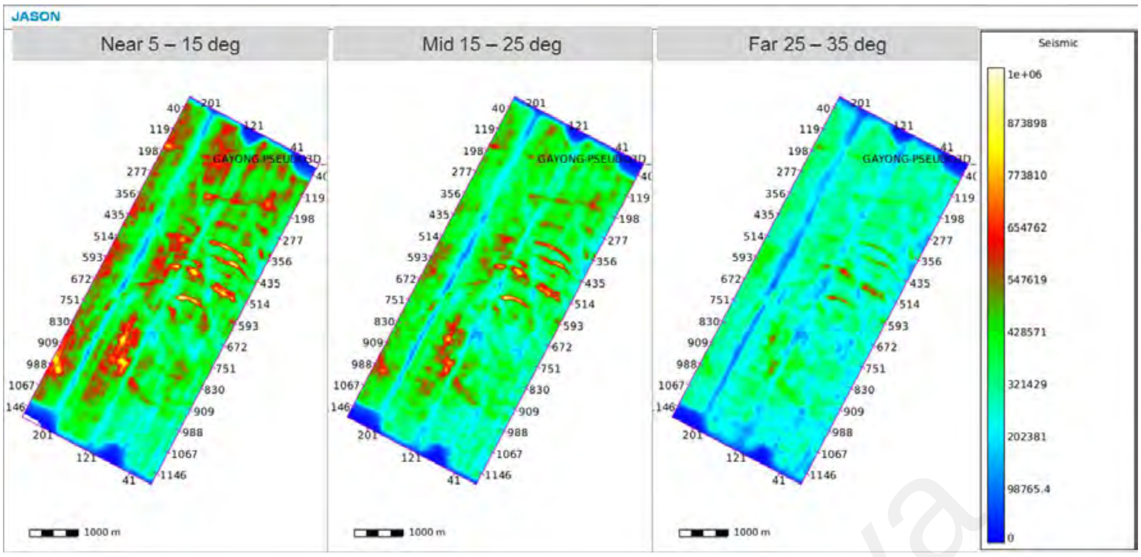

Figure 3.12: RMS amplitude extracted at window 250 – 7500ms to observe non-geological effect. Two low amplitude lines at direction NE-SW observed at all stacks are non-geological effect.

Figure 3.12 above shows the QC plot seismic RMS amplitude at each angles stacks. The result shows that the background amplitude are different indicating the requirement of amplitude balancing of these stacks. However, amplitude balancing is not required for seismic inversion process as the amplitude variation is taken care of by wavelet filter extracted at each stacks.

3.3 Petrophysical Interpretation

Petrophysical interpretation is important to link between the rock and elastic properties. In this study, the most critical interpreted logs are volume of clay, porosity total, porosity effective and water saturation at *in situ* condition. Adopted nomenclature of common log and rock properties is shown in Table 3.2.

Table 3.2: Rock Properties Nomenclature

Rock Properties	Symbol	Units	Description
Volume of clay	V_{clay}, C	fraction	Volume of clay fraction
Volume of Shale	Vshale	fraction	Volume of shale fraction (clay+silt)
Porosity Total	PHIT, $\emptyset_T$	fraction	Volume of pore space + bound water
Porosity Effective	PHIE, $\emptyset_e$	fraction	Volume of pore space - bound water
Water Saturation	SW	fraction	Water saturation of reservoir fluid
Pore pressure	PP	Mpa	The pressure exerted by a fluid filling the pores of a soil or rock

3.3.1 Volume of clay (V_{clay}) estimation

Volume of clay is critical for determination of porosity and provide lithological interpretation of volume fraction sets (sand & shale). The volume of clay was determined using Gamma Ray (GR) log of clean sand and pure clay;

$$Volume\ of\ Clay, V_{clay} = \frac{GR_{\log} - GR_{clean}}{GR_{\text{clay}} - GR_{clean}}$$

Where,

$GR_{\log}$ = gamma ray from log response

GR_{clean} = gamma ray response from clean sandstone

GR_{clay} = gamma ray response from pure clay

GR units in API.

3.3.2 Porosity estimation

Porosity has direct relationship to density and velocity (Avseth, 2000; Avseth et al., 2003 & Avseth et al., 2010) that link to impedance and seismic analysis for seismic reservoir characterization.

In this study, total porosity (PHIT) was derived from the bulk density, fluid density and matrix density. The matrix density is calculated by integrating the minerals by their volume fractions and their known individual densities values: density quartz = 2.65 g/cm^3; dry clay = 2.2 – 2.6 g/cm^3. PHIT is given by the equation below (Hook, 2003):

$$Porosity\ Total, \emptyset_T = \frac{\rho_{\text{grain}} - \rho_{log}}{\rho_{\text{grain}} - \rho_{fluid}}$$

Where,

ρ_{grain} = density of mineral selected (sand/clay)

ρ_{fluid} = density of fluid (water)

ρ_{log} = density from log response

3.3.3 Water saturation estimation

Water saturation estimation is typically based on Archie equation (Archie, 1952):

$$Water\ Saturation, {S_w}^n = \frac{R_w}{(\phi^m\ x\ R_t)}$$

Where,

Sw = water saturation of the uninvaded zone

n = saturation exponent, which varies from 1.8 to 4.0 but normally is 2.0

Rw = formation water resistivity at formation temperature

Φ = porosity

m = cementation exponent, which varies from 1.7 to 3.0 but normally is 2.0

Rt = true resistivity of the formation, corrected for invasion, borehole, thin bed, and other effects

3.4 Rock physics modeling

The objective of the rock physics modeling was to understand the rock and elastics properties changes to variation of fluid phase, saturation, porosity, pore pressure and volume of clay that is consistent with local geology. In this stage, the important modeling output are elastic logs of Vp, Vs and Density.

3.4.1 Fluid Phase and Saturation Perturbation

Fluid substitution is performed using Gassmann‟s Dry Rock Model (Khateb, 2013) as described in Appendix C. The main objective of this analysis was to ascertain sensitivity of elastics logs with different fluid type and different hydrocarbon saturation in the unconsolidated sand.

Analysis was performed for the following fluid type and hydrocarbon saturation on clean sand with Vclay < 35%.: 1) Water 100%, 2) Oil 20% and 80% and 3) Gas 20% and 80%

3.4.2 Porosity perturbation

Porosity perturbation is performed using Gasmann‟s fluid substitution to dry rock, followed by perturbing the porosity, and then putting back the original fluid in the rock to produce the perturbed porosity logs. Porosity perturbation is performed for porosity changes of + 5%, + 10%, - 5% and – 10% from the *in situ* condition.

3.4.3 Pore pressure perturbation

Pore pressure perturbation follow the fluid substitution approach to modelling the effects of changes in pressure using the Gassmann method. This method performs a fluid substitution to dry rock, perturbs the pressure, and then substitutes in a specified final fluid to give the final results. Pore pressure perturbation is performed for pressure changes of + 5%, + 10%, - 5% and – 10% from the *in situ* condition.

3.4.4 Volume of clay perturbation

Velocity-porosity-clay behavior were studied based Han‟s empirical relations (Han, 1986). At the stage, cement content is not considered and the analysis performed at depth 400 – 600m. Linear regression of Porosity-Velocity relationship at different clay cut-off were established for Vp, Vs and Density as shown in Figure 3.13, Figure 3.14, and Figure 3.15.

The volume of clay relationships with Vp, Vs and Density summarized in Table 3.3 from the GD-1. These relationships were used to generate elastics logs at different volume of clay cut-off.

Table 3.3: Velocity-density-porosity-clay relationship established from unconsolidated sand of GD-1 well

Volume of Clay	Compressional Velocity (m/s)	Shear Velocity (m/s)	Density (g/cc)
10-20%	**3.12098-(3.03682*PHIT)**	**1.63711- (2.40519*PHIT)**	**1.19358 + (0.412074*Vp)**
20-30%	**2.9924- (2.99897*PHIT)**	**1.5117- (2.3412*PHIT)**	**1.4134+ (0.323677*Vp)**
30-40%	**2.85842- (3.06386*PHIT)**	**1.38131- (2.35467*PHIT)**	**1.44281 + (0.327091*Vp)**
40-50%	**2.66366- (2.86863*PHIT)**	**1.21452- (2.1873*PHIT)**	**1.43637 + (0.35556*Vp)**
50-60%	**2.40529- (2.41031*PHIT)**	**0.992856- (1.78136*PHIT)**	**1.60543 + (0.298827*Vp)**

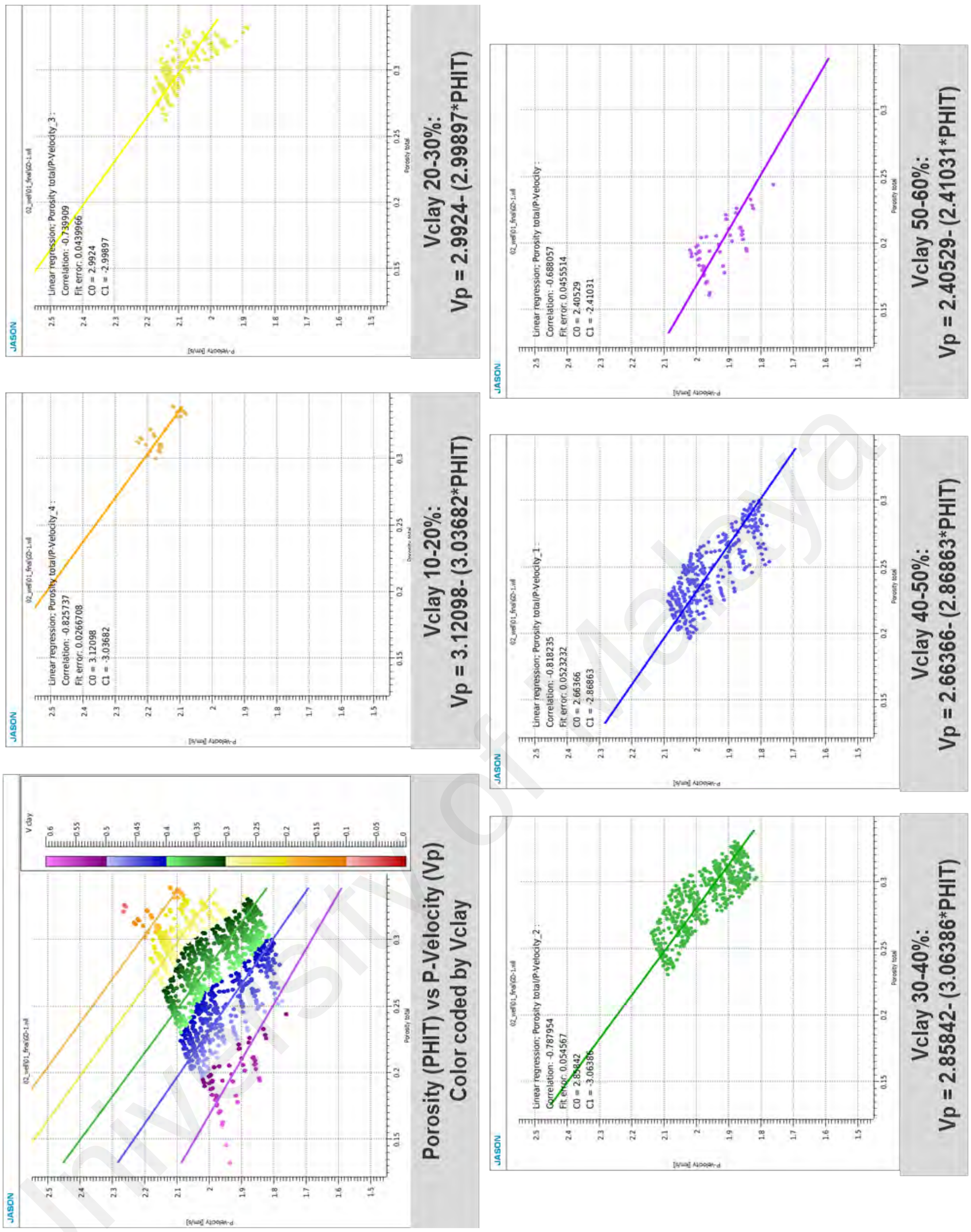

Figure 3.13: Porosity - P-Velocity - Volume of Clay relationship.

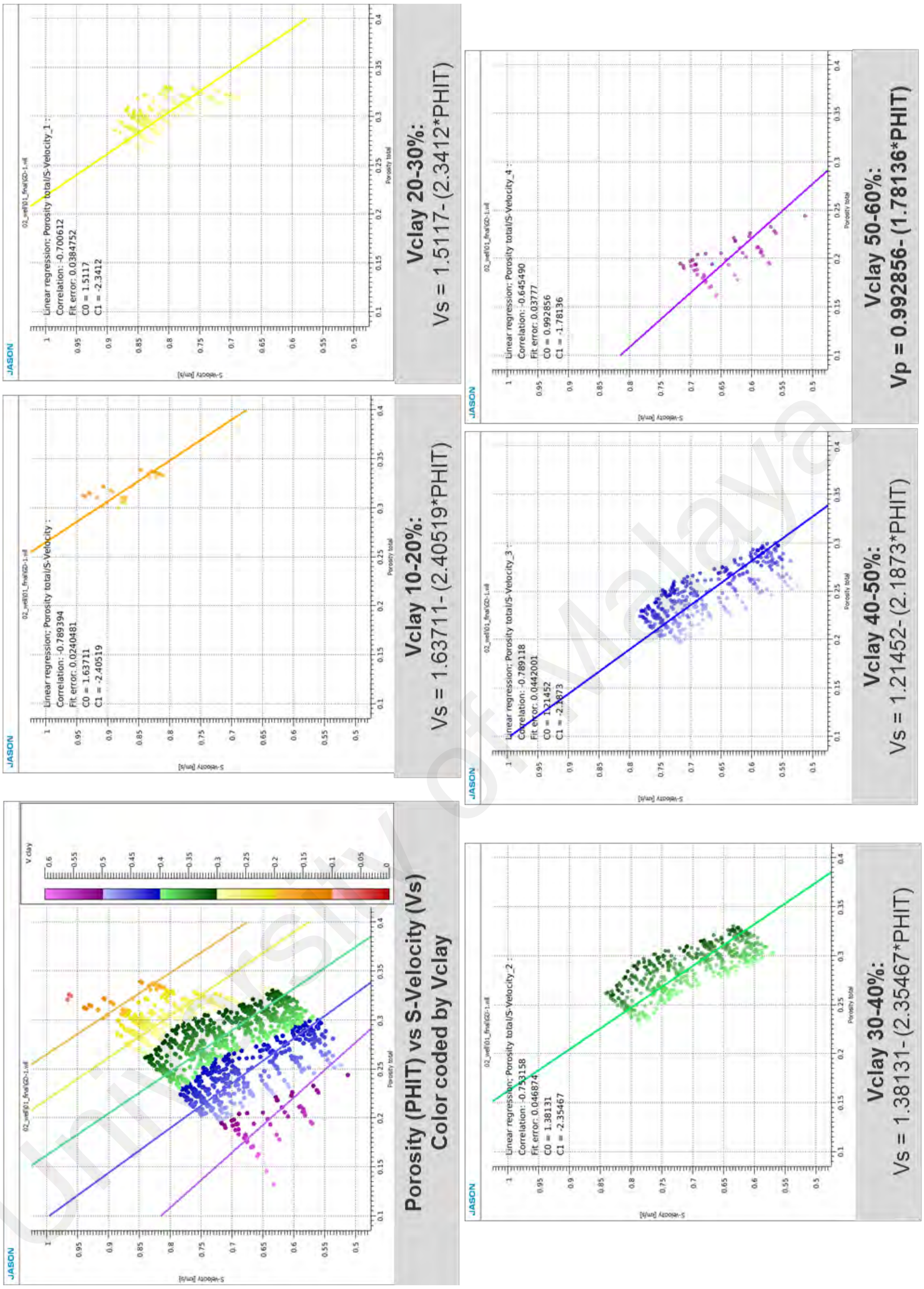

Figure 3.14: Porosity - S-Velocity - Volume of Clay relationship.

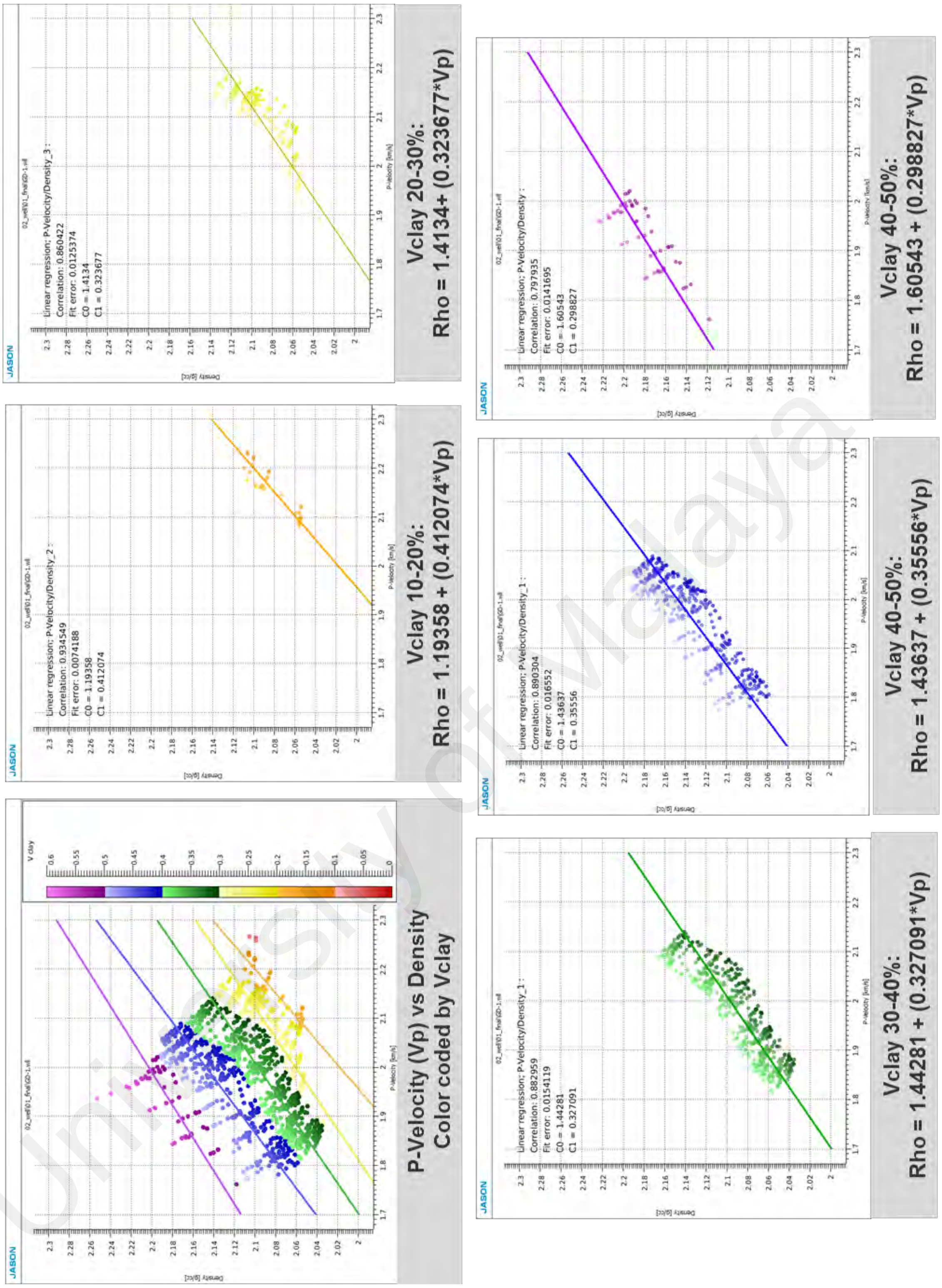

Figure 3.15: Density – P-Velocity – Volume of Clay relationship.

3.5 Seismic Forward Model & AVO crossplot

In this study, seismic forward model refers to synthetic seismic derived from the modeled elastic logs. These synthetic seismic can be compared to the actual seismic from the GD area with assumption that if the actual seismic response is similar, the rock properties in the subsurface is similar as well (Dvorkin, Gutierrez, & Grana, 2014). Figure 3.16 shows an overview of the forward model concept applied in this research. All the modeled elastic logs derived from section 3.4 were used to produce angle synthetic seismic model.

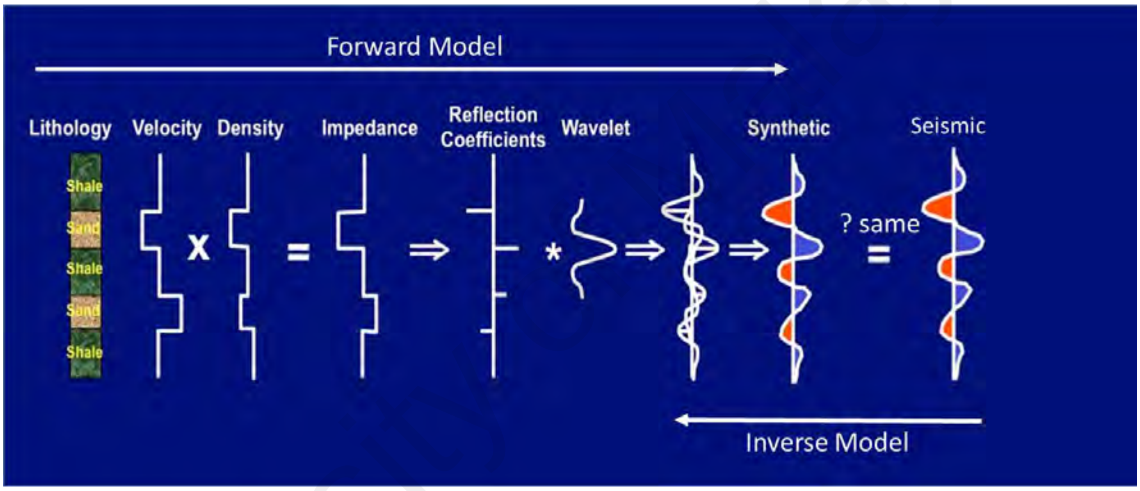

Figure 3.16: Schematic format of a seismogram forward and inverse model (after Schroeder, 2011).

Angle of reflection is calculated using the Aki-Richards linearized approximation (Aki & Richard, 1980);

$$R\ (\theta) = A\ +\ B\ sin^2\theta +\ \ C\ tan^2\theta\ sin^2\theta$$

Where,

$$A = \frac{1}{2}\ \left(\frac{\Delta\ V_p}{V_p} + \frac{\Delta\ \rho}{\rho}\right)$$

$$B\ = \frac{1}{2}\ \left(\frac{\Delta\ V_p}{V_p}\right) - 4\ \left(\frac{V_s}{V_p}\right) 2\,\frac{V_s}{V_p}{}^{2}$$

$$C\ = \frac{1}{2}\ \left(\frac{\Delta\ V_p}{V_p}\right)$$

θ = angle of incident as shown in figure below

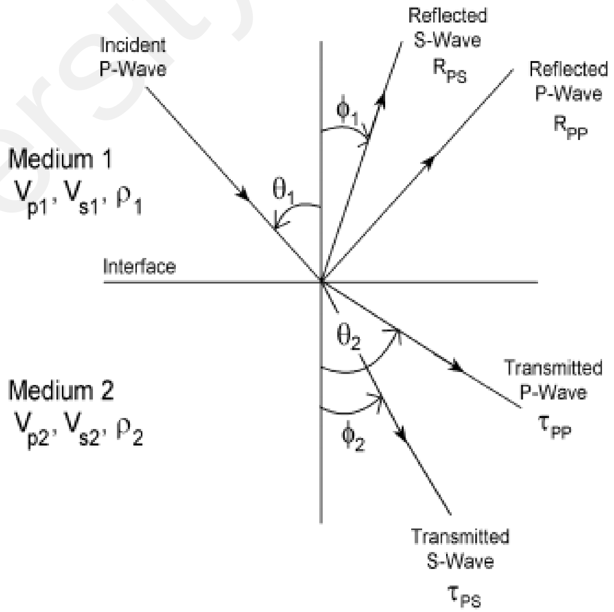

Figure 3.17: An incident p-wave produces four resulting waves, consisting of two reflected waves and two transmitted waves. Incidence angle of P-wave, $\boldsymbol{\theta_1}$ = $\boldsymbol{\theta}$ for P-wave angle reflectivity.

The main objectives of AVO crossplot analysis of the modeled synthetics are: 1) observe AVO classes based on the AVO classification schemes (Castagna & Backus, 1993; Simm & Bacon, 2014); 2) estimate relative changes of seismic amplitude from *in situ* condition (brine) to modelled rock and fluid properties. Figure 3.18: The AVO classes (Castagna & Backus. 1992; Simm & Bacon., 2014). The result should be able to give a guidance to an interpreter for reservoir/ fluid interpretation from seismic amplitude in unconsolidated sand.

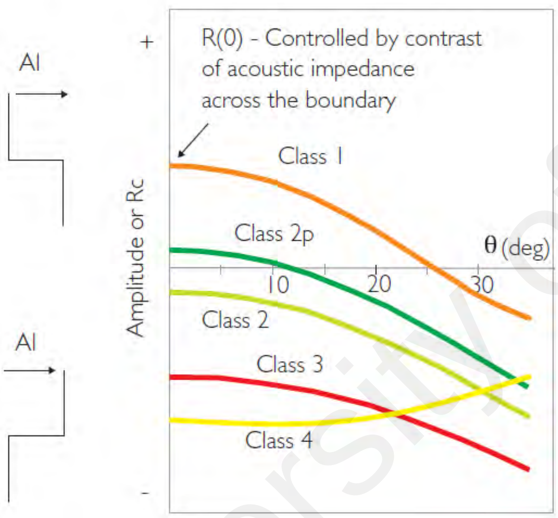

Class	Gradient	Absolute Amplitudes	Notes
I	-	Far < R(0)	+ve R(0), may have phase reversal
IIp	-	Far > R(0)	+ve R(0), phase reversal
II	-	Far > R(0)	Low amplitude at R(0)
III	-	Far > R(0)	Relatively high amplitude at R(0)
IV	+	Far < R(0)	Very high amplitude at R(0)

Figure 3.18: The AVO classes (Castagna & Backus. 1992; Simm & Bacon., 2014).

3.6 Simultaneous AVO inversion

Inversion theory is a set of mathematic technique for retrieving information of a physical system from controlled observations (Meju, 1994) and can be understood through inverse model as shown in Figure 3.16. Simultaneous inversion is a process when all the angle seismic data are simultaneously inverted for angle independent quantities as schematized in Figure 3.19. Seismic inversion has proven extremely successful for reservoir delineation and characterization because it reduces tuning and interference effects of the seismic wavelet, increases bandwidth compared to the seismic data, forces data integration, transforms the seismic data from interface properties to layer properties that are the absolute values of the rocks themselves and eases interpretation.

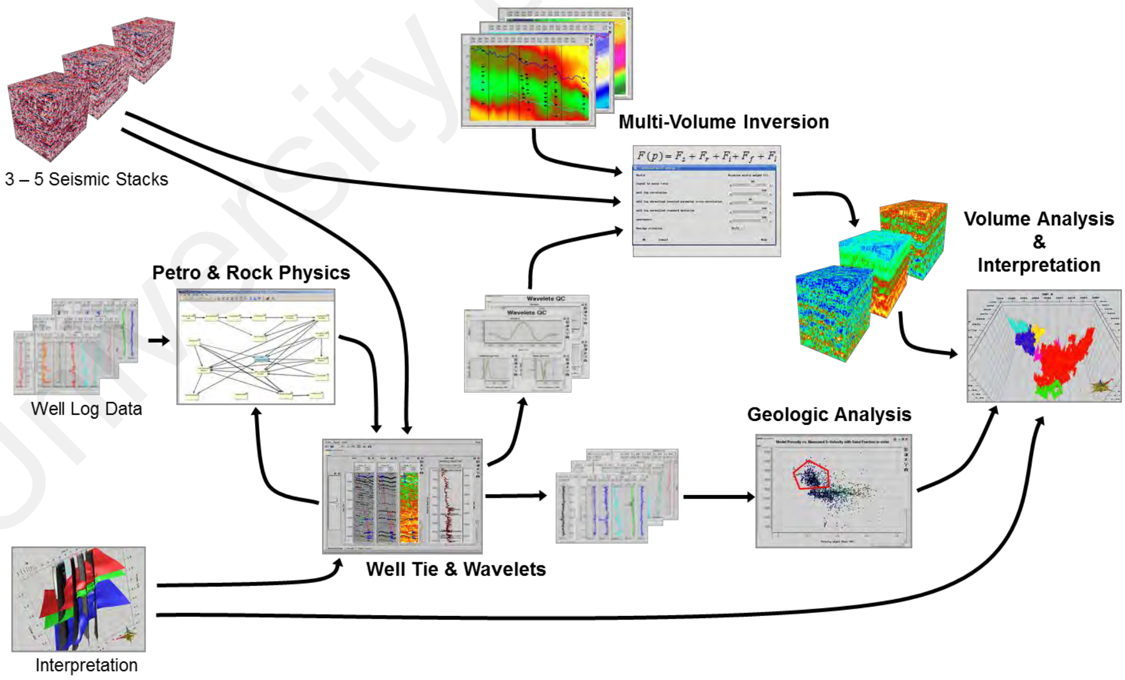

Figure 3.19: Simultaneous AVO Inversion Workflow (Adapted from Jason CGG training manual).

3.6.1 Well to seismic calibration

Well logs are measured in depth, while seismic data are in time. Well to seismic tie is a critical process to ensure the subsurface information is properly calibrated to the well data. Well checkshot was used to convert the well log information to time. After an initial depth-to-time conversion an initial wavelet is used to generate the well log synthetics and then compare to seismic. Figure 3.20, Figure 3.21 and Figure 3.22 show well to seismic calibration QC plot at three different input stacks. All the stacks showed more than 70% cross-correlation.

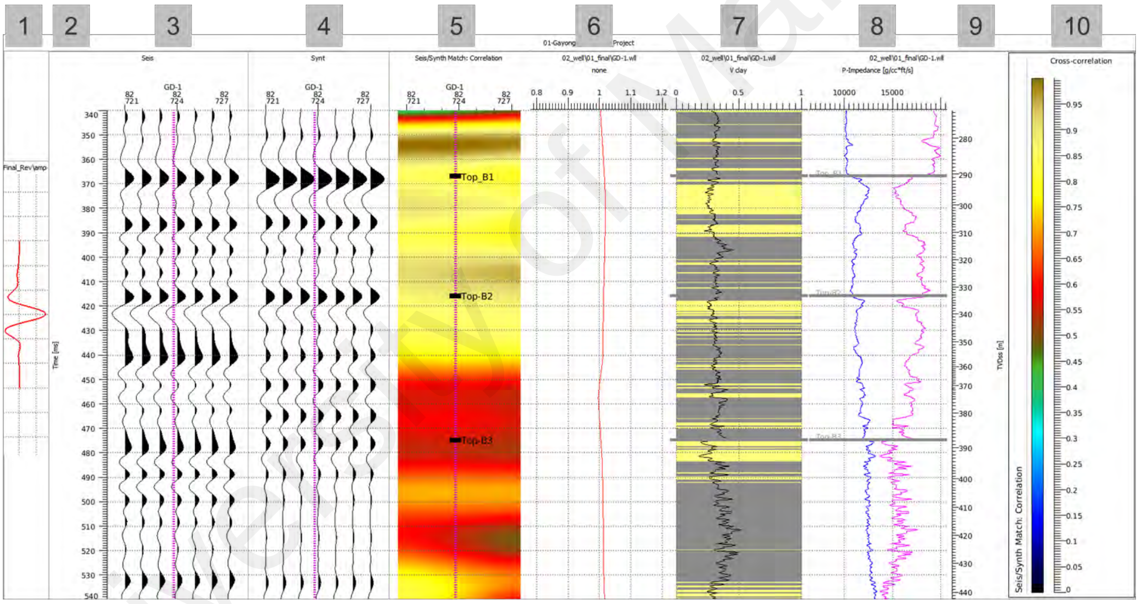

Figure 3.20: GD-1 well synthetic and seismic calibration of near stack. This well tie QC plot of each panel describes as followings. Panel 1) wavelet used to generate synthetic seismic; 2) vertical scale in two way time (ms); 3) seismic traces at the well location; 4) synthetic seismic generated from convolution of well log reflectivities and wavelet; 5) cross correlation of seismic and synthetic at each displayed traces; 6) relative drift of final time-depth curve from the well checkshot; 7) Facies sand and shale from well log; 8) AI and Vp/Vs well log; 9) vertical scale in depth and 10) legend for cross-correlation value. Observe the AI property of B1, B2 and B3 sands are higher than shale. Seismic amplitude at the top of these sands are correspond to peak of seismic amplitude (black). Over the whole interval, the seismic and the synthetic have good match with cross-correlation more than 70%. However, at the Top of B1 sand, small mismatch of amplitude observed indicating stronger well reflectivities than seismic. Thus the same mismatch of inverted seismic and well log is expected at B1 sand.

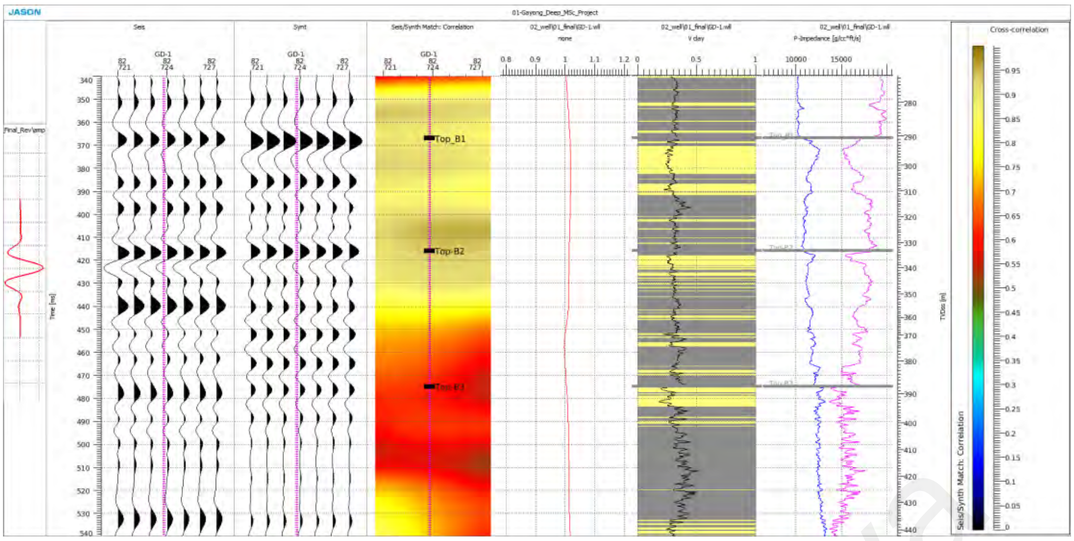

Figure 3.21: GD-1 well synthetic and seismic calibration of mid stack. AI property of B1, B2 and B3 sands are higher than shale. Seismic amplitude at the tops of these sands correspond to peak amplitude (black).

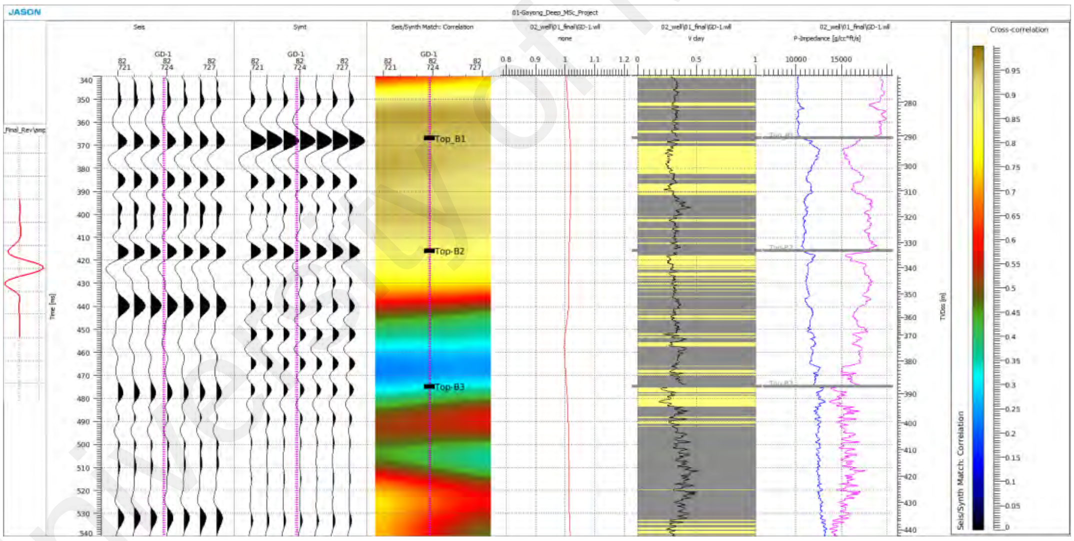

Figure 3.22: GD-1 well synthetic and seismic calibration of far stack. AI property of B1, B2 and B3 sands are higher than shale. Seismic amplitude at the tops of these sands correspond to peak amplitude (black).

3.6.2 Wavelet extraction

The seismic wavelet is the link between the earth reflectivities and the seismic data. At well location, the earth reflectivities calculated from sonic and density curves. Wavelets for each angles stacks were extracted from the input near, mid and far stacks through modeling of the well"s seismic reflectivity and then compared to the input seismic. Wavelets that produced the best match with the seismic were extracted and used for the input to the inversion process with assumption that wavelet in stationarity, the seismic data away from well control can be used together with the wavelet to estimate the earth reflectivities. The final wavelets used for seismic inversion are shown in the Figure 3.23.

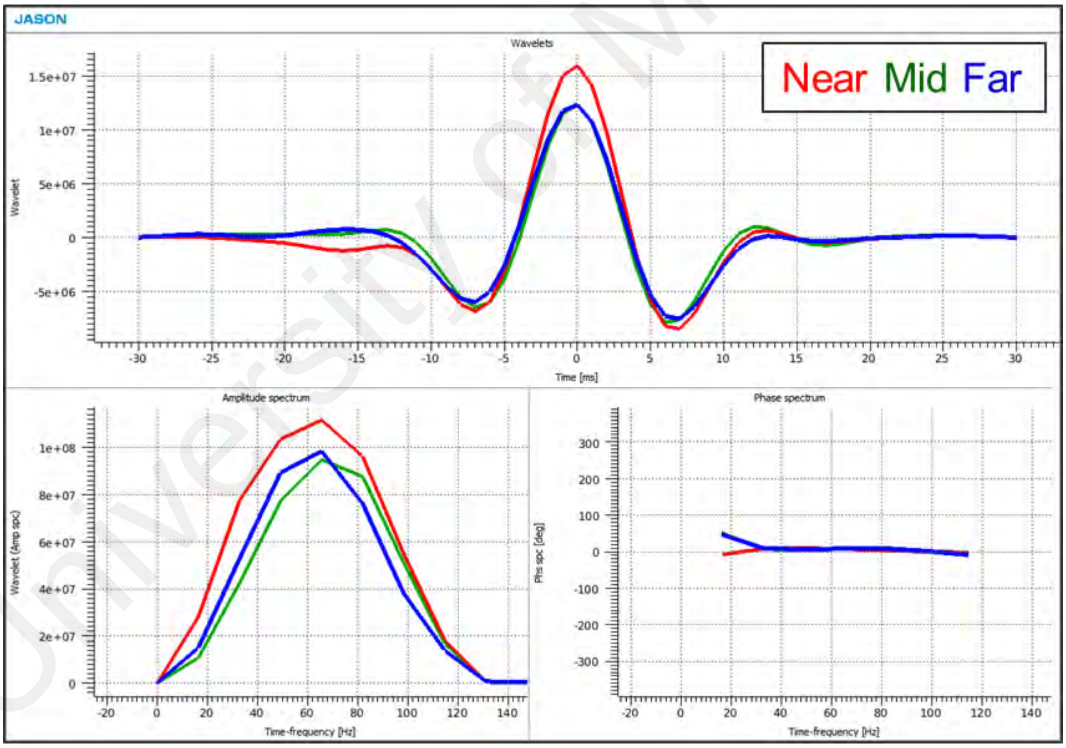

Figure 3.23: Composite of wavelets extracted from near, mid and far stacks from GD-1.

3.6.3 Low frequency model

In order to generate a structural framework, structure mapping was carried out. Global automated 3D horizon picking (Hoyes & Cheret., 2011) was used to produce seismic model grid and multiple horizons were used to generate structure model framework. Figure 3.24, Figure 3.25 and Figure 3.26 are structure time map of at the top of B1, B2 and B3 reservoir. Structure fault was not map because the fault throw in less than 100ms in the B-group has no significant impact to the low frequency model. Elastic properties from the GD-1 wells were extrapolated within the structure model to produce Vp, Vp/Vs and Density earth models. These models were then high-cut filtered to 12 Hz to produce low frequency model for input to seismic inversion process (see Figure 3.27).

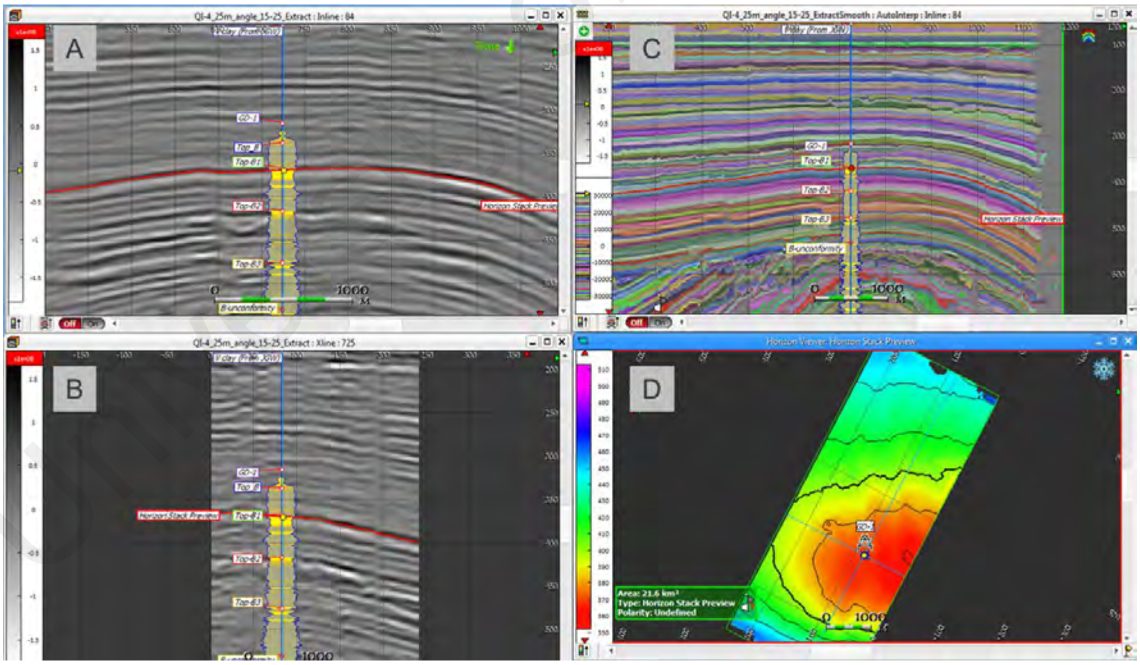

Figure 3.24: Seismic sections and interpreted horizon of top B-1 time map. A) Seismic at inline-84 across the GD-1 well with Vclay log, well formation tops and Top B-1 horizon. B) Seismic crossline 725. C) Relative Geological Time (RGT) model at inline-84. D) Top B-1 time structure map and GD-1 well location. Observe the Top B-1 reservoir map at the seismic peak, the well is located within structure crest.

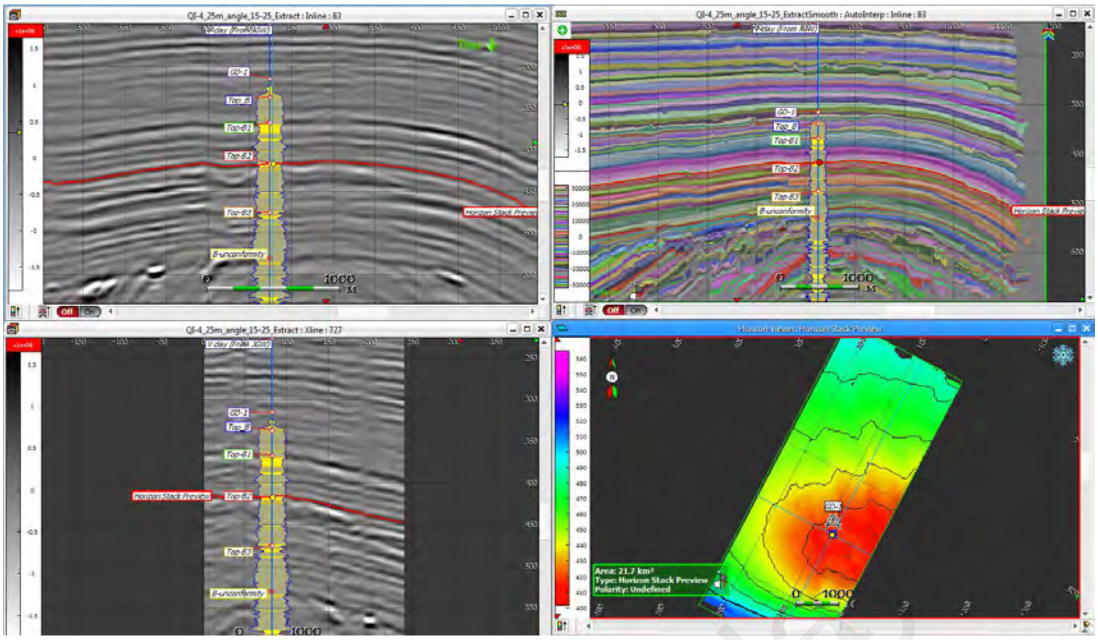

Figure 3.25: Seismic sections and interpreted horizon of top B-2 time map.

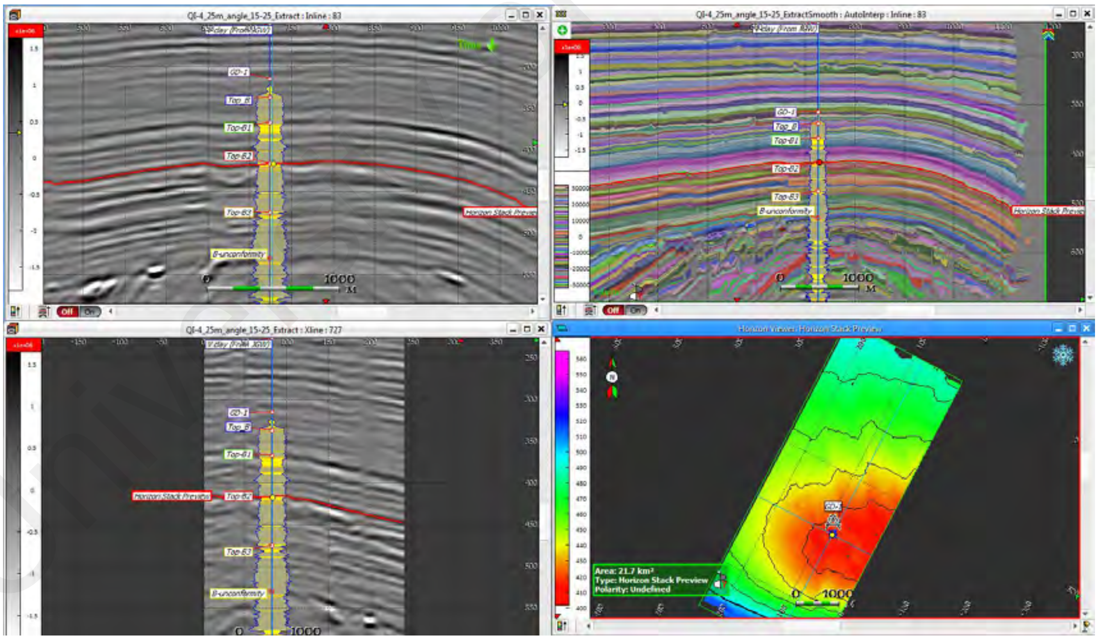

Figure 3.26: Seismic sections and interpreted horizon of top B-3 time map.

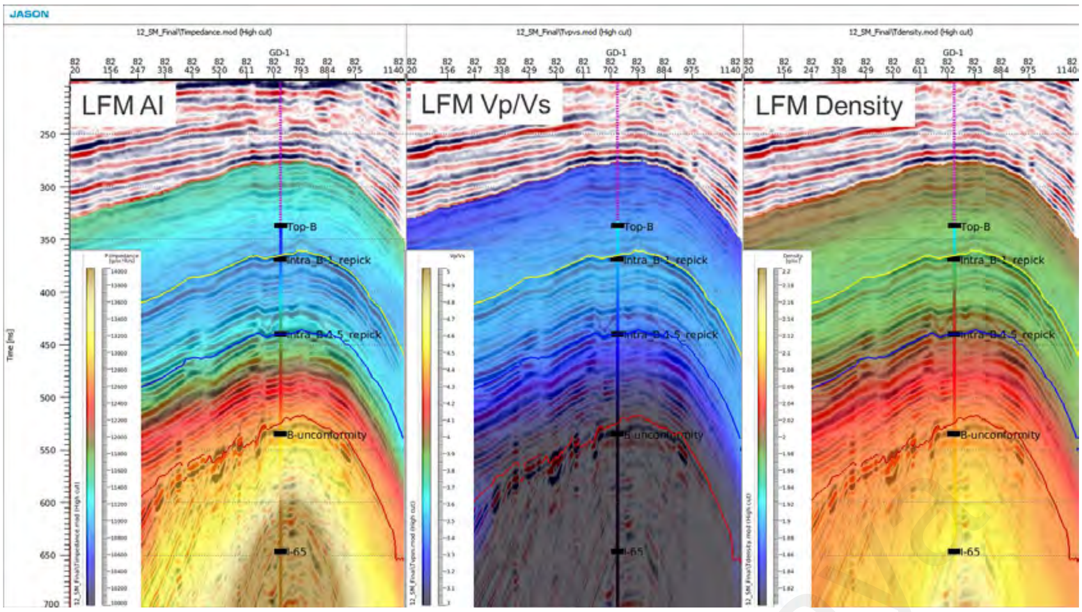

Figure 3.27: Cross section of low frequency model of AI, Vp/Vs and density.

3.6.4 Seismic Inversion and Quality Check

Simultaneous AVO/AVA Inversion builds on the CSSI technology by extending it to the offset (or angle) domain. In CSSI, the constraints applied are in terms of AI, Vp/Vs and density. An independent wavelet is used for each angle or offset volume used in the inversion algorithm.

The primary outputs are volumes of AI, Vp/Vs and density in full bandwidth (absolute) and bandlimited (relative) values. These volumes represent layer properties of the sub-surface and changes within the layer can often be related to changes in specific reservoir properties such as porosity, lithology and saturation.

The bandlimited volumes are useful as it is derived mainly from the seismic data; the influence of the low frequency model is negligible. While the full bandwidth traces can be compare directly to the elastic well logs at seismic resolution.

The inverted traces must be compared against the measured elastic logs to ascertain the quality of the inversion result. Good match of inverted trace with the well elastic log indicates good inversion quality. Figure 3.28 and 3.29 shows good match of inverted traces and well logs with cross-correlation value more than 70%, indicate to the high reliability of the inversion result.

The cross-section comparison between seismic and inverted traces give some visual comparison of the expected reflection continuity and preserved the structure information. Figure 3.30 shows continuity and preservation of the structure information in the inverted traces give higher confidence of the inversion result.

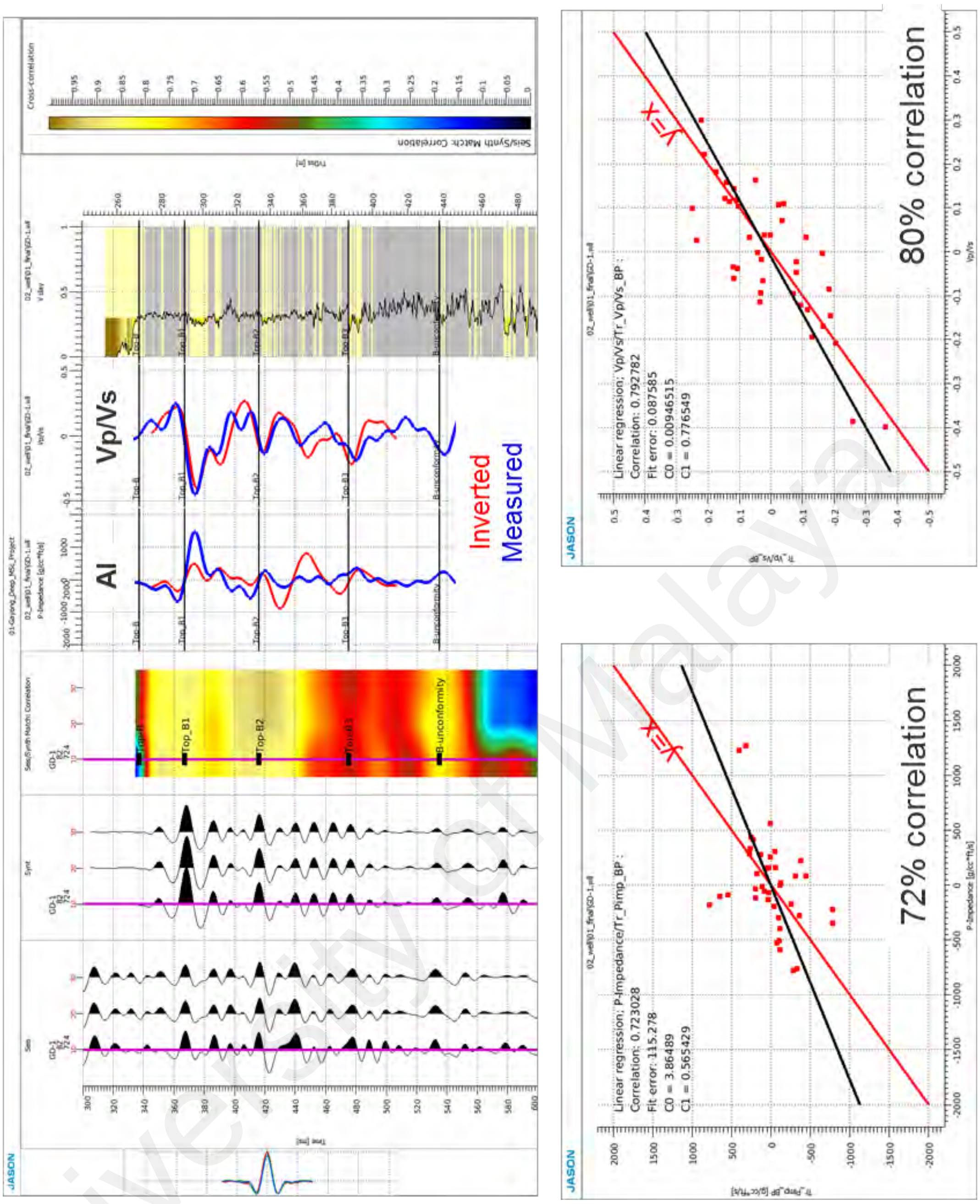

Figure 3.28: Well calibration and comparison of measured and inverted elastic logs at GD-1 well location at bandlimited bandwidth (relative domain).

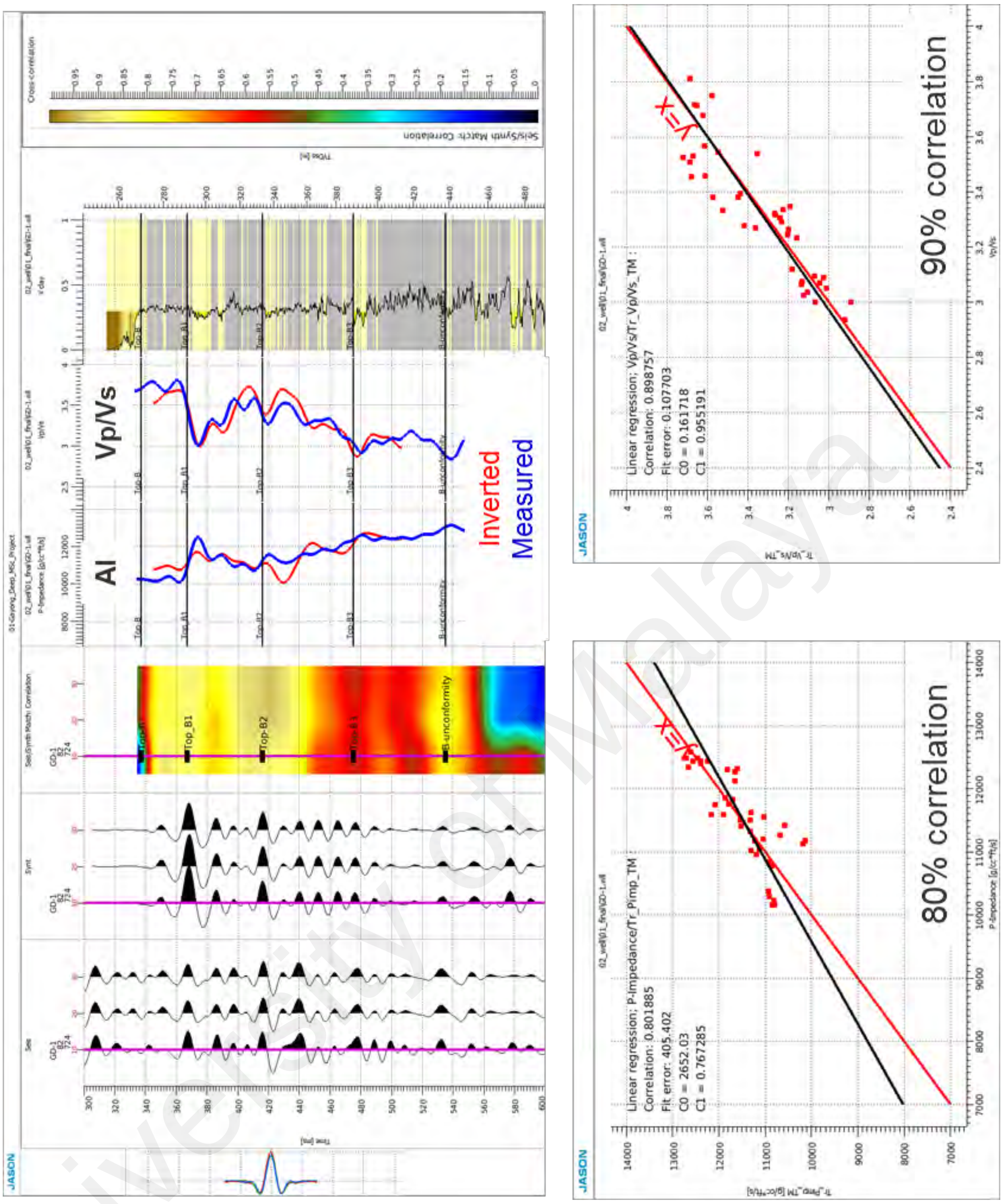

Figure 3.29: Well calibration and comparison of measured and inverted elastic logs at GD-1 well location at full bandwidth (absolute domain). The result showed high correlation of inverted and measured logs that give high confidence of inverted properties for interpretation and analysis away from the well location.

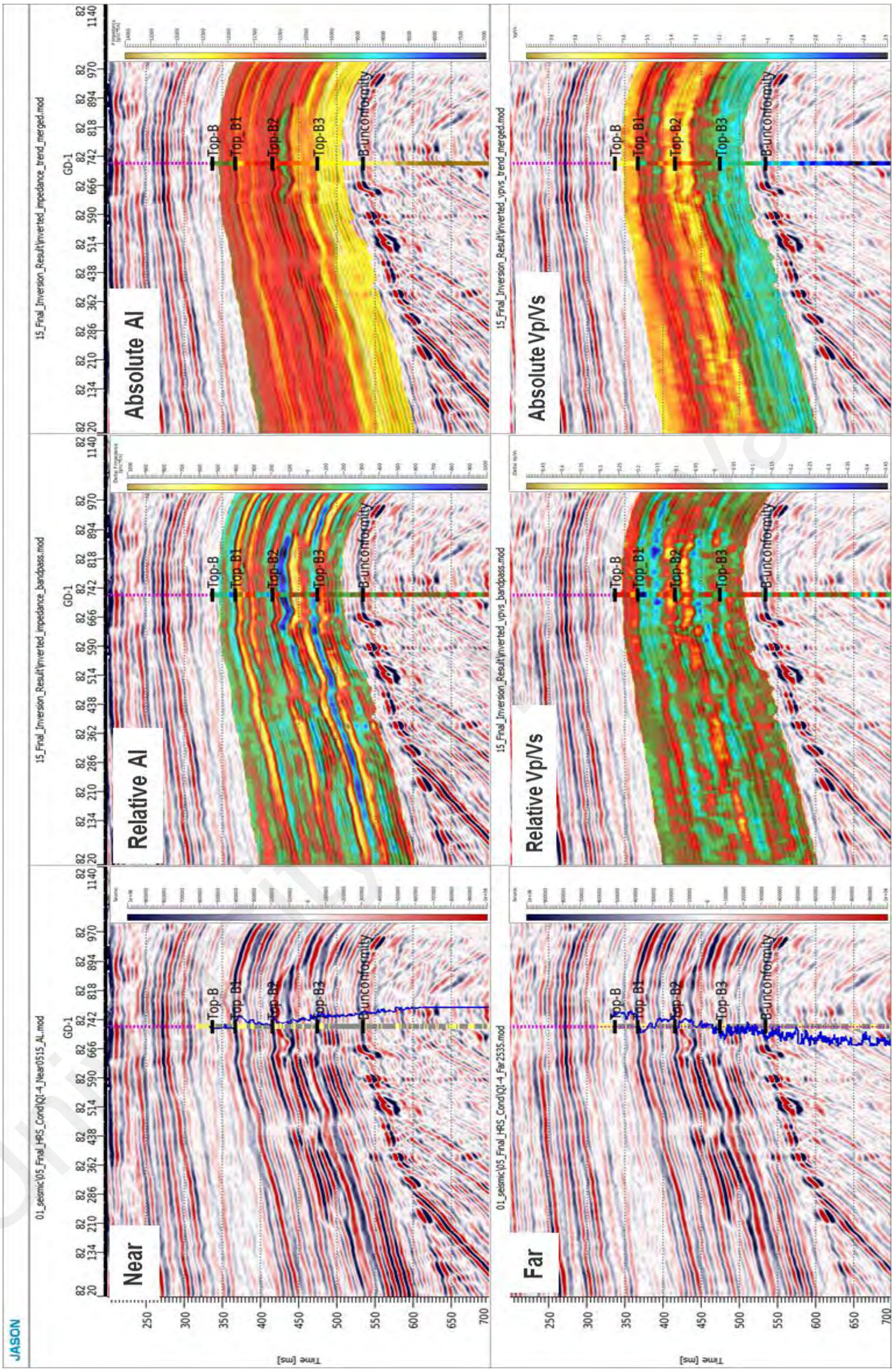

Figure 3.30: Cross section of seismic and inverted AI and Vp/Vs of bandpass (relative domain) and full bandwidth (absolute domain). Observe continuity of seismic reflectors and layers of inverted bandpass (relative) are similar. The inverted full bandwidth show two dominant contrast of AI and Vp/Vs are consistent with the low frequency trends in the figure 3.27.

3.6.5 Interpretation and analysis

Several interpretation methods and analyses were selected based on the following objectives:

I. To predict the lithology

II. To predict water saturation (if possible) and,

III. To predict reservoir pressure (if possible).

3.6.6 Analysis of cross plots and inversion results

Direct comparison of inverted traces with the modeled well log data in the calibrated rock physics template of AI-Vp/Vs able to give an initial interpretation of lithology (volume of clay), porosity, fluid type, hydrocarbon saturation and pore pressure (Figure 3.31). This direct interpretation of rock properties assumed that the depositional facies is constant throughout the whole study area. Data that falls within the modeled trend able to give an initial interpretation of the possible lithology, fluid, porosity and pressure. Figure 3.31 shows the inverted traces falls within the water bearing sand, shale and low saturation of oil sand (20% oil). This analysis result lead to several possible interpretations of lithology, fluid type and porosity.

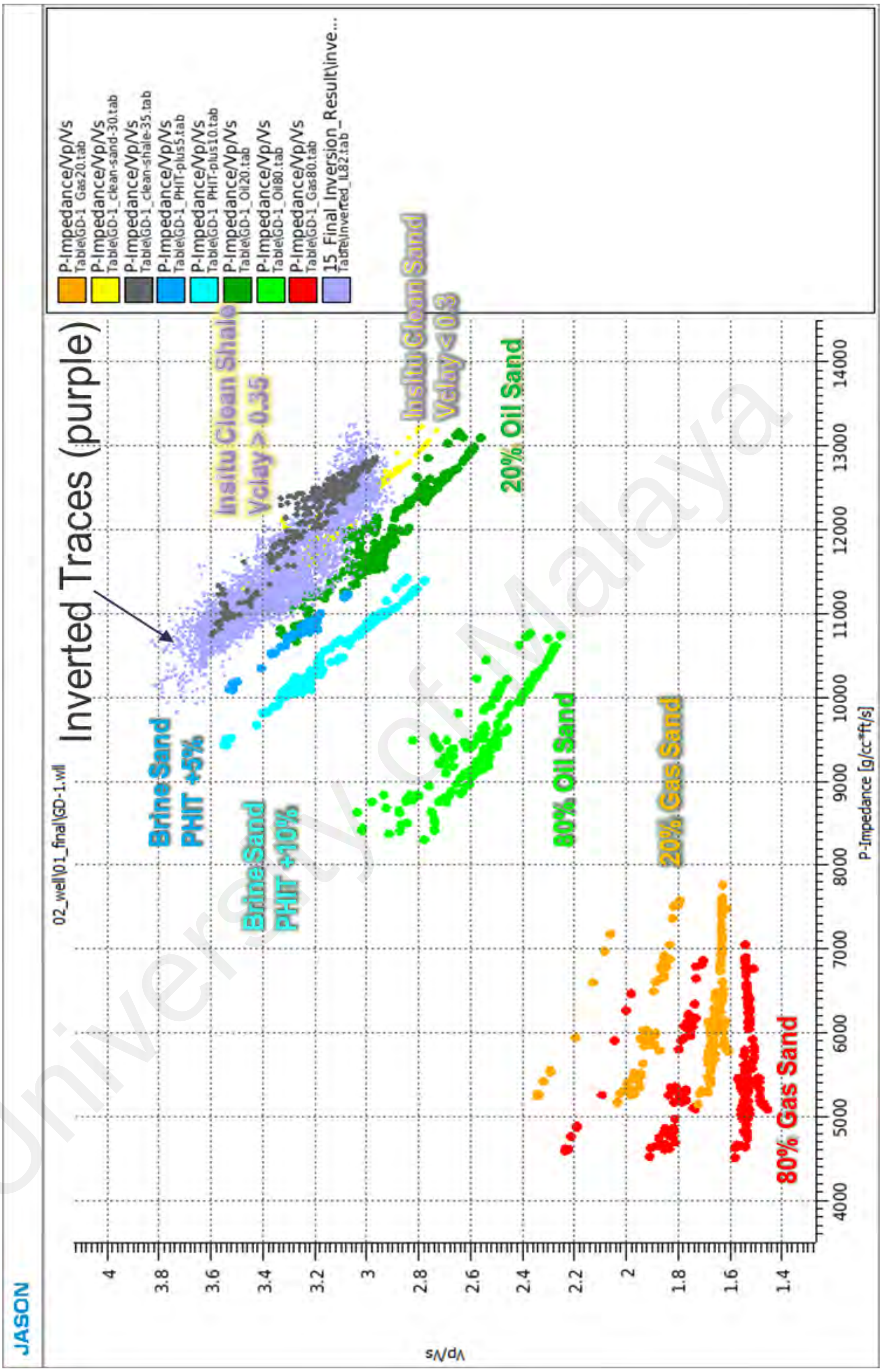

Figure 3.31: Localized AI – Vp/Vs rock physics template with modeled elastic-rock properties log. The inverted traces points are display in the purple color falls within the high porosity brine sand, clean shale and 20% oil sand.

3.6.7 Bayesian probabilistic method for lithology probability prediction

Quantification of lithology probability can be made using Bayesian probabilistic method. In this study, the prediction was made based on the well data distribution of sand and shale in the AI and Vp/Vs cross plot (Figure 3.32). Probability density function (PDF) of sand and shale generated based on the well data distribution. The PDF was applied to the well logs as initial QC to make sure the generated PDF is able to predict lithology at seismic resolution (Figure 3.33). The best PDF was then applied to the inverted traces to produce lithology probability volumes of sand, shale and most likely lithology volumes (Figure 3.34). Data outside the PDF is considered as undefined lithology.

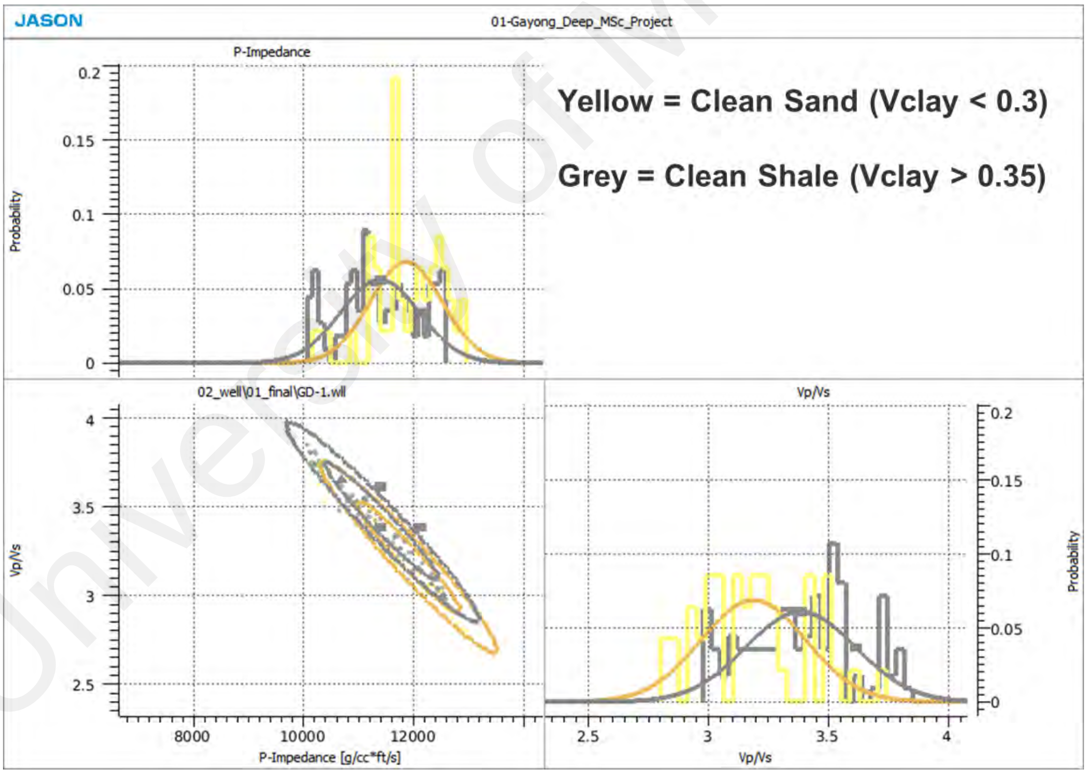

Figure 3.32: Histogram and Crossplot of AI – Vp/Vs color coded by lithology with probability density function (PDF) from GD-1 well data.

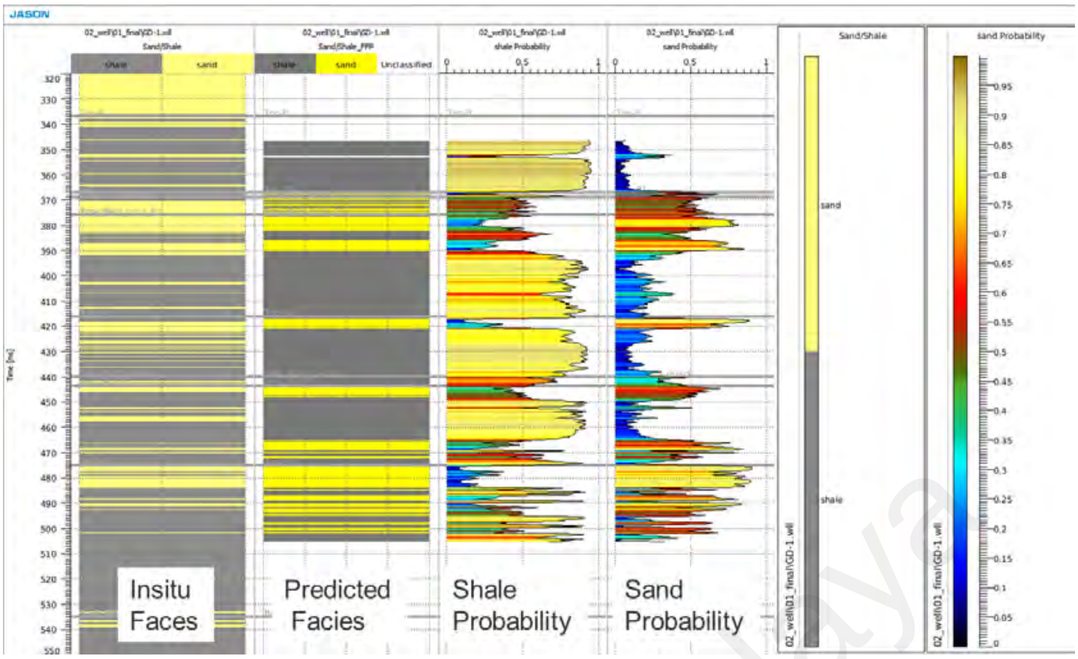

Figure 3.33: QC plot of actual and predicted lithology based on the established probability density function (PDF) at the GD-1 well location.

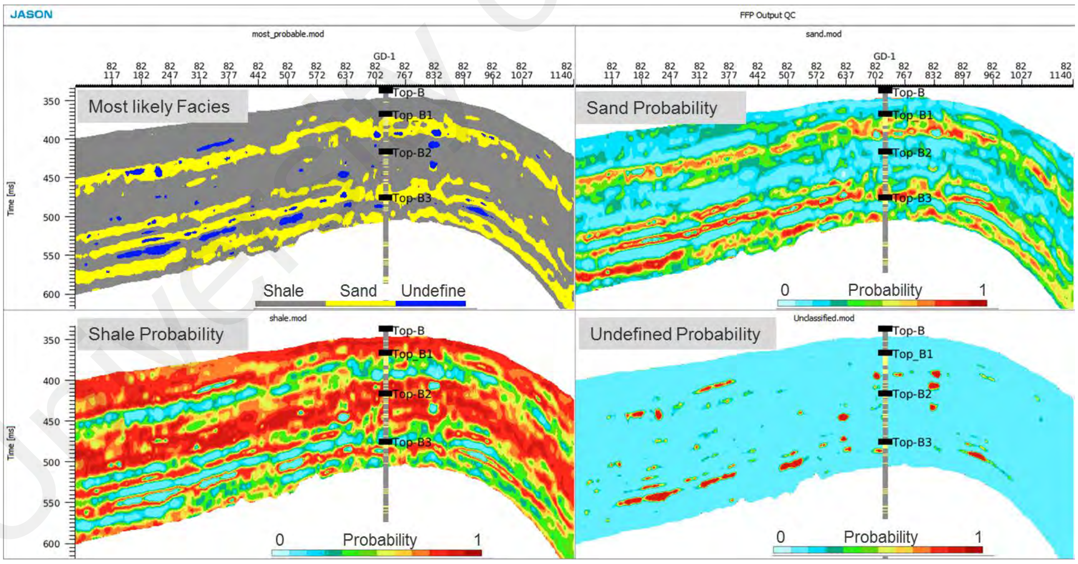

Figure 3.34: Predicted lithology probability sections and most likely lithology based on the established probability density function.

3.6.8 Porosity prediction

AI – Porosity relationship was established from the cross plot of AI and Porosity logs of GD-1 well within the B-group (Figure 3.35). Sand and shale are overlaps in the AI - porosity trend. Thus, AI – Porosity relationship was established as a single linear function for both sand and shale as the equation below;

$$PHIT = (-3.95352e - 5 * AI) + 0.803496$$

Where,

AI = Acoustic Impedance (g/cc*ft/s)

PHIT = Estimated porosity total

The porosity volume can be used to delineate reservoir porosity away from the calibrated well (Figure 3.36).

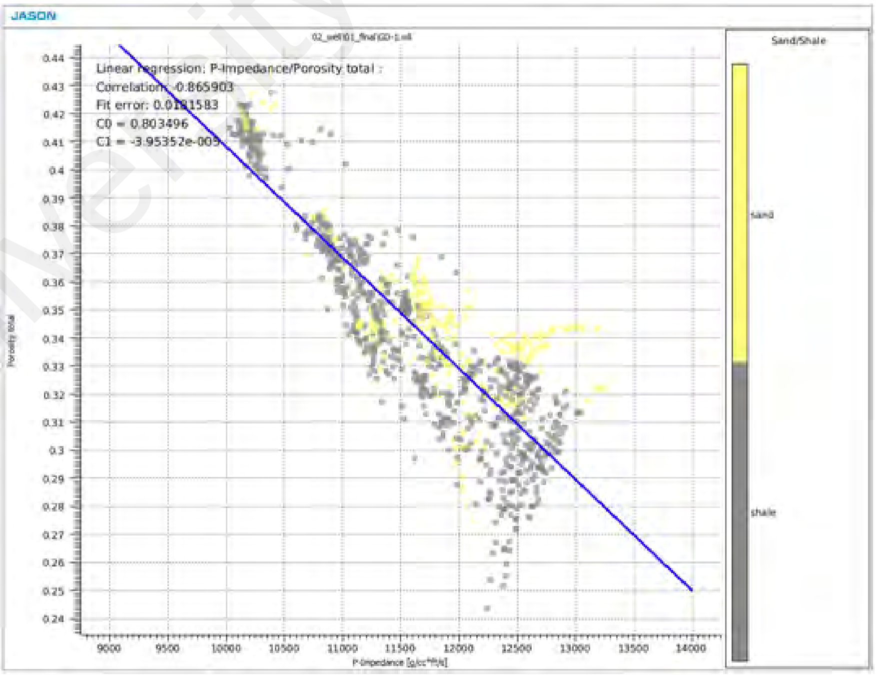

Figure 3.35: Cross plot of AI and porosity total, color-coded by lithology.

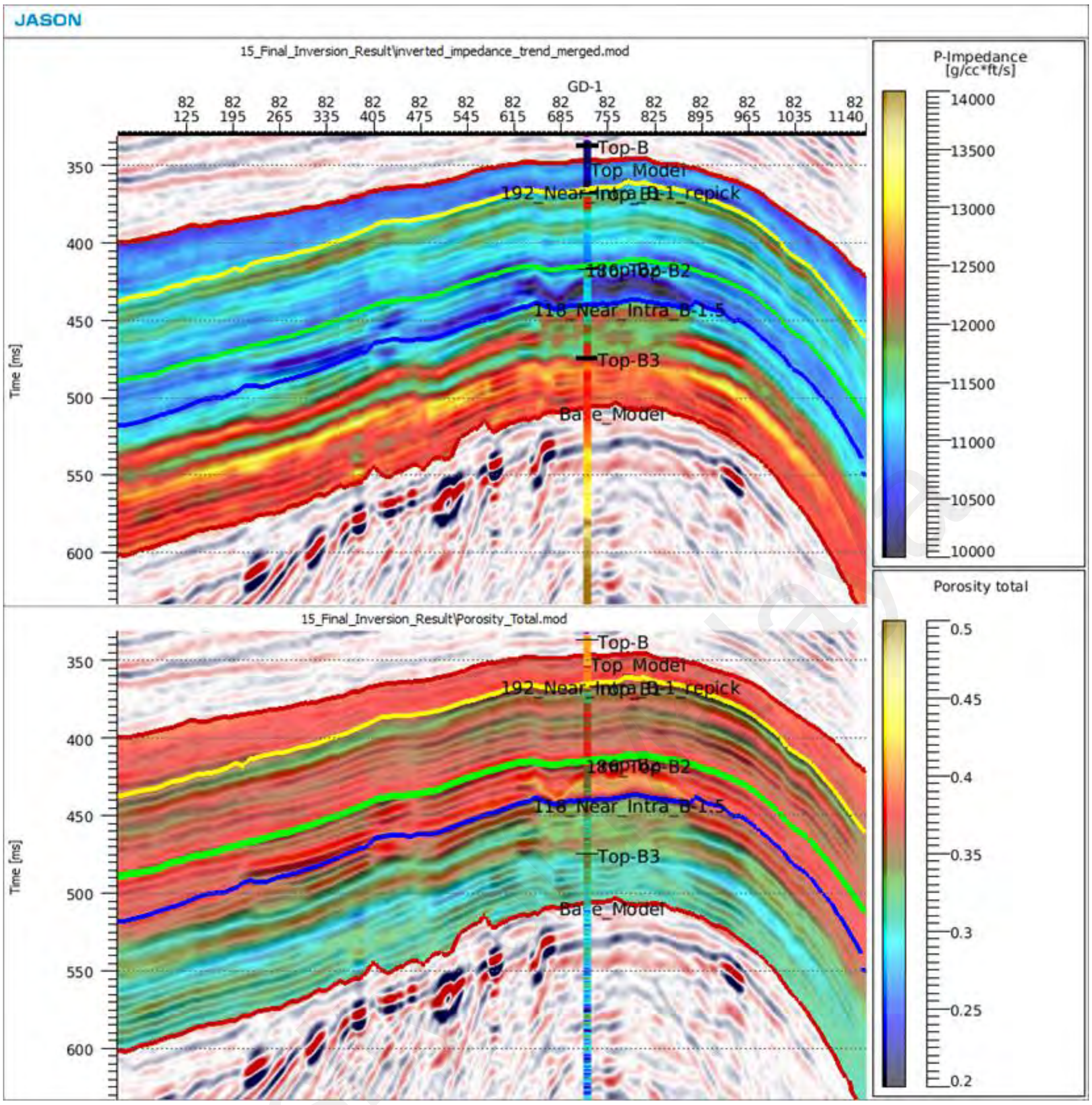

Figure 3.36: Acoustic Impedance section across GD-1 well (Top). Porosity total section across GD-1 (Bottom).

CHAPTER 4: RESULTS AND DISCUSSION

This chapter summarizes the result of each important element of this study and synthesized the analysis result through discussion towards the main research objectives. Data QC and conditioning results presented in the section 3.1 have indicated that the unconventional data of input sonic logs and the pseudo3D are feasible for AVO and inversion studies.

In this chapter, the analysis of result through rock physics modeling, AVO and inversion analysis is intended to discuss more on the reliability and the sensitivity of the unconventional input data for seismic reservoir characterization analysis for shallow gas project (see Chapter 1.1: Background and problem definition).

4.1 Rock and elastic properties of B-group unconsolidated sediments in the pilot study area

Rock physics modeling study through various perturbations of fluid type, hydrocarbon saturation, porosity, pore pressure and clay volume at the GD-1 well provide an understanding of rock and elastic properties relationship of the unconsolidated sediments in the area of interest. The result allowed the quantification of the sensitivity of elastic properties to these changes, and the expected elastic properties trend when deposited at different depositional facies. The results of each rock property perturbations are captured in the Appendix-D.

All the modeled rock-elastic properties logs were first analyzed in an AI-Vp/Vs crossplot. This is the crossplot representing localized rock physics template of unconsolidated sediment, calibrated at the GD-1 well. Figure 4.1a shows the conceptual trends for siliciclastic lithologies at constant confining pressures (Odegaard & Avseth, 2004). This can be compared with the actual localized trend obtained in this study,

Figure 4.1b where the absolute value has enabled us to quantify the property changes. Significant changes of AI and Vp/Vs can be observed from 80% oil, 20% and 80% gas as compared to the *in situ* condition (100% brine). Gas reservoir has greater impact on the elastic logs, regardless of gas saturation. The gas reservoir has very low AI and Vp/Vs with distinctive separation from others. However, in the oil case, the oil saturation is important as the 80% oil saturated has better separation as compared to 20% oil, see Figure 4.1c. Other rock properties did not give significant difference in elastic properties, but their changes follows the conceptual trend that can be used for seismic inversion interpretation (see Figure 4.1d – 4.1f).

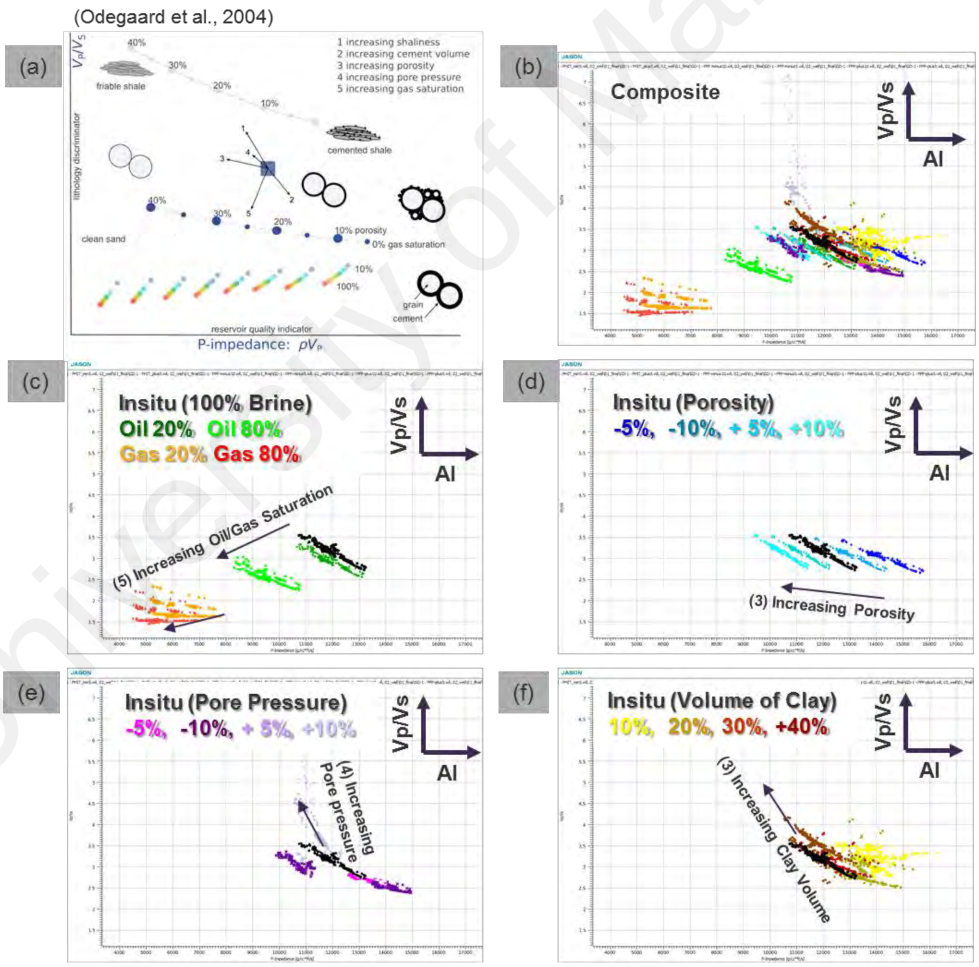

Figure 4.1: Comparison of conceptual (a) and localized (b-f) AI-Vp/Vs rock physics templates. The template for b – f are derived through rock physics modeling from various property perturbation at GD-1 well.

The sensitivity analysis of the rock-elastic properties was then carried out using seismic forward modeling. Synthetic seismic amplitude values at *in situ* condition were compared to the synthetic seismic amplitudes derived from the modeled logs at three different angle stacks (near, mid and far). Figure 4.2 shows an example of the seismic amplitude response at 20% and 80% of gas saturated sediments as compared to 100% brine saturated. The amplitude difference is significant and the seismic polarity flipped from peak to trough (at observed of time 440ms). However, in the case of porosity perturbation at 100% brine, the 5% and 10% increase of porosity did not give significant amplitude difference. Instead of amplitude brightening, the resultant amplitudes are dimming (Figure 4.3). This is because the *in situ* sand has high AI value as compared to the encasing shale. Increasing the porosity reduced the AI property of sand, and hence reduced the reflection coefficient contrast.

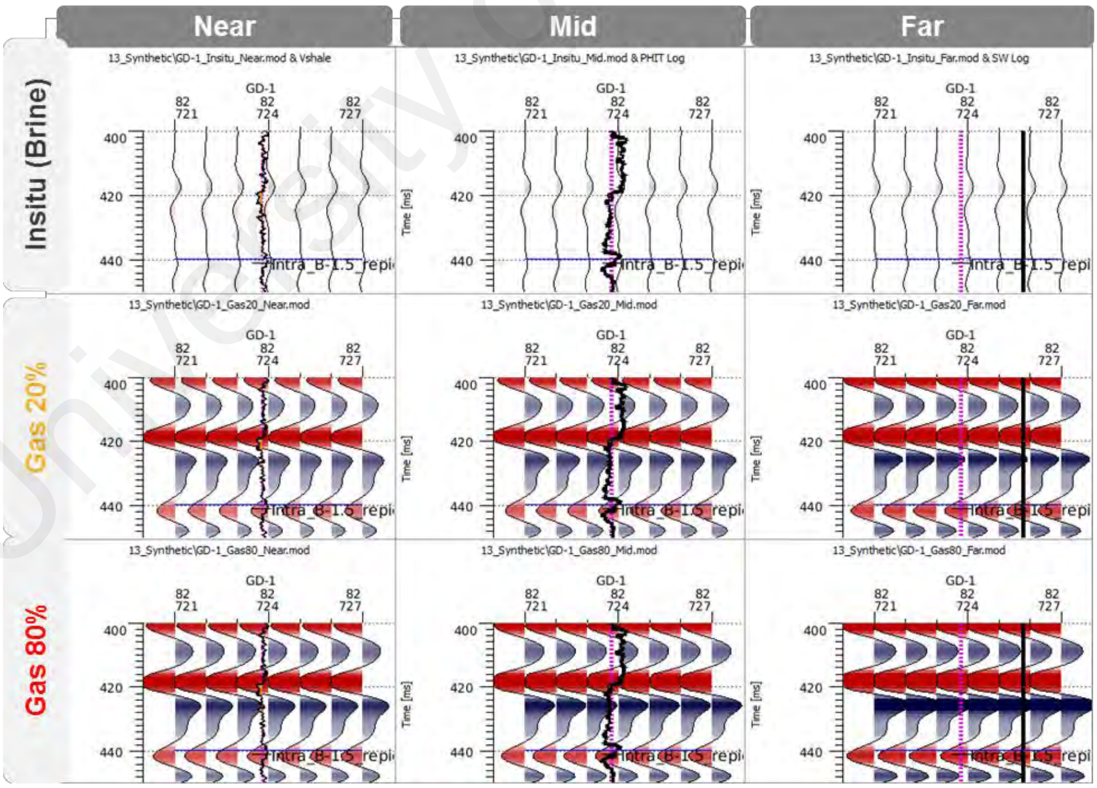

Figure 4.2: Synthetic seismic forward model responses for 20% gas and 80% gas. Observed significant amplitude brightening with gas.

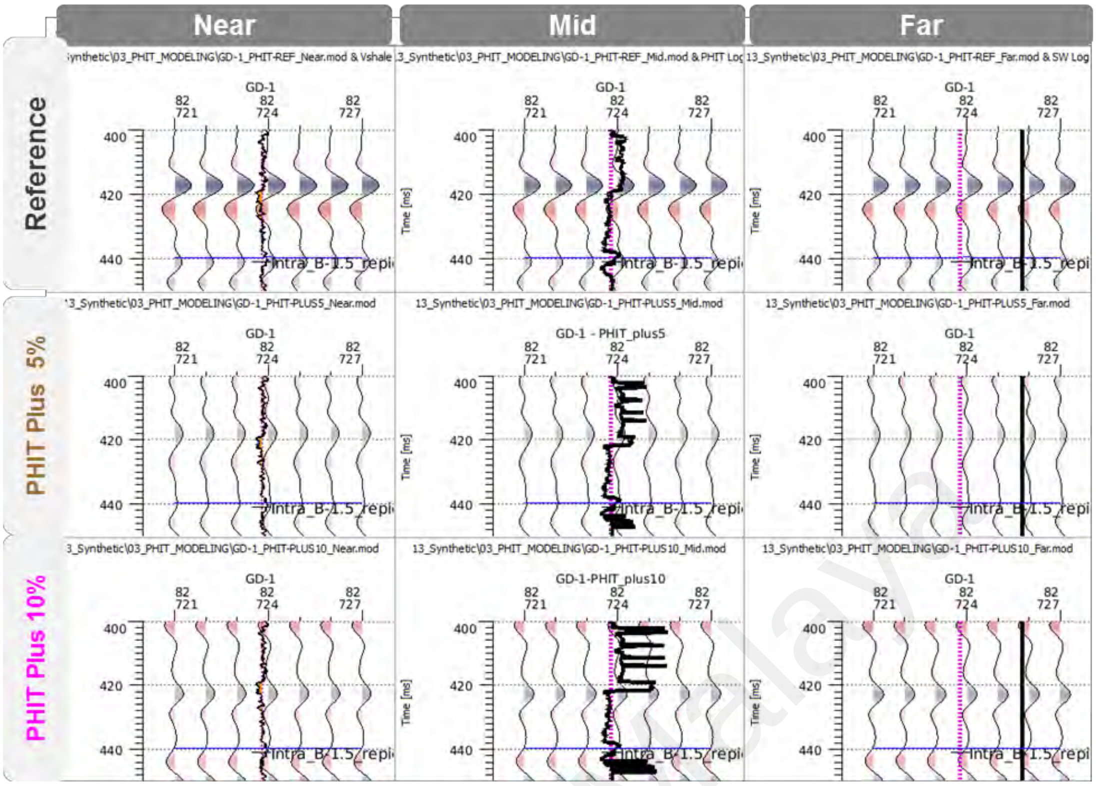

Figure 4.3: Synthetic seismic response at near, mid and far of *in situ* porosity, +5% and +10%.

Quantification of the amplitude changes and sensitivity ranking of rock properties to seismic amplitude were analyzed through histogram plots. The amplitude differences between the modeled and *in situ* seismic at each angles stacks were averaged in percent. Figure 4.4 shows the amplitude difference (%) for all the modeled scenarios. This histogram depicts that changes from 100% brine to 80% gas-filled sand should increase the seismic amplitude value by 1400 times; while 20% gas-filled, the amplitude increment is 1200 times. In the scenario of 80% oil-filled reservoir, the seismic amplitude is expected to be 400 times higher. This amplitude difference method enables us to quantify the expected seismic amplitude for gas or high saturation oil away from the calibrated well, assuming they are sharing the same reservoir properties. Instead of a general statement that the amplitude brightness at the prospect is due to the gas response, an interpreter can compare the amount of amplitude difference at the given prospect with seismic amplitude at the calibration well with 100% brine reservoir for the same stratigraphic unit and depth equivalent. The gas prospect should have amplitude within the ranges of the modeled gas. If the amplitude is less than the seismic amplitude of the modeled gas, this amplitude changes could be representing other scenarios such as different facies, pore pressure, etc. Seismic geomorphology should enable us to streamline the possible scenarios.

The sensitivity of rock properties to seismic amplitude was assessed by ranking the average relative amplitude changes to the brine sand (*in situ* condition). Figure 4.5 presents the seismic amplitude sensitivity ranking of the modeled scenarios. In this plot, the top most sensitive are 80% and 20% gas saturated, reduction of 10Mpa pore pressure and 80% oil saturated. Although the reduction of 10 Mpa pore pressure and 80% oil saturated have similar sensitivity ranking, their seismic polarity response have opposite directions. This can be clearly seen from an Amplitude versus Offset (AVO) cross plot in Figure 4.6; the 80% saturated sand has negative reflection with AVO class II response, while the reduction of 10 Mpa pore pressure has positive reflection with AVO class I. In this cross plot, seismic polarity reversal can be expected when the reservoir is 20% gas-filled, 80% gas-filled and 100% brine-filled with 10% porosity increment. Gas sand shows class III AVO response.

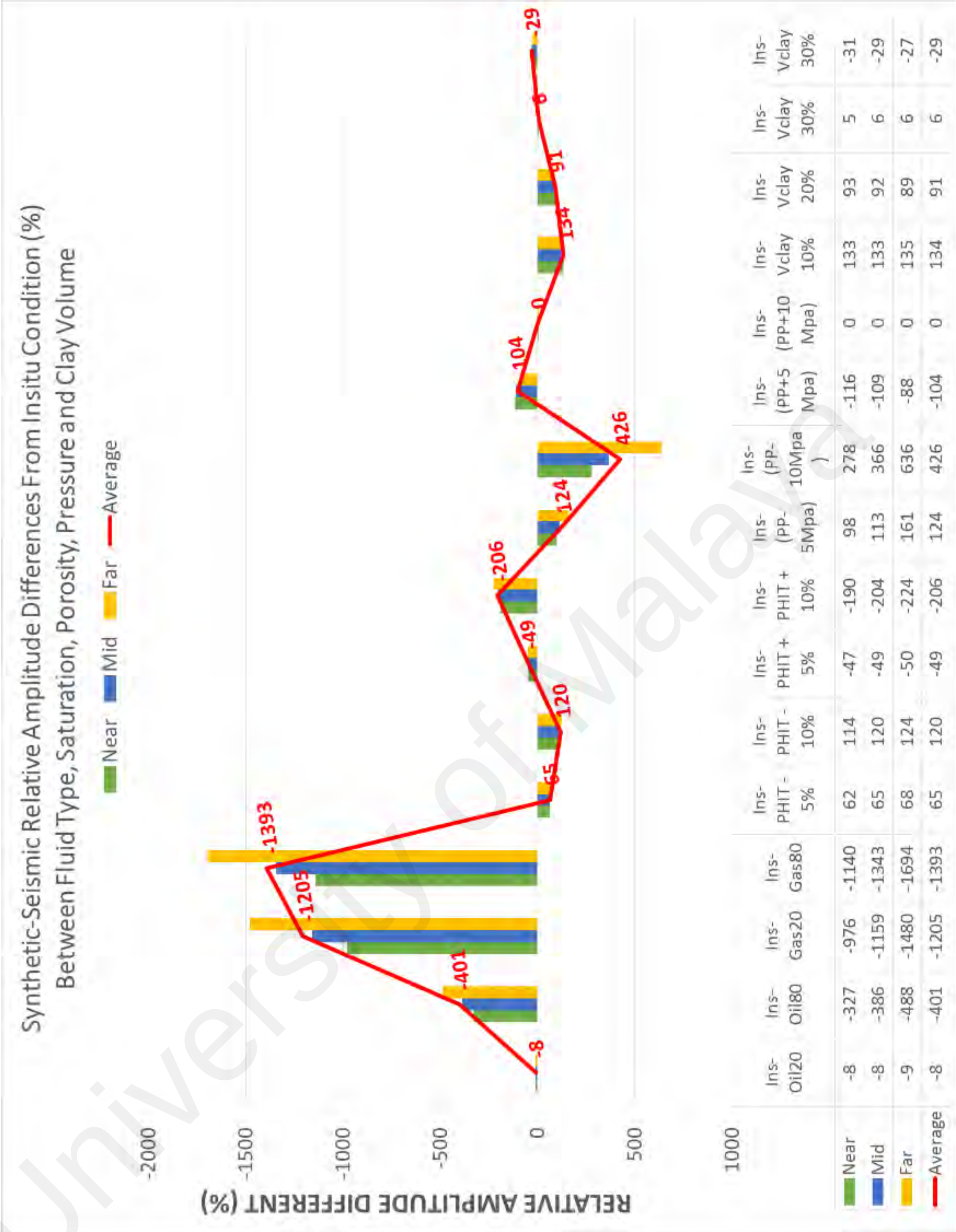

	Ins-Oil20	Ins-Oil80	Ins-Gas20	Ins-Gas80	Ins-PHIT - 5%	Ins-PHIT - 10%	Ins-PHIT + 5%	Ins-PHIT + 10%	Ins-(PP-5Mpa)	Ins-(PP-10Mpa)	Ins-(PP+5 Mpa)	Ins-(PP+10 Mpa)	Ins-Vclay 10%	Ins-Vclay 20%	Ins-Vclay 30%	Ins-Vclay 30%
Near	-8	-327	-976	-1140	62	114	-47	-190	98	278	-116	0	133	93	5	-31
Mid	-8	-386	-1159	-1343	65	120	-49	-204	113	366	-109	0	133	92	6	-29
Far	-9	-488	-1480	-1694	68	124	-50	-224	161	636	-88	0	135	89	6	-27
Average	-8	-401	-1205	-1393	65	120	-49	-206	124	426	-104	0	134	91	6	-29

Figure 4.4: Histogram of relative seismic amplitude differences from synthetic seismic angles stack of all forward model analysis

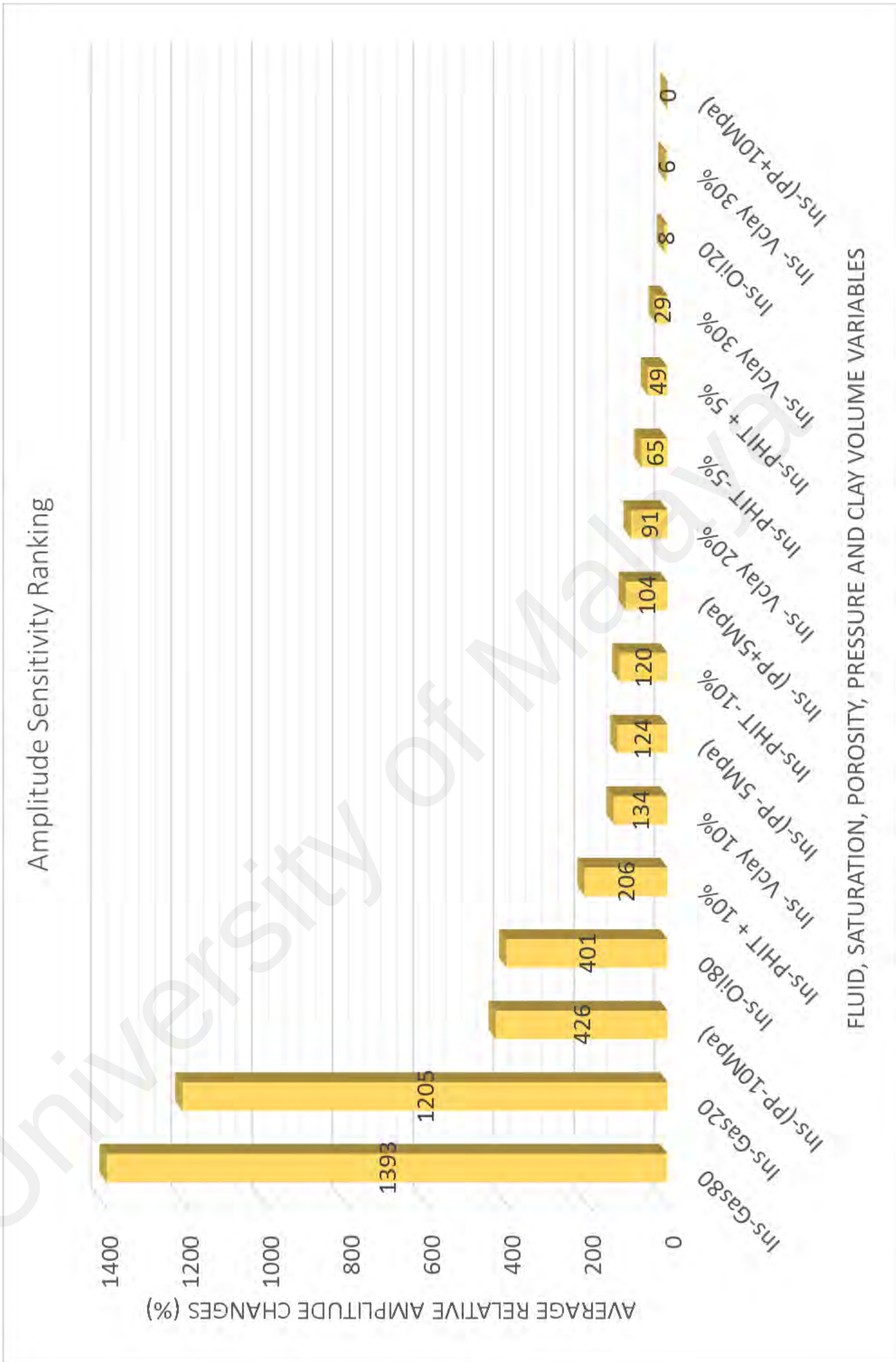

Figure 4.5: Histogram of average amplitude changes from all the synthetic seismic stacks for amplitude sensitivity ranking.

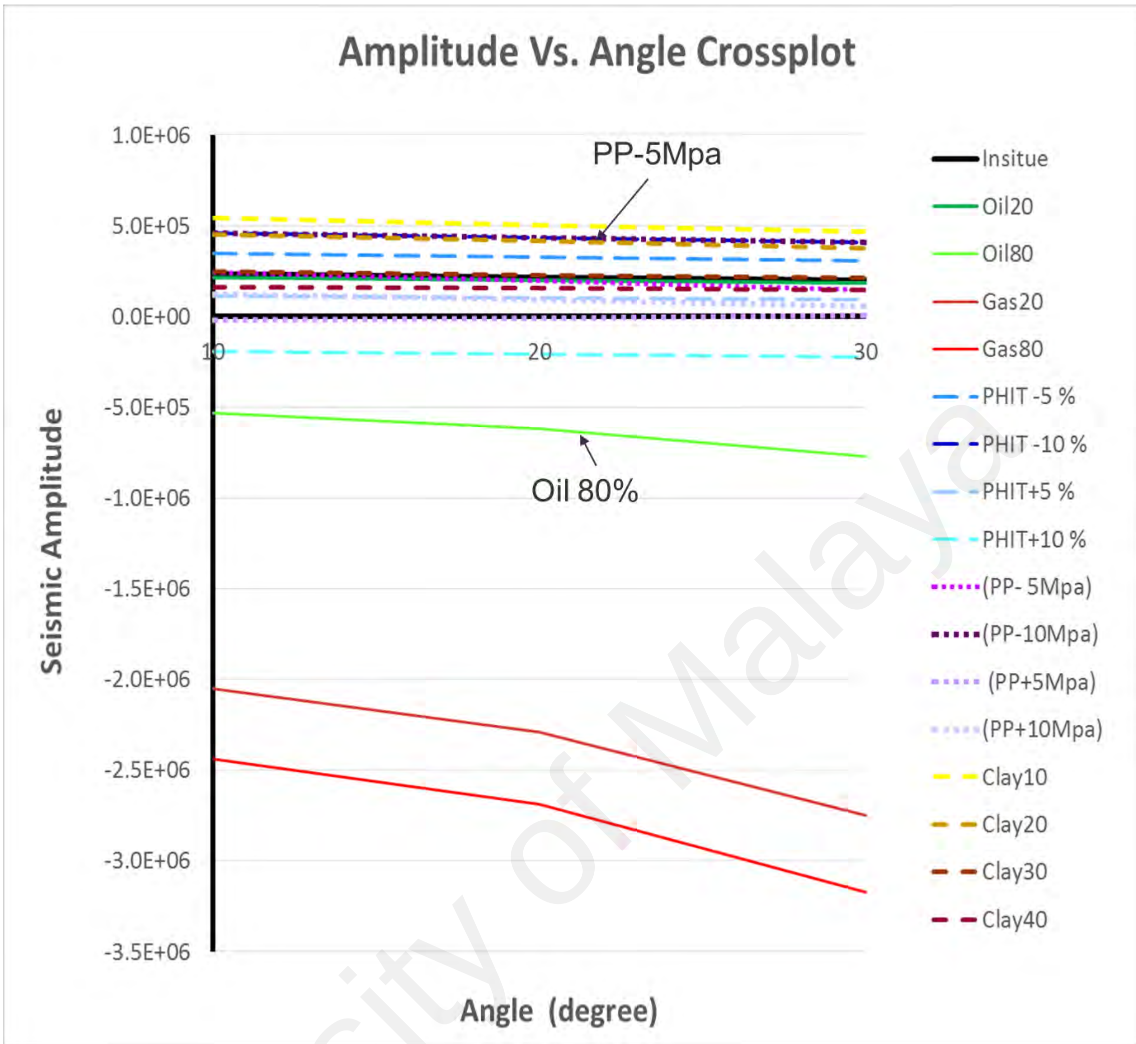

Figure 4.6: AVO crossplot summary shown is a composite of modeled synthetic seismic response from various perturbations.

4.2 Suitability of site survey seismic data for AVO and Inversion study

The conditioned seismic site survey data showed a consistent amplitude response with angles as demonstrated in the section 3.2. In order to ascertain the suitability of this site survey data for AVO and inversion study, a comparison between the measured seismic gather and synthetic seismic gather was made. In Figure 4.7, the well-to-seismic tie showed a good match. The amplitude variation with offset at each top of reservoir shows consistent AVO class between the two datasets. AVO response at top B-2 and B-3 of the synthetic and the fall on top or closer to each other, indicate the seismic data to be of in very good quality. This supporting QC plots give high confidence on the AVO and inverted traces, and good quality predictions from seismic reservoir characterization analysis are expected.

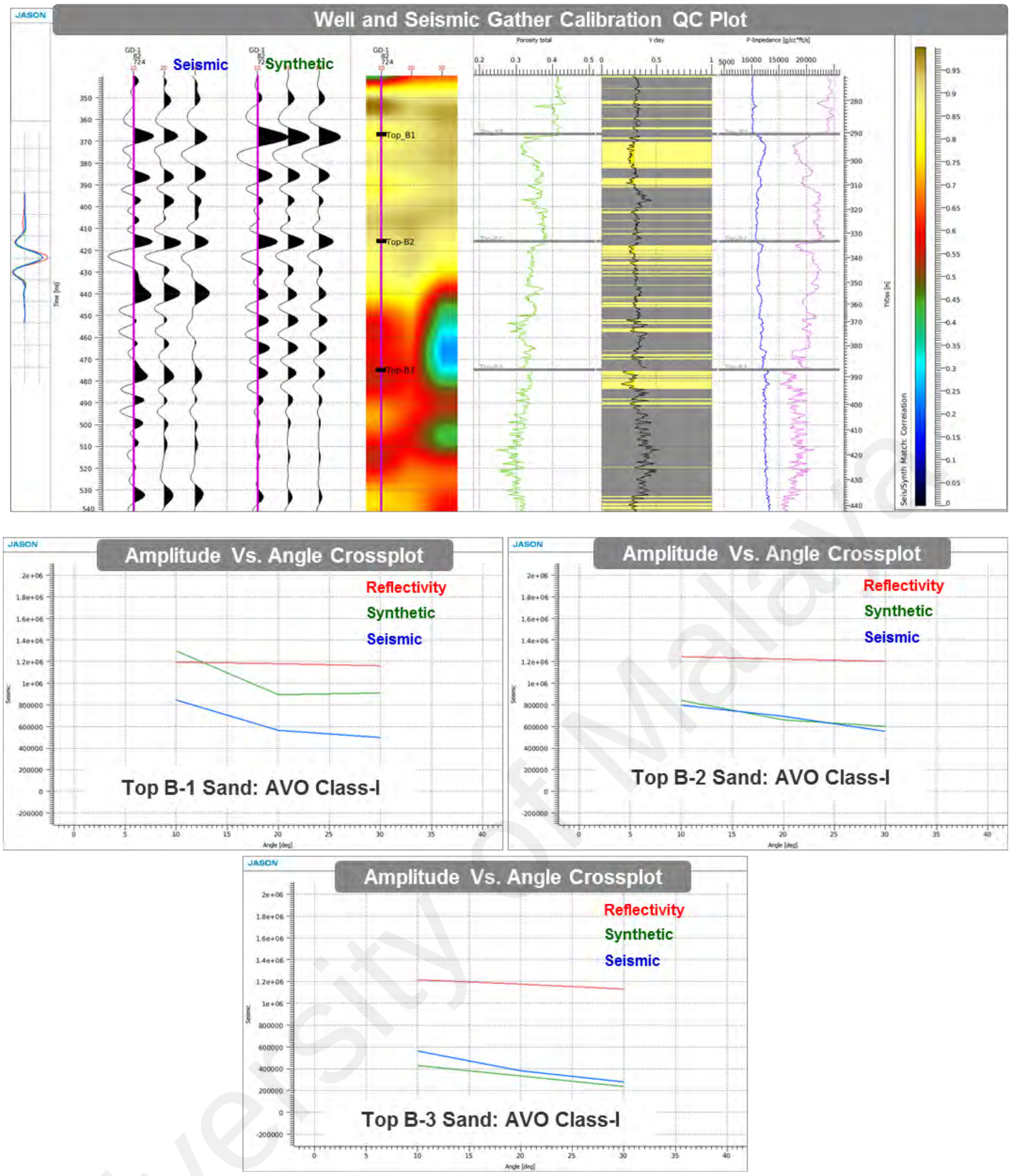

Figure 4.7: GD-1 synthetic and seismic gathers calibrations. Shown is the AVO crossplot for top sand for B1, B2 and B3 reservoirs.

4.3 Seismic reservoir prediction of lithology, porosity, fluid and pressure through forward model and inverted seismic

In the previous chapter, a first interpretation can be made by overlaying the inverted data on the localized AI-Vp/Vs rock physics template, as demonstrated in section 3.6.5 and Figure 3.31. The inverted data falls within the high porosity brine sand, 20% oil sand and shale. This first interpretation analysis indicates the lack of gas sand and normal pore pressure condition. This interpretation is consistent with the GD-1 well findings. Thus the interpretation analysis for reservoir characterization of this area only focus on the lithology and porosity predictions. Composite sections across GD-1 well of the seismic, inverted AI, inverted Vp/Vs, sand probability, shale probability, most likely facies and porosity total are derived from the site survey seismic data (Figure 4.8) and the good match with the well data give affirmation on the suitability of the site survey data for AVO inversion.

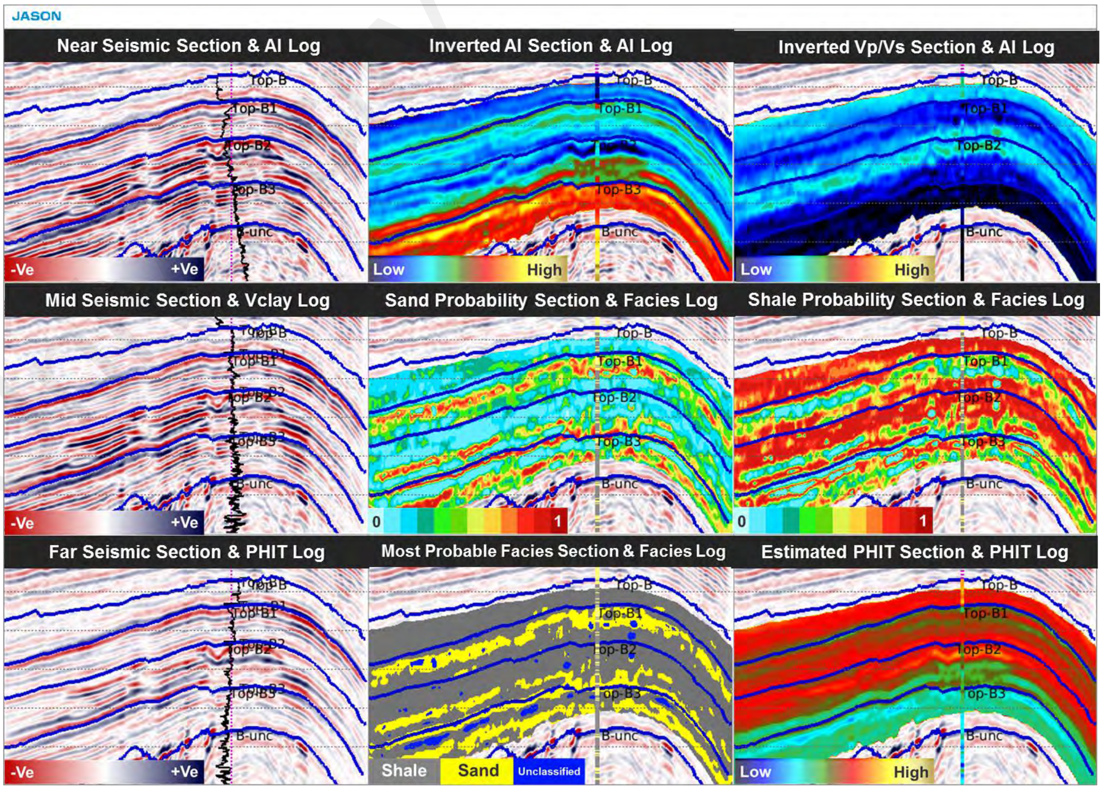

Figure 4.8: A composite section of input seismic, inverted traces and predicted lithology and porosity.

The analysis of result is extended by integration of advanced seismic attributes and predicted result for shallow gas pilot study of seismic reservoir characterization analysis at four levels of interest. Figure 4.9 is a composite analysis at the top of B-1 sand. The predicted sand match with the well result is satisfactory. On the map view, this well is located within the high porosity sand area, where the sand probability attribute is almost conformable with structure closure. The result of the forward model analysis has demonstrated that high porosity sand can produce reversed polarity response. The areal distribution of the high porosity sand confirm that the reservoir is heterogeneous. Hence, the seismic amplitude being conformable with structure closure is more likely due to facies change.

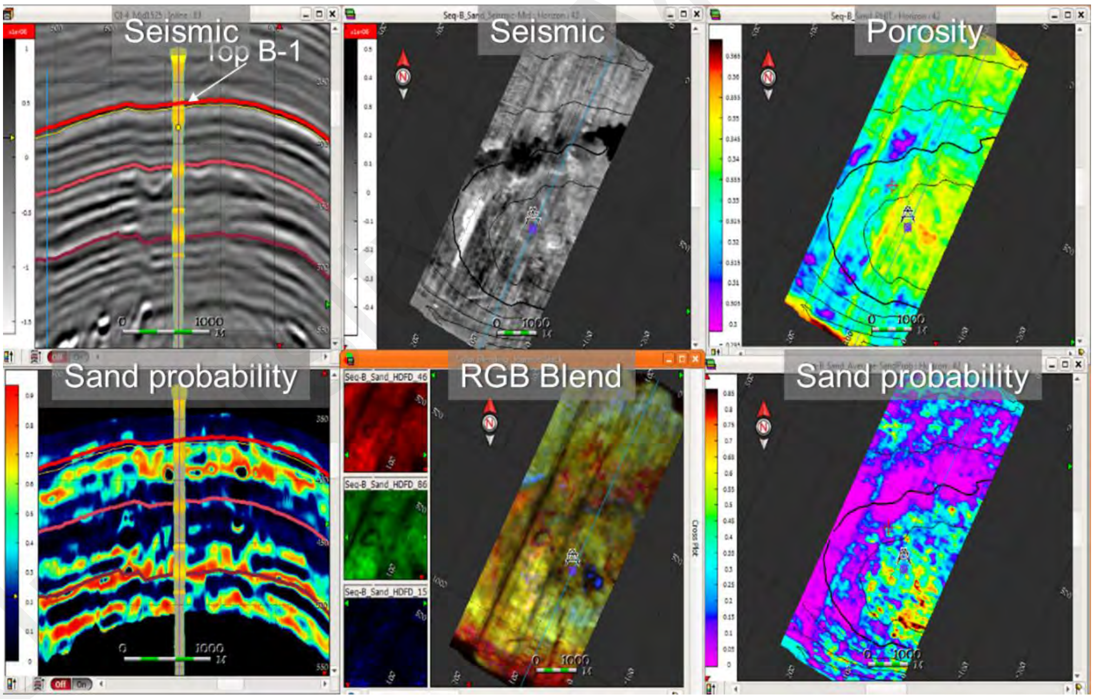

Figure 4.9: B1 sand reservoir characterization analysis. Top left: Seismic section with volume of clay log at GD-1 well, top sand horizons. Top middle: seismic amplitude on the horizon. Top right: Porosity map (PHIT). Bottom left: Sand probability section. Bottom middle: RGB color blend of decomposed frequency map extracted on the horizon. Bottom right: sand probability map extracted on the horizon.

The result of the analysis at Top B-2 shows NW-SE fault segments can be clearly observed from seismic and frequency decomposed RGB blend maps. The NE-SW lines that parallel to seismic acquisition shooting direction are artificial response which was not removed during the processing and conditioning of the seismic data. The sand quality is lesser compared to B-1 reservoir and higher heterogeneous.

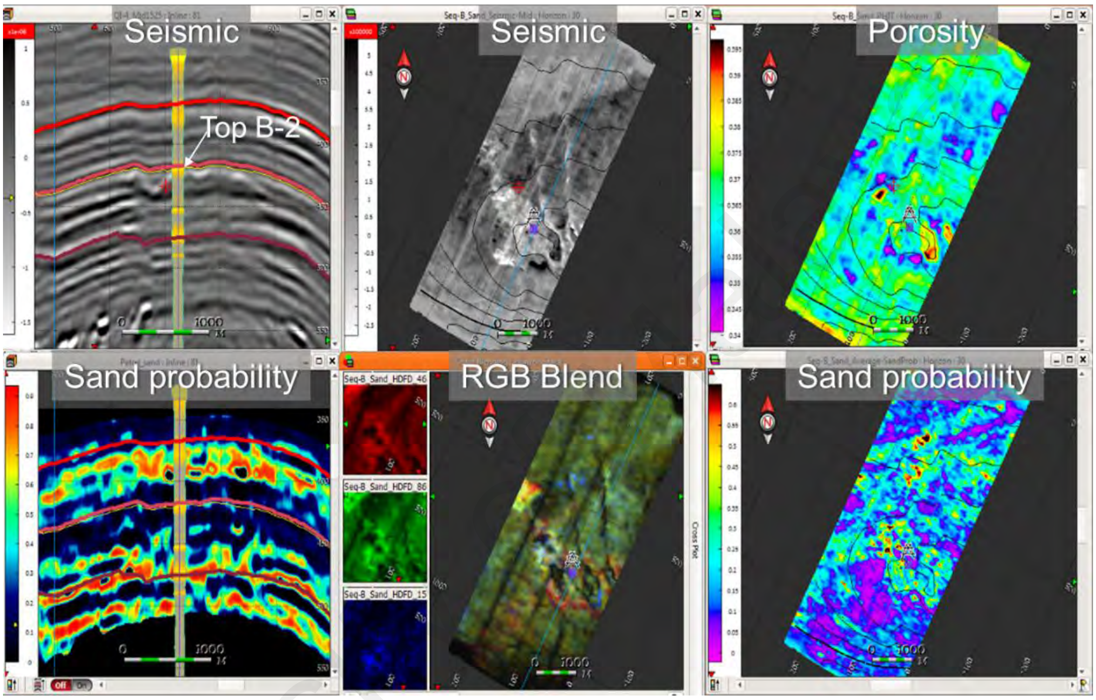

Figure 4.10: B2 sand reservoir characterization analysis. Top left: Seismic section with volume of clay log at GD-1 well, top sand horizons. Top middle: seismic amplitude on the horizon. Top right: Porosity map (PHIT). Bottom left: Sand probability section. Bottom middle: RGB color blend of decomposed frequency map extracted on the horizon. Bottom right: sand probability map extracted on the horizon.

The significant result of the analysis at Top B-3 shows NW-SE fault segments can be clearly seen in the seismic and frequency decomposed RGB blend maps. The RGB blend map also shows a low frequency trend in NE-SW direction indicating of possible different orientation of depositional facies trend. This interpretation is supported by NE-SW high porosity sand trend while the sand probability show wider spread of possible sand.

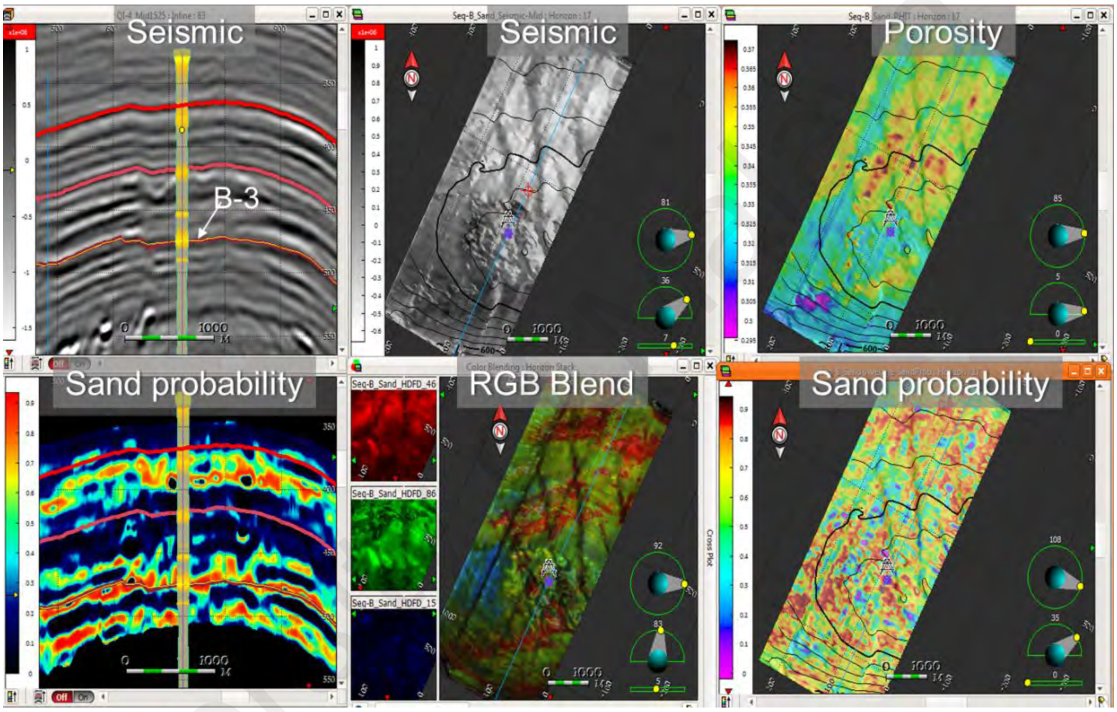

Figure 4.11: B3 sand reservoir characterization analysis. Top left: Seismic section with volume of clay log at GD-1 well, top sand horizons. Top middle: seismic amplitude on the horizon. Top right: Porosity map (PHIT). Bottom left: Sand probability section. Bottom middle: RGB color blend of decomposed frequency map extracted on the horizon. Bottom right: sand probability map extracted on the horizon.

CHAPTER 5: CONCLUSION AND RECOMMENDATION

A detailed feasibility study of seismic reservoir characterization of unconsolidated sand in part of Malay Basin has been carried out. All the analysis result in the four phases: 1) input data QC and conditioning; 2) elastic logs and seismic forward modeling; 3) seismic inversion processing; and 4) seismic reservoir characterization analysis and interpretation led to a consistent observation and conclusion. The results are encouraging. The elastic *in situ* and modeled elastics logs showed good trend match with the global AI-Vp/Vs crossplot. The established AI-Vp/Vs relation from the GD-1 well produced a clear understanding of elastic properties changes to rock type, hydrocarbon phase, porosity, water saturation and pore pressure. The resultant of seismic forward model analysis clearly demonstrated that seismic amplitude from unconsolidated shallow sand is highly sensitive to gas fill, followed by hydrocarbon saturation, porosity, volume of clay and pore pressure in that order. An excellent well-to-seismic tie with stable wavelet produced consistent AVO response between the synthetic seismic and observed seismic response thus indicating that both datasets are suitable for seismic inversion processing. High correlation value of 80 - 90% match between inverted AI - Vp/Vs trace and measured AI - Vp/Vs logs confirmed that the input site survey seismic data are feasible for seismic reservoir characterization analysis. The predicted sand response match the well response, and the interpreted sand fairway is consistent with shallow marine sand deposition.

It is therefore concluded that the AST log and pseudo3D seismic site survey data are feasible for seismic reservoir characterization analysis and interpretation. The value of site survey seismic data for seismic reservoir characterization in shallow-depth clastics has been demonstrated here. It is recommended to apply this scheme to other areas so as to improve confidence in drilling shallow gas prospects and especially placing wells at optimal drilling locations.

REFERENCES

Abhinav, K.D. (2012, Feb). *Reservoir characterization using AVO and seismic inversion techniques.* Paper presented at the Petroleum Geophysics International Conference and Exposition, Hyderabad, India.

Adekanle, A., & Enikanselu, P.A. (2013). Porosity prediction from seismic inversion properties over „XLD" field, Niger Delta. *American Journal of Scientific and Industrial Research, 4*(1), 31 -35.

Aki, K., & Richard, P.G. (1980). Quantitative seismology, theory and methods. (Volume 1). San Francisco: Freeman.

Archie, G.E. (1952). Classification of carbonate reservoir rocks and petrophysical considerations. *AAPG Bulletin, 36*(2)*,* 218–298.

Avseth, P. (2000). *Combining rock physics and sedimentology for seismic reservoir characterization of North Sea turbidite systems.* (Doctoral dissertation, Stanford University). Retreived from https://www.researchgate.net/profile/Per_Avseth

Avseth, P., Fleshe, H., & Wijngaaeden, A.J.V. (2003). AVO classification of lithology and pore fluids constrained by rock physics depth trend. *The Leading Edge, 22*(10), 1004 – 1011.

Avseth, P., Mukerji, T., & Mavko, G. (2010). *Quantitative seismic interpretation, applying rock physics tools to reduce interpretation risk.* Cambridge, United Kingdom: University of Cambridge Press.

Avseth, P. (2010). Exploration rock physics – the link between geological processes and geophysical observables. In K. Bjorlykke (Ed.) *Petroleum geoscience from sedimentary environments to rock physics* (pp.403-425). Oslo, Norway: Springer.

Banik, N., Koesoemadinata, A., Wagner, C., Inyang C., & Bui, H. (2013, Sep). *Predrill pore-pressure prediction directly from seismically derived acoustic impedance*. Paper presented at the Society of Exploration Geophysicists (SEG), *Houston, USA.*

Bianco, E. (2011). *Rock physics cheatsheet*. Retrieved from https://agilescientific.com/blog/2011/3/7/rock-physics-cheatsheet.html

Bjorlykke, K (2014). Relationships between depositional environments, burial history and rock properties. Some principal aspects of diagenetic process in sedimentary basins. *Sedimentary Geology*, 301, 1-14. https://doi.org/10.1016/j.sedgeo.2013.12.002

Brown, A.R. (2003). *Interpretation of three-dimensional seismic analysis. (*6th ed., AAPG Memoir, 42). Oklahoma, USA: The American Association of Petroleum Geologist (AAPG) & The Society of Exploration Geophysicists (SEG).

Carcione, J.M., Ursin, B., & Nordskag, J.I. (2007). Property relations between electrical conductivity and the seismic velocity of rocks. *Geophysics, 72*(5), 193-204.

Castagna, J.P., Batzle, M.L., & Eastwood, R.L. (1985). Relationship between compressional-wave and shear-wave velocities in clastic silicate rocks. *Geophysics, 50*(4), 571-581.

Castagna, J.P., & Backus, M.M (1993). *Offset dependent reflectivity - Theory and practice of AVO analysis*. Tulsa, Oklahoma: The Society of Exploration Geophysicists (SEG).

Cheng, N., Bukhari, I., Awiroot, S., & Vitoon, C. (2008). Elastic impedance inversion for reservoir delineation – A quantitative interpretation case study in the Malay Basin*: Petroleum Geology Conference and Exhibition (PGCE), Kuala Lumpur Convention Center, Kuala Lumpur* (pp. 77-80). Kuala Lumpur, Malaysia: Geological Society of Malaysia (GSM).

Chiew, K.C., & Zakaria,M.H., 2014. *Gayong Deep-1 petrophysical final evaluation report.* Kuala Lumpur: PETRONAS Carigali Sdn Bhd.

Dvorkin, J., Gutierrez, M.A., & Grana, D. (2014). *Seismic Reflection of Rock Properties*. Cambridge, United Kingdom: Cambridge University Press.

Dzhafri, N., Soo, C.N., Suhairi, S., A., Amalina, S., & Maryam, S. (2014). *Gayong Deep-1 End of Well Report.* Kuala Lumpur: PETRONAS Carigali Sdn Bhd.

Ehirim, C.H., & Chikrzie, N.O. (2017). Plane versus Elastic Wave AVO Anisotropic Synthetic Modeling in Derby Field, Southeastern Niger Delta. *American Journal of Geosciences, 4*(1), 1-6.

Eastwood, R.L, & Castagna, J.P. (1983). Basis for interpretation of Vp/Vs ratios in complex lithologies: *SPWLA 24th Annual Meeting of Logging Symposium. Calgary, Canada* (pp.103-120). Calgary Canada: Society of Petrophysicists and Well-Log Analysts (SPWLA).

Faust, L.Y. (1953). A velocity function including lithological variation. *Geophysics, 18(2),* 271-288.

Gardner, G.H.F., Gardner, L.W., & Gregory, A.R. (1974). Formation velocity and density – The diagnostic basis for stratigraphic traps. *Geophysics, 39*(6), 770-780.

Geertsma, J. & Smit, D. C. (1961). Some aspects of elastic wave propagation in fluid saturated porous solids. *Geophysics, 26*(2), 169–181.

Ghosh, D.P., Halim, M.F.A., Brewer, M., Viratno. B., & Darman, N. (2010). Geophysical issues and challenges in Malay and adjacent basins from an E & P perspective. *The Leading Edge. 29*(4), 436 – 449.

Greenberg M. L., & Castagna J. P. (1992). Shear wave velocity estimation in porous rocks: theoretical formulation, preliminary verification and applications. *Geophysical Prospecting,* 40(2), 195–209.

Han, D. (1986). The effect of porosity and clay content on acoustic properties of sandstone and unconsolidated sediment. (Doctoral dissertation, Stanford University). Retreived from https://www.researchgate.net/publication/236505782_Effects_of_porosity_and_clay_content_on_acoustic_properties_of_sandstones_and_unconsolidated_sediments.

Hacikoylu, P., Dvorkin J., & Mavko, G. (2006). Resistivity–velocity transforms revisited. *The Leading Edge, 25*(8), 1006–1009.

Hawkins, K. Ratcliffe, A., Robert, G., & Went, D. (2004). High resolution pore pressure prediction from AVO derived velocities, a North Sea Case Study. *EAGE 66th Conference & Exhibition, Paris, France* (pp. 366-369): European Association of Geoscientists & Engineers (EAGE)

Hilterman, F.J. (2001). *Seismic amplitude interpretation. (2001 Distinguish Instructor Short Course Series,4).* Houston, USA: European Association of Geoscientists & Engineers (EAGE).

Hook, J.R. (2003). An introduction to porosity. *Petrophysics, 44*(3), 205-212.

Hossain, Z., & MacGregor, L. (2014). Advanced rock-physics diagnostic analysis: A new method for cement quantification. *The Leading Edge, 33*(3), 312-320.

Hoyes, J., & Cheret, T. (2011). A review of "global" interpretation methods for automated 3D horizon picking. *The Leading Edge, 30*(1), 38-47.

Khan, A.F., and Zohdi M.S.F. (2016). *Pseudo 3D Marine Pre Stack Time Migration. Gayong Deep-1. Offshore Peninsular Malaysia*, *Data Processing Report*. Kuala Lumpur: PETRONAS Carigali Sdn Bhd.

Khateb, A.N. (2013, May). *A look into Gassmann's equation*. Paper presented at the GeoConvention. Calgary, Canada.

Krief, M., Garat, J., Stelingwerf, J., & Ventre, J. (1990). A petrophysical interpretation using the velocities of P- and S-waves (full waveform sonic). *The Log Analyst, 31*(6), 355–369.

Lubis, L.A., Ghosh, D.P., & Hermana, M. (2016). Elastic and electrical properties evaluation of low resistivity pays in Malay Basin clastics reservoirs. *IOP Conf. Series: Earth and Environmental Sciences, 38*(2016), 1-9. doi:10.1088/1755-1315/38/1/012004.

Madon, M. (1999). Basin types, techtono-stratigraphic provinces, structural styles. In Leong, K.M (Ed.). *The Petroleum Geology and Resources of Malaysia* (pp. 79-111). Kuala Lumpur, Malaysia. Petroleum Nasional Berhad (PETRONAS).

Mansor, M.Y., Rahman, A.H.A., Menier, D., & Pubellier, M. (2014). Structural evaluation of Malay Basin, its link to Sunda block tectonics. *Marine and Petroleum Geology, 58*, 736-748.

Meju, M.A. (1994). *Geophysical data analysis: Understanding inverse problem theory and practice*. (*Course Notes Series, 6).* Tulsa, Okhlahoma, USA: The Society of Exploration Geophysicists (SEG).

Miller, S.L.M., & Steward, R.R. (1990). Effects of lithology, porosity and shaliness on P- an S-wave velocities from sonic logs. *Canadian Journal of Exploration Geophysics, 26*(1), 94-103.

Mohamed, H., & Danial, R. (2013, March*). Leads and prospect delineation using rock fluid index with case example from clastics sediment, PM330*. Paper presented at the Petroleum Geoscience & Exhibition (PGCE), Kuala Lumpur, Malaysia.

Mohamed, H., Kurniawan, T., M Zaffa, F., Hamzah, M.R., Mohamed, N., Martinez, L.G., & Paton, G. (2015, Oct). *Integrated 3D quantitative analysis and interpretation of pay sand in basin floor channel complexes – case study example in deep water Sabah*. Paper presented at the Petroleum Geoscience & Exhibition (PGCE), Kuala Lumpur, Malaysia.

Morris, C.F., Letton, W., & Little, T.M. (1984, Sept). *A new sonic array tool for full waveform logging*. Paper presented at SPE Annual Technical Conference and Exhibition, Houston, Texas, USA.

Naidu, P., Santosh., Chand, S., & Saxena, U.C. (2013, Nov): *Surface related multiple elimination: A case study from east coast India*. Paper presented at the Petroleum Geophysics International Conference and Exposition, Kochi, India

Nur, F.M.J. (2014). *Gayong-2A drill site investigation survey, AVO processing report*. Kuala Lumpur: TL Geohydrographics Sdn Bhd.

Nur, A. (1992): Critical porosity and the seismic velocities in rocks. *EOS, Transactions of the American Geophysical Union, 73*(1), 43–66.

Nur, A., Mavko, G., Dvorkin, J., & Galmudi, D. (1998): Critical porosity: a key to relating physical properties to porosity in rocks. *The Leading Edge, 17*(3), 357–362.

Odegaard, E., & Avseth, P. (2004). Well log and seismic data analysis using rock physics templates. *First Break, 22*(10), 37-43.

Onajite, E. (2017). *Practical solutions to integrated oil and gas reservoir analysis, geophysical and geological Perspectives*. Amsterdam, Netherlands: Elsevier.

Ostrander, W.J. (1984). Plane-wave reflection coefficients for gas sands at nonnormal angles of incidence*. Geophysics, 49*(10), 1637 – 1648.

Panea, I., Rayner, J., Schultz, G., & Manea, C. (2013, June). *2D versus pseudo-3D seismic data processing in the AVO Analysis - A study case*. Paper presented at the *EAGE Conference & Exhibition incorporating SPE EUROPEC.* London, United Kingdom.

Paul, C.H.V, & Bruno, V.M. (2013). Depositional environment and lithofacies interpretation. In Paul, C.H.V, & Bruno, V.M. (Eds.) *Seismic Stratigraphy and Depositional Facies Models* (pp.217-362). Houton, The Netherlands: EAGE.

Ralim, A.M.N., & Mohamed, H. (2015, Nov). *Understanding the amplitudes, Peninsular Malaysia, XPM-XTS integrated studies*. Poster presented at PCSB Exploration Technical Forum. Kuala Lumpur, Malaysia.

Raymer, L. L., Hunt, E. R., & Gardner, J. S. (1980). An improved sonic transit time-to-porosity transform. *SPWLA 21st Annual Meeting of Logging Symposium. Louisiana, USA:* Society of Petrophysicists and Well-Log Analysts (SPWLA).

Ross, C.P (2000). Effective AVO crossplot modeling. Effective AVO crossplot modeling: A tutorial. *Geophysics, 65*(3), 700-711.

Roden, R., Forrest, M., & Holeywell, R. (2005). The impact of seismic amplitudes on prospect risk analysis. *The leading Edge, 24*(7), 706 – 711.

Roden, R., Forrest, M., & Holeywell, R. (2012). Relating seismic interpretation to reserve/resource calculations: Insights from a DHI consortium. *The leading Edge, 31*(9), 1066-1074.

Roger, P. (2001). *High Resolution Site Surveys*. New York, USA: Spon Press.

Schroeder, F.S. (2011). Geology and geophysics applied to industry – An Introduction to the Hunt for oil for geoscientists not within industry. Retrieved from http://archives.aapg.org/slide_resources/schroeder/index.cfm

Sidi, H.F., Ilahi, A., & Duncan, G. (2007). Seismically constrained petrophysics in the Scarborough area. *Exploration Geophysics, 38*(2), 120-124.

Simm, R., & Bacon, M. (2014). *Seismic Amplitude: An Interpreter's Handbook.* Cambridge, United Kingdom:Cambridge University Press.

Sulaiman, N., Hamzah, U., & Samsudin, A.R. (2016). Facies analysis and stratigraphic sequence of the northeast Malay Basin, Offshore Teregganu, Malaysia. *ARPN Journal of Engineering and Applied Sciences, 5*(2), 2849-2858.

Sun, B., Wang, R., Jonathan, B.S., Langley, B., Wilson, G., & Cheng, A. (2016, March). *Ultra-broadband Acoustic Logging Tool for Deep Reading Formation Evaluation*. Paper presented at Offshore Technology Conference Asia, Kuala Lumpur. Malaysia.

Suhairi, S., & Jalil, H. (2014). *Gayong Deep-1 Well Proposal Block PM315, Offshore Peninsular Malaysia*. Kuala Lumpur: PETRONAS Carigali Sdn Bhd.

Tan, D.N.K. (2009). Oil and Gas. In Hutchinson, C.S., & Tan, D.N.K (Eds.), *Geology of Peninsular Malaysia.* (pp. 365-405). Kuala Lumpur, Malaysia: The University of Malaya & The Geological Society of Malaysia (GSM).

Tjia, H.D. (1994). Inversion Tectonics in the Malay Basin: Evidence and Timing Events. *Geological Society Malaysia, 36,* 119-126.

Tjia, H.D. (1999). Geological Setting of Peninsular Malaysia. In Leong, K.M (Ed.). *The Petroleum Geology and Resources of Malaysia* (pp. 139-170). Kuala Lumpur, Malaysia. Petroleum Nasional Berhad (PETRONAS).

Tosaya C.A. (1982). *Acoustical properties of clay-bearing rocks.* (Doctoral dissertation, Stanford University). Retrieved from https://pangea.stanford.edu/departments/geophysics/dropbox/SRB/public/docs/theses/SRB_015_JUN82_Tosaya.pdf

Vardy, M.E. (2015). Deriving shallow-water sediment properties using post-stack acoustic impedance inversion. *Near Surface Geophysics, 13,*143-154.

Vardy, M.E., Vanneste, M., Henstock T.J., Morgan E., & Pinson L.JW. (2015). Can high resolution marine geophysical data be inverted for soil properties? *Proceeding of the Institute of Acoustics, 37*(1), 192-196. doi:10.3997/1873-0604.2014045

Vardy, M.E. (2016, Sept). *Remote Characterisation of Shallow Marine Sediments - Current Status and Future Questions*. Paper presented at Near Surface Geoscience Conference and Exhibition EAGE, Barcelona, Spain. doi: 10.3997/2214-4609.201602145.

Vernik, L., Fisher, D., & Bahret, S. (2002). Estimation of net-to-gross from P and S impedance in deep-water turbidites. *The Leading Edge, 21*(4), 380–387.

Versteeg, W., Verschuren, M., Henriet, J.P., & Batist, M.B., (1992). High resolution 3D and pseudo3D investigations in shallow water environment. In Weydert, M (Ed.), *European Conference on Underwater Acoustics* (pp.497-500). London, United Kingdom: Elsevier.

Werthmuller, D.A, Ziolkowsku, A., & Wright, W. (2013). Background resistivity model from seismic velocity. *Geophysics, 78*(4), 213-223.

Williams, D. M. (1990). The Acoustic Log Hydrocarbon Indicator. *SPWLA 31st Annual Meeting of Logging Symposium. Louisiana, USA:* Society of Petrophysicists and Well-Log Analysts (SPWLA).

Wollner, U., Yang, Y, & Dvorkin J.P. (2017). Rock-physics diagnostics of offshore gas field. *Geophysics, 84*(4), 121-132.

Wyllie, M. R. J., Gregory, A. R., & Gardner, L. W. (1956). Elastic wave velocities in heterogeneous and porous media. *Geophysics, 21*(1), 41-70.

Yahya, M.A. (2015). *Pseudo 3D Seismic Processing Using High Resolution Site Survey Data for Shallow Clastics AVO Study, Peninsular Malaysia*. (Unpublished dissertation proposal). University of Malaya, Kuala Lumpur.

Yoong, A.A., Lubis, L.A., & Ghosh, D.P. (2016). Application of Simultaneous Inversion Method to Predict the Lithology and Fluid Distribution in “X” Field, Malay Basin. *IOP Conf. Series: Earth and Environmental Sciences 38* (1), 1-6.